Dual Domain Echo Cancellation for Discrete Multitone Systems

Neda Ehtiati

Department of Electrical & Computer Engineering
McGill University
Montréal, Canada

April 2011

A thesis submitted to McGill University in partial fulfillment of the requirements for the degree of Doctor of Philosophy.

Abstract

Due to the tremendous popularity of the Internet in recent years and the growing market for bandwidth intensive applications, such as video on demand, high definition television and remote collaboration, there is an enormous demand for advanced broadband access technologies. Among the available broadband solutions for fixed users, the dominant one is Digital Subscriber Line (DSL) technology where the last mile connection is provided through the twisted-pair telephone lines. In a full-duplex DSL transmission, one of the technical challenges is to overcome the deteriorating effect of the echo, which is the interference of the transmitted signal into the collocated receiver. The digital echo cancellers employ adaptive filtering techniques to estimate the echo signal and then remove it from the received signal. The use of echo cancellation in DSL systems reduces the implementation complexity, improves the spectral efficiency and increases the loop reach. For discrete multitone (DMT) modulated DSL systems, the computational complexity of the echo cancellers can be reduced by making use of the structure present in the transmitted signal. However, this generally leads to a mixed adaptation structure in which the relationship between the time-domain and frequency-domain adaptive coefficients are not fully understood.

In this thesis, we introduce a general framework for studying and designing echo cancellers for DMT-based systems. This framework establishes a unified representation of the existing echo cancellation methods and provides the capability of achieving different design trade-offs between the convergence rate and the computational complexity of the echo cancellation algorithms. This capability is also exploited to design new cancellers with improved performance and/or lower complexity. In the first part of this thesis, echo cancellation for DMT-based systems is reformulated as a constrained optimization problem, where a cost function is to be minimized over an extended linear space comprised of the adaptive filter coefficients in the time and frequency domains. Based on this formulation, a new linearly constrained echo cancellation structure is proposed. This new structure offers additional flexibility in implementation by allowing the incorporation of additional constraints to improve the performance of the system. In the second part of this thesis, the echo cancellation is examined in a more general dual domain, rather than only in the time and frequency domains. A two-step design methodology is proposed providing high level of flexibility in the design process of echo cancellers. Following this methodology, a new dual domain canceller is developed, which transforms the signals and weight vector into a dual domain. The proposed dual transform domain canceller has a faster convergence rate compared to those of existing cancellers with similar computational complexity.

Sommaire

En raison de l'immense popularité de l'Internet ces dernières années et du marché croissant des applications intensives avec bande passante, comme la vidéo sur demande, la télévision haute définition et la collaboration à distance, il y a une très grande demande pour les technologies avancées avec accès à large bande. Parmi les solutions à large bande disponibles pour les utilisateurs fixes, le service dominant est le Digital Subscriber Line (DSL) (ligne numérique d'abonné), où le dernier kilomètre de connexion est assuré par des lignes téléphoniques à paires torsadées. Dans une transmission bidirectionnelle simultanée, l'un des défis techniques à surmonter est l'effet néfaste de l'écho, causé par le coulage du signal transmis dans le récepteur co-implanté. L'annulateur d'écho numérique emploie des techniques de filtrage adaptatives pour estimer le signal d'écho, puis le retirer du signal reçu. L'utilisation de l'annulation d'écho dans les systèmes DSL réduit la complexité des algorithmes, améliore l'efficacité spectrale et augmente la portée de la boucle. Pour les multitonalités discrètes (MTD) modulées par système DSL, la complexité numérique de l'annulateur d'écho peut être réduite en utilisant la structure présente dans le signal transmis. Toutefois, cela conduit généralement à des structures adaptatives mixtes dans lesquelles la relation entre les coefficients d'adaptation temporels et fréquentiels n'est pas encore bien comprise.

Dans cette thèse, nous présentons un cadre général pour l'étude et la conception des annulateurs d'écho pour les systèmes utilisant la technologie MTD. Ce cadre établit une représentation unifiée des méthodes d'annulation d'écho et permet l'application de méthodes de conception plus générales, offrant ainsi un meilleur compromis entre le taux de convergence et la complexité des algorithmes d'annulation d'écho. Cette capacité est également utilisée pour concevoir de nouveaux annulateurs avec des performances améliorées et/ou en réduire la complexité. Dans la première partie de cette thèse, l'annulation d'écho est examinée comme un problème d'optimisation sous contrainte, où une fonction de coût doit être minimisée sur un espace linéaire étendu, composé des coefficients de filtrage adaptatif dans les domaines temporel et fréquentiel. Sur la base de cette formulation, une nouvelle structure sous contrainte linéairement est proposée. Cette nouvelle structure possède une flexibilité accrue de mise en œuvre permettant l'incorporation de contraintes supplémentaires afin d'améliorer les performances du système. Dans la deuxième partie de cette thèse, l'annulation d'écho est examinée dans un domaine dual plus général, plutôt que seulement dans les domaines temporel et fréquentiel. Une méthodologie de conception en deux étapes est proposée fournissant un niveau élevé de flexibilité dans le processus de conception des annulateurs d'écho. Cette méthodologie est utilisée enfin de développer un nouvel annulateur d'écho à domaine dual, lequel transforme les signaux et le vecteur de poids dans un domaine dual. L'annulateur d'écho à domaine dual proposé possède un taux de convergence plus élevé que ceux des annulateurs

existants tout en ayant une complexité d'implantation numérique similaire.

Acknowledgments

Firstly, I would like to express my sincere gratitude to my supervisor Prof. Benoît Champagne for his guidance and constant support. I also extend my thanks to the faculty and staff of Electrical and Computer Engineering department and to the members of my Ph.D. committee. I would like to thank all of my friends at Telecommunication and Signal Processing Laboratory, especially, Aarthi, Pegaah and Parya for their companionship. My heartfelt thanks to my parents, Mohamad Ali Ehtiati and Servat Rostamkhani and my sister, Tina Ehtiati, who supported me with their love and understanding. Finally, I would like to express my deepest gratitude to my husband, Pouriya Sadeghi, for his unconditional love and support, and the sacrifices he has made in the past years.

Contents

List of Figures

List of Tables

List of Acronyms

3GPP	Third Generation Partnership Project
ADC	Analog-to-digital converter
ADSL	Asymmetric Digital Subscriber Line
AFE	Analog front-end
AM	Amplitude modulation
AWG	American wire gauge
CAP	Carrierless amplitude phase
CES	Circular echo synthesis
CDC	Circulant decomposition canceller
CO	Central office
CP	Cyclic prefix
CS	Cyclic suffix
CSA	Carrier serving area
DAC	Digital-to-analog converter
DCT	Discrete cosine transform
DFT	Discrete Fourier transform
DLC	Digital loop carrier

DMT	Discrete multitone
DOCSIS	Data-over-cable service interface specification
DSL	Digital Subscriber Line
DSLAM	Digital Subscriber Line Access Multiplexer
DSM	Dynamic Spectrum Management
DST	Discrete sine transform
DTC	Dual trigonometric canceller
DTDC	Dual transform domain canceller
EPC	Evolved Packet Core
EPON	Ethernet passive optical network
FDD	Frequency-division duplexing
FEC	Feedforward error correction
FEQ	Frequency-domain equalizer
FEXT	Far-end crosstalk
FIR	Finite impulse response
FTTTH	Fiber-to-the-home
GPON	Gigabit passive optical network
GSC	Generalized sidelobe canceller
HDSL	High bitrate Digital Subscriber Line
HDTV	High-definition television
HFC	Hybrid fibre-coaxial
IDFT	Inverse discrete Fourier transform
IEEE	Institute of Electrical and Electronics Engineers
IP	Internet Protocol

IPTV	Internet Protocol television
ISDN	Integrated Services Digital Network
ISI	Intersymbol interference
LAN	Local area network
LCA	Linearly constrained adaptive algorithm
LMS	Least mean square
LTE	Long Term Evolution
MDF	Main distribution frame
MIMO	Multiple-input multiple-output
NBN	Narrowband Noise
NEXT	Near-end crosstalk
OFDM	Orthogonal frequency division multiplexing
OLT	Optical line terminal
ONU	Optical network unit
PON	Passive optical network
PSTN	Public switched telephone network
QAM	Quadrature amplitude modulation
RF	Radio frequency
RFI	Radio frequency interference
RT	Remote Terminal
RX	Receiver
SAI	Serving area interface
SDC	Symmetric decomposition canceller
SDSL	Symmetric Digital Subscriber Line

SM	Spectrum management
SNR	Signal-to-noise ratio
SVD	Singular value decomposition
TCM	Trellis-coded modulation
TDD	Time-division duplexing
TDM	Time-division multiplexing
TEQ	Time-domain equalizer
TX	Transmitter
VDSL	Very-high-bitrate Digital Subscriber Line
VLSI	Very-large-scale integration
VOD	Video on Demand
VoIP	Voice over Internet Protocol
WDM	Wavelength-division multiplexing
WiMAX	Worldwide interoperability for Microwave Access

Notation

$\mathbf{V}(i)$	i-th element of vector $\mathbf{V}$
$\mathcal{M}(i,j)$	Element on the i-th row and j-th column of matrix $\mathcal{M}$
$\mathcal{M}(l:m\ ,\ :)$	Rows l up to m of matrix $\mathcal{M}$
$\mathcal{M}(:\ ,\ l:m)$	Columns l up to m of matrix $\mathcal{M}$
$(.)^*$	Complex conjugate operator
$\mathcal{M}^T$	Transpose of matrix $\mathcal{M}$
$\mathcal{M}^H$	Conjugate transpose of matrix $\mathcal{M}$, Hermitian traspose
$\mathcal{M}^{-1}$	Inverse of matrix $\mathcal{M}$
diag$\{\mathbf{V}\}$	Square diagonal matrix with elements of vector $\mathbf{V}$ on its diagonal
$\odot$	Component-wise multiplication operator
$\mathcal{F}_N$	N-point DFT matrix
$\mathcal{F}_N^{-1}$	N-point IDFT matrix
$\mathcal{I}_N$	Identity matrix with dimension $N \times N$
$\mathcal{O}_N$	Zero matrix with dimension $N \times N$
$\mathcal{O}_{N\times M}$	Zero matrix with dimension $N \times M$
E[.]	Statistical expectation operator

Chapter 1

Introduction

This chapter provides an overview of the thesis, which is aimed at developing and studying new signal processing algorithms for the problem of echo cancellation in discrete multitone transmissions, as used in modern Digital Subscriber Line (DSL) systems. Various broadband access technologies are discussed in Section 1.1, while a review of DSL systems and their related duplexing methods are presented in Section 1.2. The literature review of digital echo cancellation methods for DSL systems is presented in Section 1.3. The research objectives and the contributions of the thesis are discussed in Section 1.4, and finally, an outline of the upcoming chapters is presented in Section 1.5.

1.1 Broadband Access Technologies

In recent years, the demand for broadband access technologies has increased tremendously with the emphasis on delivering multimedia services, such as voice, data and video, over a single connection. The evolution of the Internet and the growing mar-

ket for bandwidth intensive applications, such as Video on Demand (VOD), high-definition television (HDTV) and remote collaboration, have resulted in an increasing pressure on the bandwidth provisioning in broadband networks. There are numerous competing technologies providing broadband data access, each having its own limitations with respect to the bandwidth, reliability, cost and coverage [1].

The broadband solutions can be divided into two categories: fixed-line and wireless technologies. Fixed-line (or wired) technologies offer a dedicated physical connection to each end-user. Examples of such technologies include optical fiber, DSL, hybrid fibre-coax (HFC) and broadband power line systems. In wireless broadband technologies the connection between the end-user and the network access point is provided by a radio frequency link. Examples of such technologies are Worldwide interoperability for Microwave Access (WiMAX) and the 3rd Generation Partnership Project Long Term Evolution (3GPP LTE). For fixed users, wired technologies are generally preferred to the wireless ones due to the high cost of wireless bandwidth, the shared nature of the radio channel between the users, and non-uniform coverage of wireless networks.

Considering the available wired technologies, fiber-to-the-home (FTTH) which is an all-fiber architecture is a superior option in terms of achievable data rate and reliability. However, the deployment of FTTH networks has been slowed down due to two main reasons; one is the high cost of the installation of optical fibers to the end-user location (e.g., home) and the other is the availability of competing solutions via existing infrastructures such as copper telephone lines and coaxial cables. Consequently, instead of having all-fiber networks, hybrid solutions are widely deployed where the transmission path includes a combination of optical fibers with telephone

lines or coaxial cables. Among these solutions, the dominant one is DSL technology, with a market share of 65% in 2008 [1]. In DSL systems, the last mile connection, i.e., the connection between the end-user and the central office (CO), is delivered through copper telephone lines.

1.2 Overview of DSL Systems and the Echo Problem

The earlier standards in DSL systems, namely high bitrate DSL (HDSL) and Symmetric DSL (SDSL), provided bitrates up to 1.16 Mbps over twisted-pair copper wires. In contrast , more recent standards, in particular very-high-bitrate DSL (VDSL) and VDSL2, can achieve symmetric rates up to 100 Mbps, offering support for the transmission of video channels for Internet Protocol television (IPTV) [3]. These higher data rates are achieved by using advanced signal processing techniques and by decreasing the distance between the CO and the end-users. The latter is feasible by deploying intermediary units connected to the CO through optical fiber.

As noted, DSL systems provide broadband access over copper telephone lines. In these systems, the available bandwidth is shared between the voiceband telephone transmission, which requires the lower frequency band from 0 up to 4 kHz, and the digital high data rate transmission, which occupies the higher end of the frequency band above 4 kHz. The available higher frequency band is further divided between the upstream transmission, which is from the subscriber to the CO and the downstream transmission, which is from the CO to the subscriber or the remote terminal (RT).

In these systems, the upstream and downstream signals are sent over a single pair of wires. Therefore, a hybrid circuit is utilized to do the conversion from the four-wire connection on the transceiver side to the two-wire connection on the network

side. Ideally, signal should travel from the twisted-pair line into the receiver and from the transmitter into the line. However, there is always leakage of signals from the transmitter into the collocated receiver, which is known as electrical echo.

In DSL systems, the upstream and downstream signals are transmitted simultaneously, resulting in a form of transmission known as full-duplex. The common duplexing techniques mainly used in DSL systems are frequency-division duplexing (FDD), digital duplexing and echo cancellation [2].

In FDD, a frequency gap separates the bands used for the transmission of the upstream and downstream signals. This is achieved by using precise analog filters, with sharp transition characteristics, thereby providing the desired level of the protection against the echo. However, the design and implementation of an accurate brick-wall analog filter is very difficult and expensive. In addition, in recent DSL standards which accommodate various frequency band plans, the use of fixed filters is prohibitive. Another duplexing method is digital duplexing where the signals in the two directions are kept orthogonal to each other by adding cyclic suffix (CS) [5]. This technique can address the issue of having various frequency band plans, but it remains applicable to the short loops with lengths under 1 km [6, 7].

In systems with echo cancellation, digital adaptive filters are used to estimate the echo and remove it from the transmitted signal [8]. The benefits of using digital echo cancellers are multiple; the requirements on the front-end filters can be relaxed; the need for a frequency gap between the downstream and upstream is removed, resulting in a higher spectral efficiency; finally, for systems with digital duplexing, the use of echo canceller makes the service available on longer loops.

Multicarrier modulation is a widely-used modulation scheme in both wireless and

wired communications systems for frequency-selective channels, i.e., channels with severe channel-induced intersymbol interference (ISI). In this technique the channel is divided into orthogonal subchannels (or tones). Due to their narrowband nature, these subchannels have relatively flat-fading behaviour and therefore, the ISI on each tone is negligible [9]. In DSL systems, the multicarrier modulation is realized in the form of discrete multi-tone modulation (DMT) which is well-suited for digital implementation. This technique is widely used in the context of the wireless communications, where it is commonly known as orthogonal frequency division multiplexing (OFDM).

In this thesis, we examine the problem of echo cancellation for DMT-based systems, with the main focus on the DSL networks. However, since the main assumption made about the system is the use of the DMT modulation, the results of our work are applicable to the OFDM-based wireless networks as well. Indeed, concepts similar to the echo cancellation have already been used in certain wireless communication applications, such as intercarrier interference cancellation and full-duplex relaying [10, 11, 12, 13].

1.3 Echo Cancellation Methods for DMT-Based Systems

The echo cancellation is generally performed by using adaptive filtering methods such as least mean square (LMS). In these methods, the echo channel is emulated by a finite impulse response (FIR) filter whose weights are updated adaptively. The echo signal is calculated by the linear convolution of the known transmitted signal with the filter coefficients, and then the estimated echo is subtracted from the received signal. Finally, the resulted error signal is used to adaptively update the filter coefficients also known as tap weights.

For DMT-based systems, the above general echo cancellation with LMS filtering can be applied in the time domain. In this implementation, the echo signal is calculated by multiplying the echo weight vector with the Toeplitz data matrix containing the transmitted signal samples. Moreover, a similar matrix multiplication is required in the adaptive weight update step. Due to the aforementioned matrix multiplications, the time-domain LMS echo canceller is characterized with very high computational cost.

In [14], Cioffi and Bingham proposed a mixed time- and frequency-domain echo canceller to reduce the complexity of the traditional time-domain LMS echo canceller. In this canceller, the echo emulation is performed in the time domain; however, the echo weights are updated independently (i.e., on a per-tone basis) in the frequency domain instead of the time domain as done in the traditional method. Later, in [15], Ho *et al.* proposed the circular echo synthesis (CES) method, where the Toeplitz data matrix is decomposed into a sum of a circulant and a residual matrix, with the former being diagonalized by means of the Fourier transform. Consequently, the CES complexity is reduced by performing the emulation partially in the time and frequency domains, while a per-tone weight update is done entirely in the frequency domain. However, not all tones are used (excited) in DMT-based systems due to certain requirements of power masks or bit allocation algorithms. Therefore, the filter weights corresponding to the unused tones remain unchanged during the weight update step, and as a result, this method suffers from slow convergence. Addressing the convergence issues of this method, in [15], it was proposed to transmit dummy data with reduced power on the unused tones. However, as shown in [16], this approach generates extra interference requiring a more complex equalizer at the receiver and

higher order front-end filters to comply with the power mask [4].

Other methods have been proposed in the literature in order to improve the convergence rate of the mixed time- and frequency-domain echo cancellers. In [17], Ysebaert *et al.* suggested the circulant decomposition canceller (CDC), where the Toeplitz data matrix is expressed as a sum of a circulant and a skew-circulant matrix. Similar to the CES canceller, in this method the echo is emulated jointly in the time and frequency domains; however, the tap-input vector used for the weight update, usually has sufficient excitation on all tones. Later, in [18], Pisoni and Bonaventura extended and modified this echo canceller by using discrete trigonometric transformations. Eventually, in [19], Pisoni *et al.* introduced a canceller similar to the self-orthogonalizing filter, where the singular value decomposition (SVD) of the correlation matrix is used to boost the slow modes.

Other echo cancellation methods for DMT-based systems have proposed modifications to these mixed time- and frequency-domain echo cancellers in order to lower the complexity and/or improve the performance of these cancellers. For instance in [20], Jones showed that the proper choice of the delay between the transmitted and received symbols can help reduce the complexity of the system. In [21], Ysebaert *et al.* added double talk cancellation to the receiver, i.e., removing the effect of the far-end signal in order to improve the convergence of the adaptive weight update. In [22], they also proposed an asynchronous echo canceller (integrated with the double talk cancellation) to be used when there is a misalignment between the transmitted symbols and received symbols. Moreover, there are other methods for echo cancellation which perform both the echo emulation and the weight update in the frequency domain, such as in [23, 24], where per-tone echo cancellers were proposed.

1.4 Thesis Objectives and Contributions

The main objective of this thesis is to develop and study improved approaches for digital echo cancellation in DMT-based systems. As pointed out above, various methods have been presented in the literature where the specific structure present in the DMT-modulated signals has been used to design a canceller with low computational complexity while having satisfactory performance. While these methods typically employ mixed adaptation structures in which the filtering is performed partially in the time and frequency domains, the relationship between the adaptation of the filter coefficients in these two domains is not currently well understood. In this thesis, we introduce a general framework for studying and designing echo cancellers that more systematically exploit the intrinsic connection between the representations of the echo synthesis filter in two domains. This general form provides a unified representation of the existing echo cancellers. In addition, the proposed models offer a better understanding of different parts of the canceller and of the impacts of each part on the overall performance in terms of the convergence rate and the computational complexity. These more general models are also used to design new cancellers with improved performance.

In the existing echo cancellers, two weight vectors are used; one weight vector in the time domain and the other one in the frequency domain. These two weight vectors are related by means of Fourier transformation. In the first part of this thesis, a framework is established to characterize the relationship between the time- and frequency-domain weight vectors of the existing echo cancellers in a more systematic way. This is achieved by forming an extended linear space, containing the weight vectors in both time and frequency domains. In this extended space, the echo cancel-

lation can be identified as a constrained optimization problem where a cost function is to be minimized satisfying a certain set of constraints. These constraints can be set primarily to ensure a proper mapping of the weights from the frequency domain into the time domain or vice versa.

By expressing the echo cancellation problem as a constrained optimization, constrained echo cancellers can be designed based on the various available algorithms for constrained adaptive filtering. In this thesis, we derive linearly constrained echo cancellers based on the constrained LMS algorithm by Frost in [25] and the generalized sidelobe canceller (GSC) structure by Griffiths and Jim in [26]. The proposed linearly constrained cancellers are developed using a general joint time- and frequency-domain formulation. Therefore, the existing cancellers, performing the echo emulation in these two domains, can be considered as special approximative realizations within this general framework.

As discussed above, the proposed linearly constrained echo canceller framework provides a unified representation of existing cancellers, and more importantly, it supplies the means to incorporate additional processing constraints into the echo canceller design so as to improve their performance. As an example application, we study the echo cancellation in the presence of radio frequency interference and show that additional constraints can be imposed through our new formulation in order to make the system more robust against such interference.

The second part of this thesis explores the dual domain filtering used in echo cancellation algorithms. In the existing echo cancellers, the main focus is on the filtering in the time and frequency domains, which is a straightforward choice for DMT-modulated signals, where the representation of the transmitted signal is avail-

able in both of these domains at the transceiver. In these methods, the design of the echo canceller is initiated by choosing a technique to decompose the Toeplitz data matrix, and then the rest of the design follows from this decomposition. Such a design procedure is restraining, since the chosen decomposition explicitly constrains the domains in which the echo emulation and the adaptive weight update are performed and it also defines the transformation matrices involved. Therefore, this decision has a direct impact on the computational complexity and the convergence rate of the cancellers.

In this thesis, we take a bold step and propose to reverse the order of echo canceller design procedure. In this proposed design procedure, a generic dual domain decomposition of the Toeplitz data matrix is assumed and the echo canceller is designed in two steps. In the first step, the structure of a general dual domain echo canceller is developed based on generic transforms. In the second step, the criteria for an appropriate decomposition for this structure are determined and then based on these criteria a specific decomposition is chosen.

The proposed design order has the advantage that the structure of the echo canceller can be optimized without having any a priori limitations imposed by the choice of the decomposition. In addition, the use of a generic dual domain decomposition of the Toeplitz data matrix in the proposed structure makes it possible to perform the echo cancellation in any dual domain rather than only in the time and frequency domains.

Following the aforementioned two-step design procedure, a novel dual transform domain canceller (DTDC) is developed. In this canceller, the time-domain signals and weight vectors are mapped into a dual domain defined by a pair of generic unitary

matrices. This canceller performs an LMS adaptive weight update in the dual domain with low computational complexity. The implementation of this dual domain canceller using the appropriate decomposition is referred to as dual trigonometric canceller (DTC).

The decompositions used in existing DMT-based echo cancellers can be regarded as special cases of the proposed general decomposition of the Toeplitz data matrix. Therefore, the new DTDC structure establishes a unified representation of these cancellers in a general dual domain framework. The existing cancellers comply with the dual domain operation in the echo emulation part but perform the adaptive weight update in a single domain to reduce the complexity of the algorithm. As a result, the DTDC structure provides an analytical tool to study the existing cancellers from a unified prospective, as well as, a framework to design new generalized cancellers with a better performance and/or lower complexity.

Furthermore, a constrained dual domain echo cancellation is proposed where the linear constraints ensure the proper mapping of the weights in the dual domain. A comprehensive study of the constrained and unconstrained dual domain cancellers shows that the constrained canceller has a faster convergence rate, similar to that of the time-domain LMS canceller. This improved convergence rate is achieved at the expense of increased computational complexity. Therefore, a combined dual domain canceller is proposed which is mainly based on the unconstrained dual domain canceller, while the constrained adaptive weight update is used infrequently. As it is shown later, the proposed combined dual domain canceller has a convergence rate close to that of the time-domain LMS canceller, while having much lower complexity, similar to those of the existing yet slower cancellers.

The main contributions of this thesis are summarized below:

Linearly Constrained Adaptive Cancellers:

i. Formulation of the echo cancellation for DMT-modulated systems as a linearly constrained optimization problem, where the constraints are originally used to ensure the proper mapping of the weights from the frequency domain into the time domain.

ii. Development of two new implementations for the constrained echo cancellers; one based on the work by Frost in [25] and another based on the GSC structure by Griffiths and Jim in [26].

iii. Implementation of the mixed time- and frequency-domain echo cancellers using the constrained structure and examination of the impact of different choices of constraints on the convergence rate of the cancellers.

iv. Appending additional constraints to the constrained echo cancellers to improve the performance of the system.

Dual Transform Domain Cancellers:

i. Introduction of a general form decomposition for the Toeplitz input data matrix, which provides a unified representation of the various decompositions used in the existing echo cancellers.

ii. Development of a two-step echo canceller design method, where finding a proper structure and an appropriate decomposition for the canceller are performed independently.

iii. Proposing a new dual transform domain canceller (DTDC), providing a unified representation of the existing echo cancellers.

iv. Development of dual trigonometric canceller (DTC) based on the DTDC structure and using the appropriate decomposition.

v. Development of linearly constrained dual domain echo cancellers that develops the incorporation of the linear constraints for the dual domain cancellers.

vi. Development of a combined DTC algorithm, which has a faster convergence compared to the existing cancellers with a similar level of complexity.

vii. Presentation of two implementations for multirate dual domain cancellers where the polyphase decomposition of the signals is used to reduce the complexity of the algorithm.

The algorithms and the contributions of this thesis have been published in peer-reviewed journals and refereed conferences. The list of publications is as follows:

Journal papers

J-1 N. Ehtiati and B. Champagne, "Constrained adaptive echo cancellation for discrete multitone systems," *IEEE Trans. on Signal Processing*, vol. 57, no. 1, pp. 302-312, Jan. 2009.

J-2 N. Ehtiati and B. Champagne, "A general framework for dual domain echo cancellation for discrete multitone systems," to be submitted to *IEEE Trans. on Commun.*

Conference papers

C-1 N. Ehtiati and B. Champagne, "Linearly constrained adaptive echo cancellation for discrete multitone systems," in *Proc. IEEE Int. Sym. on Signal Processing and Information Technology*, Giza, Dec. 2007, 6 pages.

C-2 N. Ehtiati and B. Champagne, "Dual transform domain echo canceller for discrete multitone systems," in *Proc. IEEE Global Telecommunications Conf.* Honolulu, HI, Dec. 2009, 6 pages.

C-3 N. Ehtiati and B. Champagne, "Comparative evaluation of the dual transform domain echo canceller for DMT-based systems," in *Proc. IEEE Int. Conf. on Acoustics, Speech, Signal Processing*, Dallas, TX, Mar. 2010, 4 pages.

C-4 N. Ehtiati and B. Champagne, "Dual domain echo cancellers for multirate discrete multitone systems," in *Proc. 44th Asilomar Conf. Signals, Systems and Computers*, Pacific Grove, CA, Nov. 2010, 5 pages.

1.5 Thesis Organization

An overview of various broadband access technologies with the main focus on the DSL systems is presented in Chapter 2, along with the background of the mathematical framework for the characterization of DMT signals and associated transceiver structure.

In Chapter 3, the above literature review is expanded and the existing methods for echo cancellation in DMT-based systems are reviewed. Some of these methods, such as time-domain LMS, circular echo synthesis, circulant decomposition and symmetric decomposition echo cancellers are studied in more detail. This review includes both

the symmetric and the multirate versions of these cancellers.

In Chapter 4, the linearly constrained adaptive echo cancellation is introduced. In particular, the proposed linearly constrained adaptive echo cancellation method is derived based on the mixed time- and frequency-domain echo cancellers. The proposed cancellers are examined with different set of constraints, including the addition of extra linear constraints to improve the robustness of the canceller in the presence of radio frequency interference.

In Chapter 5, the echo canceller design is examined in the dual domain. A general decomposition of the Toeplitz data matrix is assumed and, based on this general form, a two-step echo canceller design methodology in the dual domain is developed. Considering this design strategy, a new dual domain echo cancellation method is presented. In addition, the constrained echo cancellation is also considered in the dual domain. Later, by integrating these two algorithms, a new combined dual domain echo canceller is proposed, and its computational complexity and convergence behaviour are examined.

The methodology and results of computer simulation experiments are presented in Chapter 6 . Finally, concluding remarks are provided in Chapter 7. Some of the utilized linear algebra terminologies are reviewed in Appendix A, and some of the mathematical proofs related to analytical development are presented in Appendix B.

Chapter 2

DSL Systems Background

In this chapter, various broadband technologies are discussed with main focus on the DSL technology. In Section 2.1, different broadband access techniques are briefly reviewed, and the DSL history is presented in Section 2.2. The DSL physical medium is explained in Section 2.3, while the structure of DSL transmitters, receivers and the mathematical framework for DMT signals are discussed in Section 2.4. Finally, some recent advances in DSL technology are discussed in Section 2.5.

2.1 Broadband Access Technologies

From the early 1960's, when voiceband modems were first commercially introduced, providing data access on the regular telephone lines to residential customers[1], the call for higher data rates and better quality of service has grown tremendously. Over the years, the diversification of the in demand services, e.g., Internet browsing, voice over Internet Protocol (VoIP), remote collaboration, IPTV, *etc.* has resulted in the

[1]The first commercial modem, the Bell 103, was released by AT&T in 1962.

development of various broadband technologies, such as DSL, optical fiber, wireless access, coaxial cable modems and power line communications. The consideration of various factors, such as the cost of implementation, the existence of an infrastructure and the demand for particular services, has led to the emergence of a conglomerate of solutions combining different technologies rather than having a single dominant preference. In the following, we briefly discuss and compare these technologies.

Optical fiber

The high cost of the installation of fiber networks has been the main reason that the ideal scenario of having optical fiber connected to each customer premises has not been attained yet. However, intermediate solutions have been proposed, where the transmission path includes a combination of fiber with telephone lines or coaxial cables. In recent years, passive optical network (PON) over combined fiber has provided a reliable high bandwidth access [27].

Generally, the connection of the customers to the PSTN is established via the CO while, previously the customers were connected to the CO through telephone (copper) lines, in the PON structure, they are connected to an intermediary optical network unit (ONU) through copper lines, and multiple ONUs are connected to a single optical line terminal (OLT), located at the CO, through dedicated fibers using a passive optical splitter [28]. Accepted variants of PON are: gigabit PON (GPON), used mainly in US and Europe, and Ethernet PON (EPON), mostly used in Japan. Both technologies are classified as time-division multiplexing (TDM) PONs where the link to the OLT is accessed by different ONUs for the downstream and upstream transmission using TDM techniques [29].

The GPON technology provides up to 2.5 Gbps downstream and 1.2 Gbps upstream with split ratio (maximum number of ONUs connected to a single splitter) up to 1:64, while the EPON provides a symmetric 1 Gbps with split ratio 1:16 in range of 20 km [1]. A recent development in this field is the proposal of wavelength-division multiplexing (WDM) PONs. In this method, each ONU is assigned an individual wavelength, resulting in higher bandwidth being accessible to each ONU, where a combination of such methods can support split ratio up to 1:1000 [29].

Coaxial cable

Coaxial cable was traditionally used for broadcasting television channels; however starting in the 1990's, this medium is also being used for providing VoIP and broadband access. The main drawback of this technology is that most of the installed infrastructure for cable networks is unidirectional; therefore, there have to be some adjustments to allow a bidirectional transmission [3]. In recent years, a combination of optical fiber and coaxial cable known as hybrid fibre-coaxial (HFC), has been employed where the part of the transmission between the cable head-end and fiber nodes is done via optical fiber and the rest of the path to the customer premises is done via coaxial cable [30]. The transmission over HFC is standardized by data-over-cable service interface specification (DOCSIS), which makes it more accessible for various services and service providers [31].

Wireless broadband alternatives

Wireless broadband technologies originate either from fixed wireless networks such as wireless LAN or from mobile cellular communication systems. A recent technology

in the former category is Worldwide interoperability for Microwave Access (WiMAX) and in the latter is the 3rd Generation Partnership Project Long Term Evolution (3GPP LTE) [1]. WiMAX provides broadband access to fixed or mobile customers and is described in the family of 802.16 IEEE standards. This technology uses some advanced signal processing techniques such as OFDM modulation scheme, multiple-input multiple-output (MIMO) and smart antenna systems, providing rates up to 10 Mbps [32, 33]. 3GPP LTE is proposed as the next generation of cellular mobile communication standard following the 3GPP, providing downlink rates up to 100Mbps. This technology uses Evolved Packet Core (EPC) architecture with an all-IP network structure, where all services, such as data and voice are communicated through a packet switch domain. The EPC also facilities the handover to other services such as fixed lines or other wireless networks [34, 35].

Power line transmission

One of the fixed mediums that has gained momentum in recent years for broadband access is the existing network of power lines [36]. These lines have been used previously for the transmission of low data rate control signaling and automatic meter reading; however, the recent advances in VLSI and signal processing techniques have made the high rate data transmission over power lines more attainable [37]. In order to combat various noise sources in this medium and its frequency selective nature, multirate filter banks and wavelet techniques are used [36]. One of the advantages of transmitting over power lines is its accessibility, since its infrastructure exists even in most remote areas. Furthermore, some recent approaches even suggest using the wiring inside homes to form a LAN.

xDSL transmission

The term Digital Subscriber Line (DSL) refers to the broadband service provided over the copper telephone lines. This technology is discussed in detail in the remaining of this chapter. A comparison of deployment of xDSL versus the other described broadband technologies is given in Fig. 2.1, where it can be seen that xDSL systems are dominant with a 65% share of the market. In addition, in Table 2.1, the achievable rates and coverage of the mentioned broadband technologies are compared with various DSL standards, to be presented in the next section. As discussed earlier, the current trend is in technologies relying on the combination of fiber with copper lines or coaxial cables. Such infrastructures are used in recent standards for DSL systems such as very-high-bitrate DSL (VDSL).

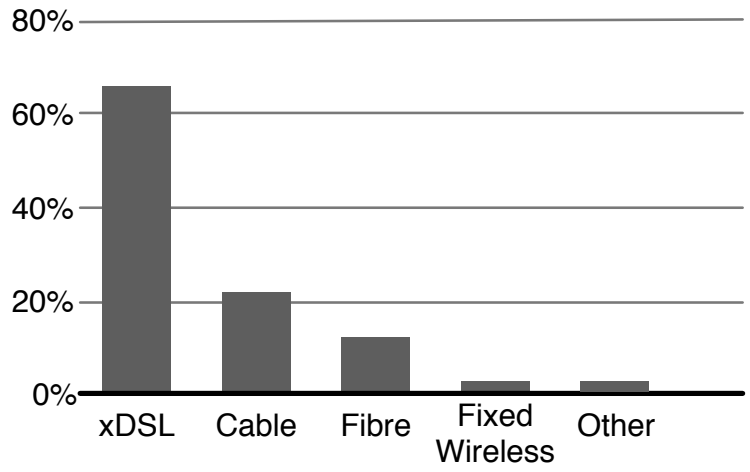

Fig. 2.1 Broadband deployment by technology in 2008 [1].

Table 2.1 Comparison of various broadband technologies [1].

Technology	Capacity	Maximum range
HFC	0.5 - 3 Mbps per user	up to 100km (using amplifiers)
Fiber	1Gbps per channel per fiber	20 km
WiMAX	10 Mbps	1 - 2 km
ADSL	1.5 - 12 Mbps	5.4 km
ADSL2+	12 - 24 Mbps	2.7 km
VDSL1	13 - 52 Mbps	1.3 km
VDSL2	52 - 100 Mbps	0.5 km

2.2 xDSL Technologies

Until recently, the transmission of data over the PSTN was done using voiceband modems, which could provide data rates up to 56 kbps. These modems transmit data over the frequency band used for voice call transmissions in analog form over an end-to-end PSTN connection. This situation changed dramatically with the introduction of DSL systems, where the digital data is sent on the local loop, between the user terminal and the CO, by exploiting the much wider bandwidth available on the wireline. In DSL systems, a DSL Access Multiplexer (DSLAM) is used at the CO to separate the data service from the telephone service and redirect them for transmission through their corresponding networks [2].

The earliest member of the DSL family of technologies is the Integrated Services Digital Network (ISDN) introduced in the mid 70's. This standard was mainly focused on offering voice communication and low-rate data transmission, accommodating symmetric rate of 160 kbps over 5.5 km distance [38]. In 1986, high bitrate DSL (HDSL) was introduced, providing 784 kbps over one twisted pair or higher rates such as 1.16 Mbps and 2.32 Mbps by using two or three twisted pairs [39]. Compared to T1/E1

lines which provide similar rates, HDSL was easier to implement since it did not require the removal of bridged taps and the use of repeaters; it also resulted in less destructive interference to other services [3]. The following generation of HDSL, called HDSL2, provided similar data rates over only a single twisted pair. This improvement was possible by using various signal processing techniques, such as trellis-coded modulation (TCM) error correcting codes [40]. In 1990, Symmetric DSL (SDSL) was introduced on a single twisted pair providing symmetric multirate services [41].

In the deployment of DSL services to residential customers, the asymmetrical services became more desirable, since for these applications the demand for downstream bandwidth is much higher than for the upstream one. In addition to different demands on each direction, the asynchronous use of spectrum admits of a theoretical justification. As discussed in [2], the received signal loss increases with the frequency and so does the received crosstalk noise[2]. Therefore, there is a frequency above which two-way transmission on the same band is not possible. Consequently, below this frequency limit, the spectrum can be assigned to both directions (full-duplex), while above this limit, it is assigned to either of directions depending on the demand.

The Asymmetric DSL (ADSL) was introduced in the late 1990's providing 12 Mbps in the downstream direction and up to 1.024 Mbps in the upstream direction [42]. In early implementations of ADSL, the voice and data transmissions were separated by a pair of lowpass and highpass filters known as splitter [3]. Installation of the splitter had to be done by a technician and sometimes, a second pair of wiring was needed at the customer premises, which was not desirable. These requirements were relaxed by the introduction of a variant of ADSL known as *splitterless* where, instead of

[2]For crosstalk definition see Section 2.3.3.

splitters, in-line lowpass filters need to be installed in series with each telephone at the customer premises, which often can be done by the customer him/herself [43]. Further enhancements to ADSL, providing higher data rates and better reach, are ADSL2 and ADSL2+ as addressed in [44]. In the downstream direction, ADSL2 can support up to 12 Mbps while ADSL2+ can support up to 24 Mbps; in the upstream direction, both standards can support up to 3.5Mbps.

Very-high-bitrate DSL (VDSL) is the latest main standard for DSL systems. VDSL is mainly focused on the hybrid optical/copper networks, where the ONUs are connected via fiber to the CO, and the length of the copper connection between ONU and the customer premises is usually less than 1 km. The VDSL1 standard can provide data rates between 13 to 26 Mbps symmetrically, or 52 Mbps downstream and 6.4 Mbps upstream when employed asymmetrically. The more recent VDSL2 standard can achieve symmetric rates up to 100 Mbps [3]. Since VDSL operates on shorter loops, it faces some issues specific to this setting. For example, the far-end side crosstalk (FEXT) becomes the dominant source of interference, as discussed later.

2.3 Twisted Pair Transmission

All the DSL standards discussed in the previous section are implemented on standard copper telephone lines. In this section, we therefore discuss the structure of the copper network, its characteristics and main impairments. The first telephone service introduced by Alexander Graham Bell in 1877 was implemented on single wire connection, using the ground as a return path. Later, the single wire was replaced by a pair of wires, for added reliability. In addition, it was recognized that twisting the two wires in a pair together decreases the crosstalk from external sources. The term

twisted-pair loop refers to the twisted-pair of copper wires between the CO and the customer, designed to provide a reliable and low-cost means for voice communications. However, the introduction of data services on these networks during the last 25 years changed this priority and eventually resulted in structural modifications. In recent years, optical fiber has been deployed farther and farther in the telephone networks, making high rate DSL services such as VDSL possible. In this work, our focus is on the *last mile*, which refers to the copper wire connection from the CO or ONU to the customer premises [3].

2.3.1 Loop plant structure

An all copper last mile configuration is depicted in Fig. 2.2. In this configuration, the CO is usually connected via high-speed data lines or optical fiber to the rest of the network. A CO can serve over 100,000 telephone lines, where they are grouped into feeder cables each including 1,500 to 4,000 lines [2]. At the CO, a main distribution frame (MDF) is used to physically connect each line from the feeder cable to the appropriate CO equipment cable. The other end of the feeder cables connect to serving area interfaces (SAI), which spread out to distribution cables each serving between 200 to 800 lines. An SAI can be a passive access-point or, as used recently, it can host a digital loop carrier (DLC), which is a digital multiplexer connected by T1-carrier lines or by fiber to the CO. Distribution cables lead to pedestals which serve between 4 to 12 lines, each connecting to a single customer.

In systems employing DLC, multiple lines from customers can be multiplexed and their signal transmitted on a single line, reducing the need for dedicated copper lines.

[3] It should be noted that mile is used literary and the actual distance can be more than that.

In addition, the DLC also decreases the length of the loop on the customer side, which is preferable in DSL transmissions. The data signals from the customers in DSL systems are transmitted to DSLAM, which separate the data from the voice services; DSLAM can be located in either the CO or the SAI.

As discussed earlier, the use of optical fibers in the telephone network is getting closer to the customer's side. As depicted in Fig. 2.3, the CO can be connected by fiber to an ONU while copper wires are used to connect the ONU to the customer premises.

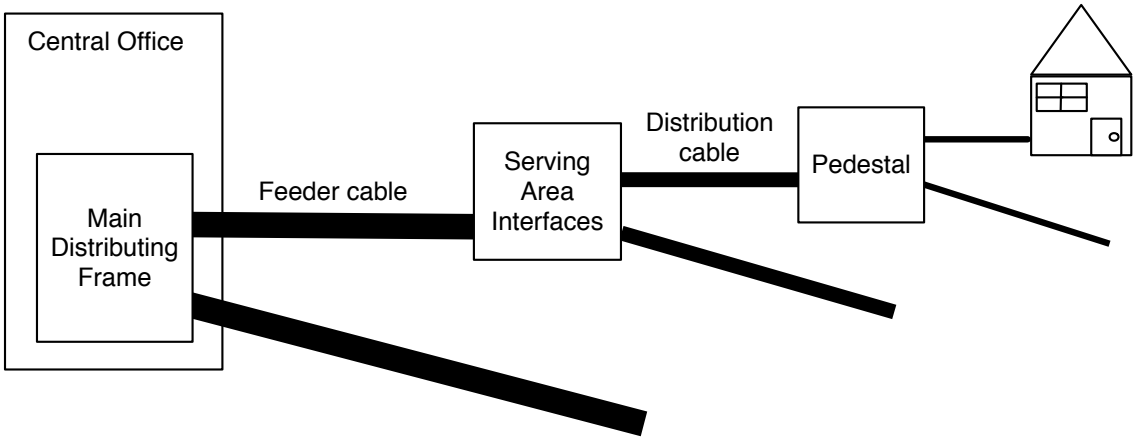

Fig. 2.2 All copper DSL system loop plant.

2.3.2 Characteristic of copper lines

The basic cable used in the copper part of the PSTN consists of a group of electrically insulated twisted-pairs in a shield, with the number of pairs typically equal to 25, 50 or 100. The wires used in the cable may have different diameters, and accordingly different impedances. In North America, twisted-pairs are defined by the American wire gauge (AWG), indicating their diameters, where the mostly used ones are AWG

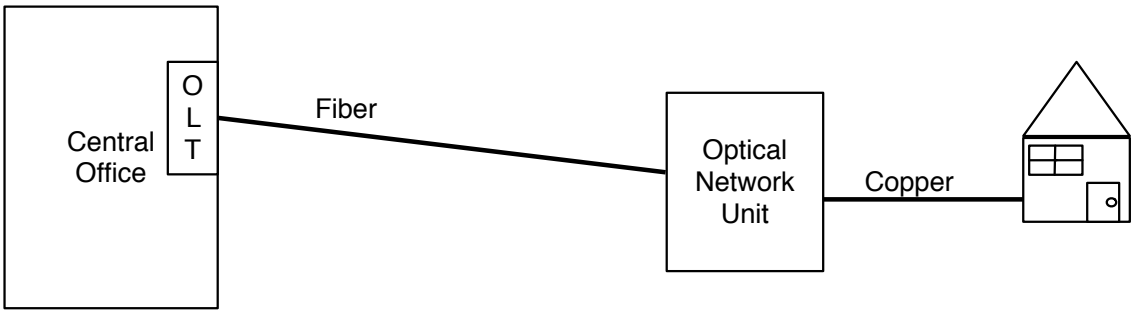

Fig. 2.3 Fiber-copper DSL system loop plant.

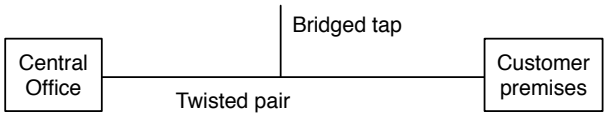

Fig. 2.4 A twisted pair with bridged tap.

19, 22, 24 and 26 [3].

The PSTN is designed to have the capability to accommodate fast connection to new customers, and therefore, there are many unterminated lines in the network. These open circuit lines, known as *bridged taps*, are foreseen for the future growth of the network, as depicted in Fig. 2.4. Bridge taps do not affect the telephony system, but have a degrading effect on DSL system performance as they result in spectral nulls and phase distortions [3].

Another common technique used in PSTN, which affects DSL signals, is that of loaded loops. In this technique, a series of inductors known as loading coils are placed at equal distances along the line to flatten the frequency response in the voice communication band. This method has such a drastic effect on DSL signals that DSL connections can not be achieved on loaded loops.

Knowing the cable structure between the CO and customer premises, the transfer

function and the impedance of the transmission path can be calculated using the standard ABCD modeling technique for two-port networks [45]. The primary parameters of line per unit length (including the series and shunt impedances) used in the ABCD model can be calculated based on the diameter of the wires; for derivation and more details we refer the reader to [45].

2.3.3 Crosstalk interference

One of the main sources of interference limiting the performance of DSL systems is crosstalk, which is the electromagnetic coupling between the twisted-pair of wires in a cable. There are two types of crosstalk, as shown in Fig. 2.5. One is near-end crosstalk (NEXT), which occurs when the transmitted signal on a pair couples back to another receiver close to the transmitting side. The other one is far-end crosstalk (FEXT), which is when the transmitted signal on a pair couples to another receiver close to the receiving side. In the DSL system, all the pairs in the cable can cause crosstalk on the desired signal transmitted through one pair, and it is highly dependent on the frequency. The NEXT power is proportional to $f^{3/2}$, where f denotes the frequency, and does not depend on the cable's length or attenuation. However, FEXT is proportional to f^2 and depends on the cable's length and transfer function [46]. Usually NEXT is more damaging than FEXT, because the FEXT signal is attenuated by the line transfer function. The power spectral density of various crosstalk sources affecting an ADSL transmission is shown in Fig. 2.6.

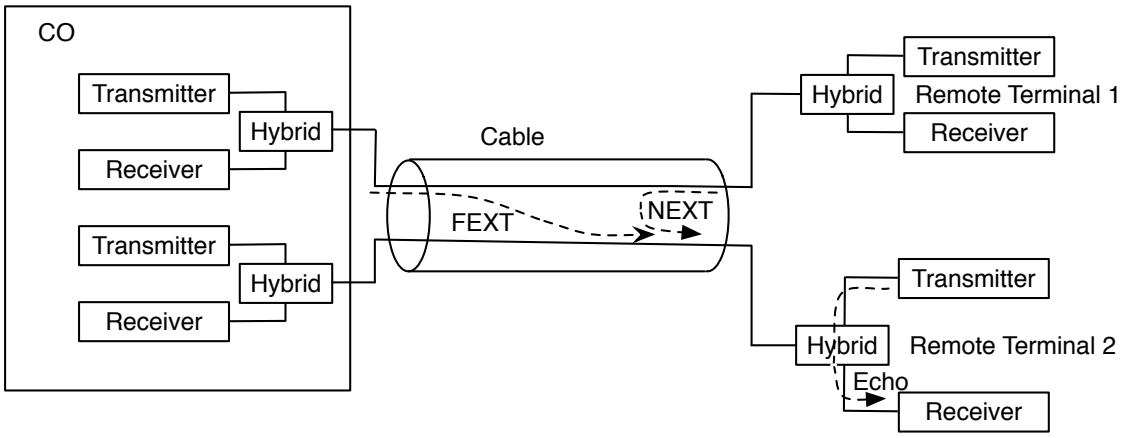

Fig. 2.5 Crosstalk, as seen by remote terminal 2.

2.3.4 Radio frequency noise

In DSL systems, twisted-pair lines, specially the aerial lines, act as an antenna for the radio frequency (RF) signals present in the environment, resulting in RF interference (RFI). Predominantly, this RF interference consists of the ingress from the AM radio broadcasts and amateur radio transmissions. The level of the ingress from both of these sources at the receiver can be higher than the level of the crosstalk and the background noise. The RF ingress can be modeled as narrowband interference compared to the bandwidth of the DSL signal. DSL systems that employ multitone modulation (discussed in the next section) are expected to be protected against such narrowband interference. However, because of the time windowing of the received signals the interference leak to neighbouring tones and can potentially affect several tones [3]. There are various techniques to suppress RFI in DSL systems; analog techniques are mostly concerned about the saturation effect in the analog-to-digital converter (ADC) of the

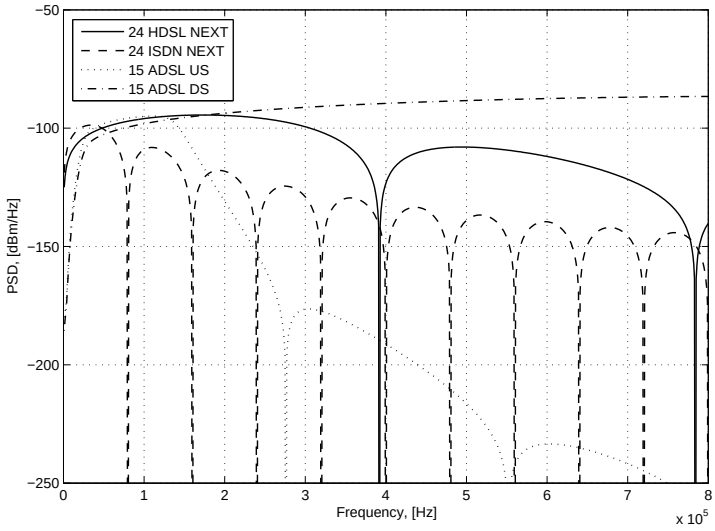

Fig. 2.6 Power spectral density of different crosstalk sources (the number indicated for each type of disturber denotes the number of disturber of that type).

modem in the analog front-end; digital techniques mostly attempt to cancel out these interference sources [3].

2.3.5 Hybrid circuitry

In DSL systems, the downstream and upstream data are sent over a single pair of wires. Therefore, a hybrid circuit is required to do the conversion from two-wire to four-wire network, as depicted in Fig. 2.5. The detailed structure of a hybrid circuitry is shown in Fig. 2.7; this structure is known as a bridge. Ideally, the signal must travel from the twisted-pair line into the receiver and from the transmitter into the line. However, there is always leakage of signals from the transmitter into the collocated receiver which is known as echo. One of the parameters controlling echo is the reference impedance Z_{ref} of the hybrid circuit. In particular, if this impedance

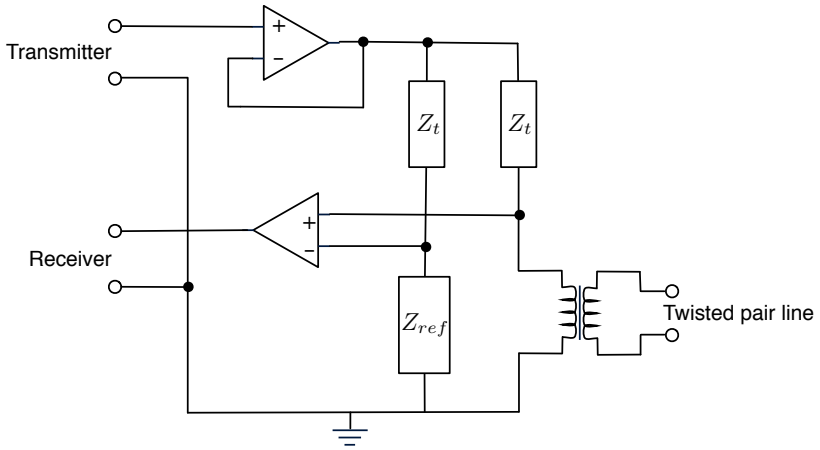

Fig. 2.7 Hybrid circuitry [2].

matches (is equal to) the line impedance there will be no echo. In practice, the lumped impedance as in the hybrid circuit can not match the distributed impedance of the line exactly and the maximum isolation yield by an analog hybrid circuit is 15-20 dB. It should be noted that the value of the transmit impedance Z_{t} needs to be equal to the conjugate of the line impedance in order to achieve maximum energy transfer.

2.4 DSL Transceiver Structure

The main focus of this thesis is on asymmetric multicarrier DSL systems, which is utilized in standards such as ADSL and VDSL. The term *asymmetric* is used to indicate that the bandwidths assigned for the upstream and the downstream are not equal, while *multicarrier* refers to the modulation used and is further discussed below. The overall structure of such a transceiver is shown in Fig. 2.8.

In this transceiver structure, the scrambler is used to randomize the transmitted data, which usually improves the performance of the adaptive components, e.g., equal-

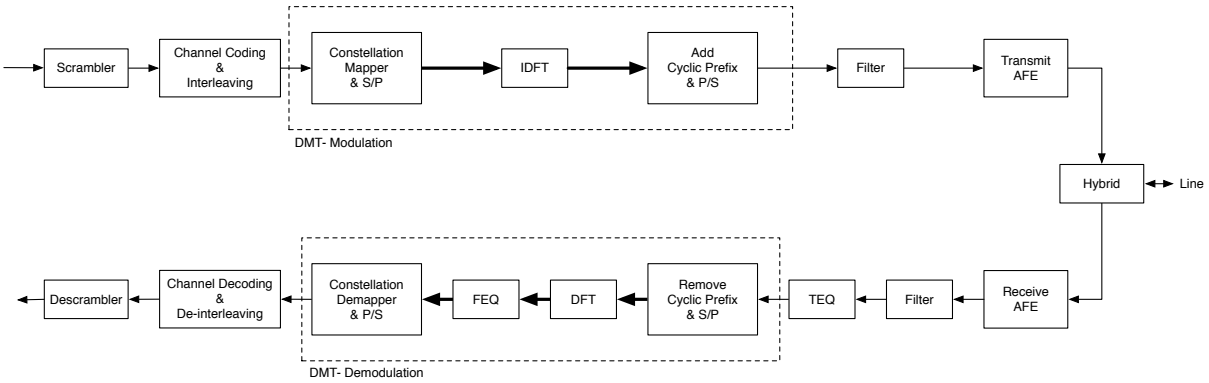

Fig. 2.8 DSL transceiver [3].

izers. Forward error correction (FEC), such as Reed-Solomon coding, makes the system more robust against channel errors [47]. The multicarrier modulation known as discrete multitone (DMT) is used to modulate the signal, which is described in detail in the next section. The transmit filter is used to comply with the power masks enforced by various DSL standards for controlling the interference on other services. The transmit analog front-end (AFE) serves as interface between the digital part and the analog part, performing digital-to-analog conversion with proper filtering. The bottom part, in Fig. 2.8, represents the receiver section, where all the operations performed in the transmitter is reversed.

2.4.1 Discrete multitone modulation

Multicarrier modulation is a widely used modulation scheme in wireless and wired communications systems, based on dividing the channel into orthogonal subchannels (or tones). This modulation is suitable for channels where severe ISI is present, since each subchannel has relatively flat fading, and therefore the ISI on each tone is small [9]. Multicarrier modulation also provides a convenient structure for utilizing

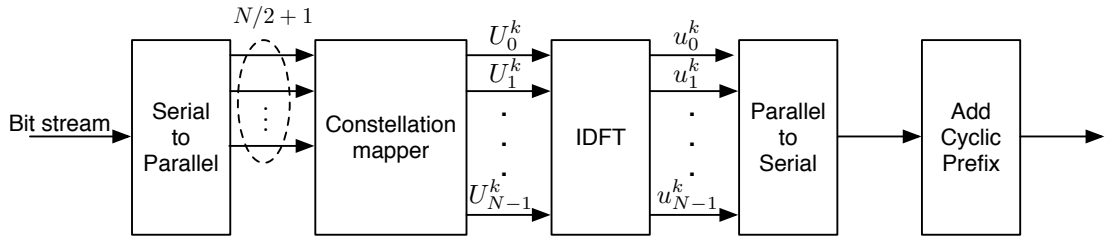

Fig. 2.9 DMT transmitter structure.

precoding and adaptive bit loading. These algorithms are often employed in DSL systems to allocate more power, bits or proper channel coding to individual subchannels based on their signal-to-noise ratio (SNR) [3].

In wired communication systems, a widely used form of multicarrier modulation well-suited to digital implementation is discrete multitone modulation (DMT), also known as orthogonal frequency division multiplexing (OFDM), in the context of wireless communication. This implementation, as discussed below, uses discrete Fourier transform (DFT) for signal modulation/demodulation and provides an ISI free transmission by appending a cyclic prefix.

The transmitter for a DMT modulated system is shown in Fig. 2.9. In this transmitter, the serial bit stream from the source is first divided into $N/2+1$ sub-streams (for reasons explained later, note that N is even), each sub-stream is then mapped into a M-ary quadrature amplitude modulation (QAM) constellation, e.g., 4-QAM. The resulting symbol U_n^k represents a tone or a subchannel, where k is the symbol period and n is the tone number. For baseband systems, such as DSL, in order to ensure that the modulated signal at the output of the IDFT is real valued, the symbols must have conjugate symmetry [2], i.e., $U_n^k = U_{N-n}^{k*}$ for $n = 1, \cdots, N/2-1$, $U_{N/2}^k$ is real and the term U_0^k, which corresponds to the DC value, is also set to zero .

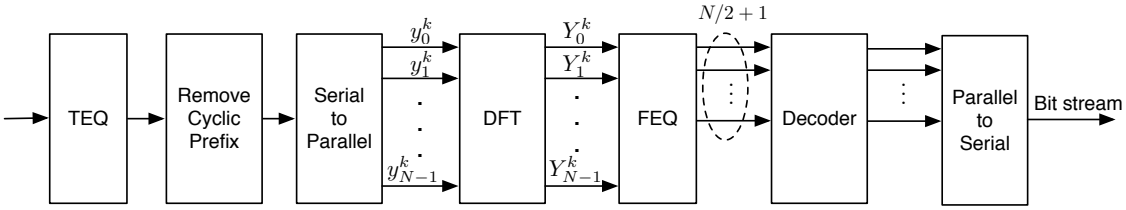

Fig. 2.10 DMT receiver structure.

Subsequently, the modulated time-domain signal, i.e., u_i^k for $i = 0, \cdots, N-1$, is obtained as the inverse discrete Fourier transform (IDFT) [48]:

$$u_i^k = \frac{1}{N} \sum_{n=0}^{N-1} U_n^k \; e^{j\,2\pi ni/N} \qquad i = 0, \cdots, N-1. \tag{2.1}$$

Following the IDFT and parallel to serial conversion of the output u_i^k, a guard period of υ samples is added to the beginning of each symbol. Referred to as cyclic prefix (CP), this guard period eliminates the ISI between the symbols, as explained below. Therefore, an output symbol has a length of $N + \upsilon$ and contains the cyclic prefix and the modulated symbol. The receiver of a DMT modulated system, is shown in Fig. 2.10, where the dual of each operation performed in the transmitter is applied in reversed order to recover the transmitted bit stream, with the additional time- and frequency-domain equalizations.

Specifically, after the time-domain equalizer (TEQ), the CP is removed and the symbol is demodulated using the DFT, i.e.,

$$Y_n^k = \sum_{i=0}^{N-1} y_i^k \; e^{-j2\pi ni/N} \qquad n = 0, \cdots, N-1 \tag{2.2}$$

where y_i^k, $i = 0, \cdots, N-1$ denotes the received time-domain samples of the k^{th}

symbol. As shown later, the effect of the channel can be removed by a per-tone frequency-domain equalizer (FEQ). Finally, an inverse mapping is applied to the FEQ output to recover the original bit stream.

In DMT, the υ samples of the CP added to each symbol are chosen to be the same as the last υ samples of the symbol. We denote the CP added symbol as $\tilde{\mathbf{u}}^k$, where[4]

$$\tilde{u}_i^k = \begin{cases} u_{N+i}^k & \text{for } -\upsilon \le i \le -1 \\ u_i^k & \text{for } 0 \le i \le N-1 \end{cases}$$

Let this symbol $\tilde{\mathbf{u}}^k$ be sent through a channel with finite impulse response, represented by vector $\mathbf{h} = [h_0, h_1, \cdots, h_{l_c}]$ of length $l_c \le \upsilon$, and denote the received signal *frame* as $\tilde{\mathbf{y}}^k = [y_{-\upsilon}^k, \cdots, y_{-1}^k, y_0^k, \cdots, y_{N-1}^k]$. Each entry of $\tilde{\mathbf{y}}^k$ results from the linear convolution of input samples from $[\tilde{\mathbf{u}}^{k-1}, \tilde{\mathbf{u}}^k]$ with $\mathbf{h}$. In particular,

$$y_i^k = \sum_{l=0}^{\upsilon-i} h_l\, \tilde{u}_{i-l}^k + \sum_{l=\upsilon-i+1}^{l_c} h_l\, \tilde{u}_{N+\upsilon-i-l}^{k-1}, \quad \text{for } -\upsilon \le i \le 0 \tag{2.3}$$

$$y_i^k = \sum_{l=0}^{l_c} h_l\, \tilde{u}_{i-l}^k, \qquad \text{for } 0 \le i \le N-1 \tag{2.4}$$

$$= \sum_{l=0}^{l_c} h_l\, u_{(i-l)_N}^k, \qquad \text{where } (n)_N \equiv \text{modulo } N \tag{2.5}$$

$$= h_i \otimes u_i \qquad \text{for } 0 \le i \le N-1 \tag{2.6}$$

where (2.5) follows from the CP concatenation, and in (2.6) $\otimes$ represents the circular convolution. In other words, the addition of the CP has transformed the linear convolution into a circular one. In practice, the samples y_i^k for $-\upsilon \le i \le 0$ are discarded at the receiver. It is therefore convenient to define the received signal *frame*

[4]We use the notation as in [9].

as $\mathbf{y}^k = [y_0^k, \cdots, y_{N-1}^k]$, in terms of which (2.6) can be written compactly as

$$\mathbf{y}^k = \mathbf{h}^k \otimes \mathbf{u}^k. \tag{2.7}$$

Both sides in (2.7) can be transformed by the N-point DFT, resulting into

$$\mathbf{Y}^k = \mathbf{U}^k \odot \mathbf{H} \tag{2.8}$$

where $\odot$ denotes component-wise multiplication, and $\mathbf{Y}^k$, $\mathbf{U}^k$ and $\mathbf{H}$ are the N-point DFT (i.e., frequency domain representation) of the received signal $\mathbf{y}^k$, the transmitted signal $\mathbf{u}^k$ and the channel $\mathbf{h}$, respectively. As shown in (2.8), the effect of the channel can now be removed using a per-tone FEQ, where for each tone

$$\hat{U}_n^k = Y_n^k / \hat{H}_n^k \qquad n = 0, \cdots, N-1 \tag{2.9}$$

where $\hat{H}_n^k$ is an estimate of the complex channel gain at tone n, and $\hat{U}_n^k$ is the corresponding equalized output. Removing the effect of the channel using (2.9) is possible provided that the length of the CP exceeds that of the channel impulse response. In practice, the channel impulse response can be quite long which requires adding a long CP and therefore increases the redundancy of the system. To avoid this problem, the length of the channel is reduced using a time-domain equalizer TEQ, as discussed previously. The DMT structure discussed above is used mainly in VDSL and ADSL systems with similar subcarrier spacing, which facilitates the compatibility between these two standards.

2.4.2 Duplexing methods and echo cancellation

In DSL systems, a bidirectional data transmission can be achieved either by having two pairs of wires between the transmitter and the receiver or by having a single pair and using a duplexing method. The former approach is only possible when an extra pair is available, which is mostly prohibitive. The common scenario is to implement a bidirectional transmission on a single pair where a duplexing technique such as time-division duplexing (TDD), frequency-division duplexing (FDD), digital duplexing and echo cancellation is employed. These techniques are briefly discussed below.

Time-division duplexing

In time-division duplexing, the transmitter on both sides transmit the data on non-overlapping time slots, resulting in reduced total achievable data rate. In this method, the echo is avoided and, in case of coordinated transmission from multiple users, NEXT is also prevented.

Frequency-division duplexing

In frequency-division duplexing, the available frequency bandwidth is divided into non-overlapping bands for the upstream and the downstream transmission. This method, like TDD, can avoid echo and NEXT, at the price of a reduction in data rate. It also requires precise analog filters for its implementation. The frequency band plan for ADSL is shown in Fig. 2.11.

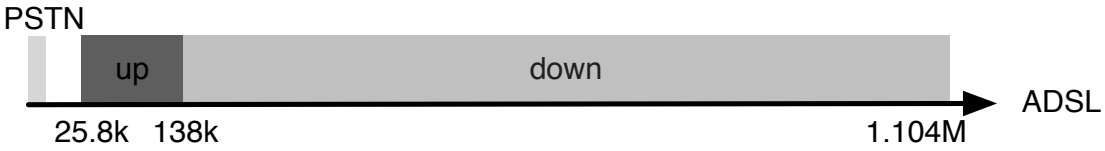

Fig. 2.11 Frequency band plan for ADSL [3] (k = kHz, M = MHz).

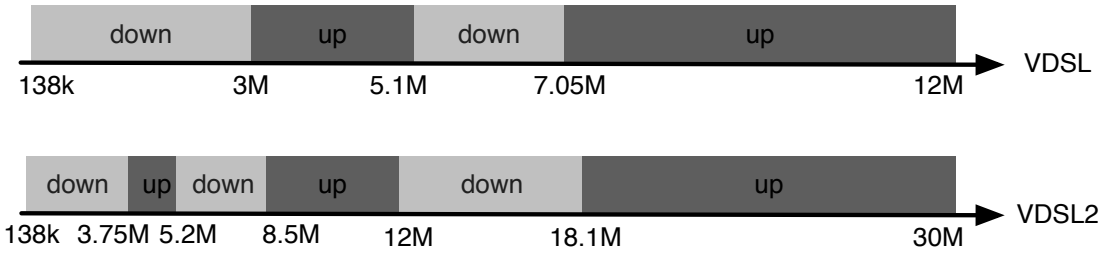

Fig. 2.12 Frequency band plan for VDSL and VDSL2 [3] (k = kHz, M = MHz).

Digital duplexing

In recent DSL systems, such as VDSL, several frequency band plans are available for dividing the frequency bandwidth between upstream and downstream, as shown in Fig. 2.12. In such systems, having FDD with fixed analog filters is prohibitive, and another duplexing method known as digital duplexing or *Zipper* is used, where subcarriers can be assigned in various ways to the upstream or downstream. The two directions are kept orthogonal to each other by proper alignment of the transmitted and received frames, and by adding cyclic suffix (CS), which is similar to a CP but added at the end of the symbol [5]. Zipper duplexing is used in systems designed for shorter loops, such as in VDSL1. On loops longer than 1 km, such as used in VDSL2 applications, the propagation delay of the line can not be compensated by the CS and other methods such as echo cancellation and TEQ must be used [6, 7].

Echo cancellation

In systems with echo cancellation, digital adaptive filters are used to estimate the echo and remove it from the transmitted signal [8]. In such systems, the requirements on the front-end filters can be relaxed and frequency overlap between downstream and upstream is allowed. In flexible duplexing methods such as Zipper, as discussed above, echo cancellation is also required in longer lines. More generally, at low frequencies, where NEXT is at the same level as FEXT, higher data rates can be achieved if the subcarriers can be used for both directions, which then requires the use of echo cancellers [5]. Echo cancellation option is considered for ADSL systems in [49] and some of the available chips with this capability are AD20msp930 by Analog Devices Inc., GEMINAX by Infineon Technologies AG, MB86670A by Fujitsu Microelectronics Europe and TA1080 by Tioga Technologies.

2.4.3 Bit loading and power allocation

In DMT-based systems, power allocation and bit distribution algorithms can be implemented very conveniently. These algorithms determine the number of the bits and the power allocated to each subchannel.

Based on the theory of capacity of AWGN channel, the number of bits loaded on the n^{th} subchannel, i.e., b_n, is given by:

$$b_n = \log_2(1 + \frac{\mathcal{E}_n\, g_n}{\Gamma\, \sigma_n^2}) \tag{2.10}$$

where $\mathcal{E}_n$ is the transmitted energy on this subchannel, g_n is the coding gain of the FEC, Γ is the Shannon gap, which depends on the constellation being used, received

noise variance and desired symbol error rate, and σ_n^2 is the noise power spectral density [2]. For a fixed total power system, the energy on each subchannel $\mathcal{E}_n$ can be derived based on the water-filling algorithm, which basically allocates more power to subchannels with higher SNRs. Using (2.10) and assuming that other parameters are known for each subchannel, the proper number of bits b_n allocated to the n^{th} subchannel can be derived. It should be noted that the values of b_n resulted from (2.10) are not necessary integer, there are algorithms to compute bit allocation for *integer* b_n values [50].

After the initial bit and power allocation, the receiver can monitor the SNRs of each subchannel: if the SNR on one of the subchannels drops below a certain threshold, bit swapping is performed. In this technique, a bit is swapped between the affected subchannel and a subchannel that can accommodate the additional bit, and the power on subchannels are decreased and increased respectively, to maintain the same noise margin [51].

2.5 Recent Advances in DSL Technology

In this chapter, we have discussed some of the available broadband wired-line technologies and studied the general medium and parameters of DSL transmission systems. Before embarking on the discussion of echo canceller design for DMT-based systems in the next chapter, we discuss, for completeness, some of the recent advances in the DSL communication area.

One of the major limitations of DSL systems is crosstalk interference from other services. Therefore, in recent years, spectrum management (SM), which studies the methods to control this interference, has received considerable attention. SM coordi-

nates the behaviour of DSL terminals in the loop to achieve the maximum capacity of the overall system, while maintaining a tolerable level of interference on the existing services. Several methods have been proposed based on, e.g., limiting the total power, forcing spectral masks, limiting power on specific frequencies, adjacency control, controlling the number of neighbouring pairs on one cable binder *etc.* [52].

Static SM, which is traditionally used in DSL systems, is based on operating under worst possible conditions. Therefore, the power masks required by these schemes are very conservative and in many cases prevent the transmission link from achieving its maximum data rate (without interfering with existing services). Therefore, in recent years Dynamic Spectrum Management (DSM) techniques have been developed, promising rates up to 500Mbps on a single twisted pair [53].

DSM can be achieved at various levels of coordination between the services sharing a cable binder. The introduction of new loop structures also facilitates achieving these levels of coordination. For example, in VDSL, the presence of the ONU at a very short distance from customers can act as a single entity to co-ordinate transmission on the loop plant [54]. In so-called Level-0 of DSM, the power and rate allocation is performed autonomously, using water-filling technique as discussed earlier [55, 56]. In a Level-1 of DSM, the DSL modems use iterative water filling for allocating power, where different users try to achieve maximum rate while controlling the crosstalk on other users. As shown in [57, 58], the rates achieved by this technique are very close to the ones achieved by optimal rate and power allocation. In DSM Level-2, it is assumed that the binder information is known and the optimization is performed over the binder [59]. This level of coordination usually referred to as *spectrum balancing* is discussed in various works, e.g., [60, 59, 61]. Spectrum balancing is mostly used

in cases where there is a high level of crosstalk interference, such as the crosstalk of shorter lines on longer lines. It is also possible to perform the DSM Level-2 on a per band basis, in which coordination is maintained across a group of adjacent tones [62]. The highest level of DSM, Level-3, mostly known as *vectored DSL* or multiple-input multiple-output DSL *(MIMO-DSL)*, is presented in [54, 63, 64]. In this method the spectrum maintenance centre has control over the transmission and reception of signals sent over coordinated multiple DSL lines. The interference in the downstream is eliminated via precoding technique while in the upstream, it is eliminated by successive cancellation [64].

The latest innovation in DSL technology, known as *binder DSL* or *Gigabit DSL*, is discussed in [53, 65, 66, 67]. In this technology, the differential-mode vectoring [54], is transformed into common-mode vectoring, where the transmitted signal is measured with respect to a common ground. The common-mode vectoring doubles the degrees of freedom of the system, which can be used to achieve gigabit services.

Chapter 3

Echo Cancellation in DMT-based Systems

In this chapter, we review the existing methods for echo cancellation in DMT-based systems. In Section 3.1, a brief overview of the existing literature on this topic is given. In the Sections 3.2 - 3.5, some of these methods are studied in more detail, specifically: time-domain synthesis, circular echo synthesis, circulant decomposition and symmetric decomposition echo cancellers. This review includes both the symmetric and the multirate version of these cancellers. Finally, some other methods of asynchronous and double talk echo cancellers are presented in Section 3.6.

3.1 Overview of Echo Cancellation Methods for DMT-based Systems

As discussed earlier, in high-rate data transmission over twisted-pair loops, a hybrid circuit is used to connect the 4-wire part of the network to the 2-wire circuitry. Vari-

ous methods have been discussed in the literature for cancelling echo in these systems using adaptive echo cancellers, e.g., [68, 69, 70, 71, 72]. In DSL systems based on the DMT modulation, the direct time-domain implementation of the basic echo canceller is characterized by high computational cost; however, this can be improved by exploiting the structure present in the transmitted signal. The work in [14], by Cioffi and Bingham is one of the early works in this field, where a mixed time- and frequency-domain echo canceller is proposed. In this data-driven echo canceller, the echo emulation is performed in the time domain (including the cross-tones echo emulation) and the echo weights are updated independently in the frequency domain, resulting in lower complexity of the echo canceller.

Later, in [15], Ho *et al.* proposed the circular echo synthesis (CES) method, where the circular part of the echo is also emulated and cancelled efficiently in the frequency domain and only the residual echo is cancelled in the time domain. This canceller also performs a per tone weight update entirely in the frequency domain, which further reduces its complexity. However, not all the tones are used (excited) in DMT-based systems, because of certain power masks requirements or due to the bit allocation algorithm. As a result, this method suffers from slow convergence since the filter weights corresponding to the unused tones remain unchanged after the weight update step. To improve the convergence, transmission of dummy data with reduced power on the unused tones is proposed in [15]. However, as shown in [16], this approach generates extra interference demanding a more complex equalizer at the receiver; it also requires higher order front-end filters to comply with the power mask [4]. Some of the practical aspects of CES echo canceller is discussed in [73], and a faster training procedure is presented in [74].

To overcome the convergence issues of the CES canceller, other methods have been proposed in the literature. In [17], Ysebaert *et al.* suggested the circulant decomposition canceller (CDC). In this method, similar to the CES canceller, the echo is emulated jointly in the time and frequency domains; however, the tap-input vector used for the weight update usually has sufficient excitation on all tones. Later, in [18], Pisoni and Bonaventura extended and modified this echo canceller by using discrete cosine and sine transformations. Eventually, in [19], Pisoni *et al.* introduced a canceller similar to the self-orthogonalizing filter, where the singular value decomposition (SVD) of the data correlation matrix, which is derived in [75], is used to speed up the slow-modes of adaptation.

Other methods for echo cancellation in DMT-based systems propose modifications to the CES canceller in order to lower its complexity and/or improve its performance. For instance in [20], Jones has shown that the proper choice of the delay between the transmitted and received symbols can help to reduce the complexity of the system. In [21], Ysebaert *et al.* have added double talk cancellation to the receiver, i.e., removing the effect of the far-end signal to improve the convergence of the adaptive weight update. In [22], they have also proposed an asynchronous echo canceller (integrated with double talk cancellation), which is used when there is a misalignment between the transmitted symbols and received symbols. Double talk cancellation for CES canceller is also discussed in [76].

There are other methods for echo cancellation, which perform both the echo emulation and weight update in the frequency domain, such as in [23, 24, 77]. In [23], Bogucka and Wesolowski considered the effect of both the intersymbol interference or interblock interference and the intercarrier interference separately. Their proposed

approach requires a higher order IFFT in the canceller than in the transmitter that results in increased complexity but improves the adaptation rate of the canceller. A per-tone frequency-domain echo canceller and equalizer for DMT-based systems is discussed in [24, 78] by Van Acker *et al.* In this structure, the design objective function is optimized for each tone separately, resulting in an improved convergence at the expense of increased complexity, similar to the method in [23].

The above methods mostly rely on one FIR filter to model the echo channel, which requires several hundred of taps since usually the echo impulse response has a long tail. The complexity of the system can be reduced by certain methods that combine the use of two filters to model the echo channel. In [79], Kwon *et al.* proposed an echo canceller based on the cascade of a lattice and orthogonalized IIR filter, each modeling the fast changing head and the slow dying tail of the impulse response of the echo channel, respectively. In [80], Lin and Wu examined an echo canceller based on the FIR- interpolated FIR structure, presented in [81]. This structure also achieves reduced complexity by cascading two FIR filters each modeling the head and the tail of the echo channel separately. In the following sections, some of these methods are studied in more detail, specifically: the time-domain, circular echo synthesis, circulant decomposition and symmetric decomposition echo cancellers are discussed.

3.2 Time-Domain Echo Canceller

Consider a symmetric DMT transceiver, as shown in Fig. 3.1, where the common length of the modulating IDFT and demodulating DFT is denoted by N and a cyclic prefix of size v is added to each symbol frame. The true echo channel, which includes the effect of the transmitter and receiver front-end filters, hybrid circuitry and the

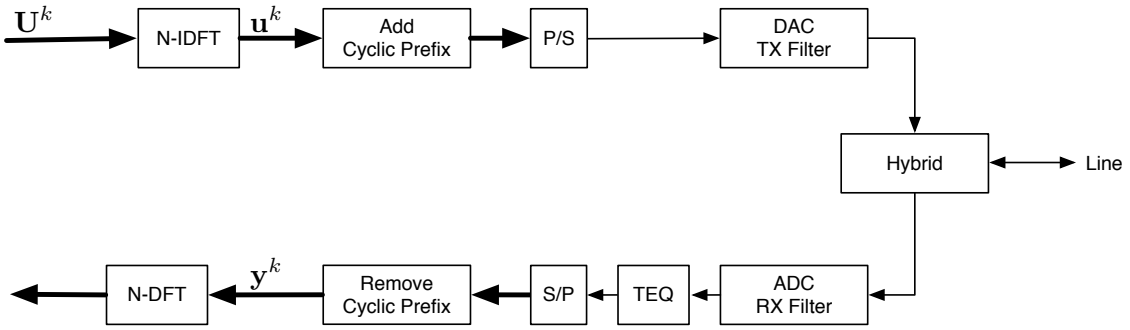

Fig. 3.1 DMT transceiver block diagram

time-domain equalizer (TEQ), is assumed to be linear and time-invariant. It is represented by its vector of impulse response coefficients $\mathbf{h} = [h_0, h_1, \cdots, h_l, 0, \cdots, 0]^T$ of length N, where zero-padding is used. The received signal, containing the far-end signal, additive noise and echo at symbol period k is given by

$$\mathbf{y}^k = [y_0^k, y_1^k, \cdots, y_{N-1}^k]^T = \mathbf{y}_e^k + \mathbf{n}^k \tag{3.1}$$

where $\mathbf{y}_e^k$ is the echo signal and $\mathbf{n}^k$ contains the far-end signal and noise.

The echo frame can be either synchronized with the far-end frame or asynchronous, where there is a delay of Δ samples between the echo and far-end frames (both positive and negative values of Δ are possible). As can be seen from Fig. 3.2(a), in the synchronous case, the echo signal affecting the received signal at period k is generated by the transmitted frames at period $k-1$ and k while in the asynchronous case, it is generated by the transmitted frame at periods $k-1$, k and $k+1$.

The echo signal is generated by the linear convolution of the echo channel with the time-domain samples of the echo reference symbols. Using a matrix representation,

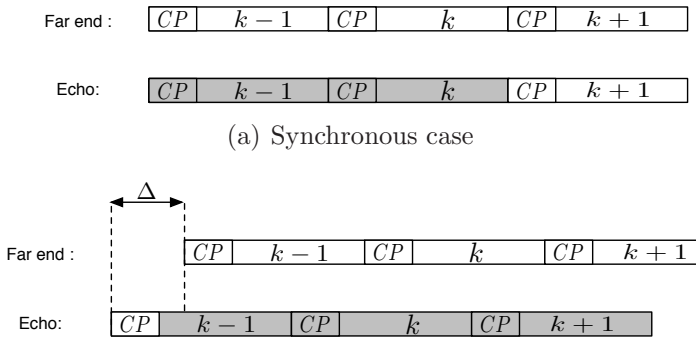

Fig. 3.2 Frame synchronization between the echo reference symbols and far-end symbols (the figure is from [4]). Echo frames that may affect the k^{th} far-end frame are shown shaded.

this can be expressed as

$$\mathbf{y}_e^k = \mathcal{U}^k \, \mathbf{h} \tag{3.2}$$

where $\mathcal{U}^k$ is an $N \times N$ Toeplitz matrix consisting of elements from symbols, $\mathbf{u}^{k-1}$ and $\mathbf{u}^k$ for synchronous scenario, or $\mathbf{u}^{k-1}$, $\mathbf{u}^k$ and $\mathbf{u}^{k+1}$ for asynchronous scenario. In this thesis, we define $\mathcal{U}^k$ for a general asynchronous case with delay Δ samples, where the synchronous case follows with $\Delta = 0$.

Hence, taking into account the nature of the cyclic prefix and the temporal rela-

tionship between the far-end and echo frames in Fig. 3.2(b), $\mathcal{U}^k$ is defined as

$$\mathcal{U}^k \triangleq \begin{bmatrix} u_{\Delta}^{k} & \cdots & u_{0}^{k} & u_{N-1}^{k} & \cdots & u_{N-\upsilon}^{k} & u_{N-1}^{k-1} & \cdots & u_{\Delta+\upsilon+1}^{k-1} \\ \vdots & \ddots & & & & & & \ddots & \vdots \\ u_{N-1}^{k} & & & & & & & & u_{N-1}^{k-1} \\ u_{N-\upsilon}^{k+1} & & & & & & & & u_{N-\upsilon}^{k} \\ \vdots & & & & & & & & \vdots \\ u_{N-1}^{k+1} & & & & & & & & u_{N-1}^{k} \\ u_{0}^{k+1} & & & & & & & & u_{0}^{k} \\ \vdots & \ddots & & & & & & \ddots & \vdots \\ u_{\Delta-\upsilon-1}^{k+1} & \cdots & u_{0}^{k+1} & u_{N-1}^{k+1} & \cdots & u_{N-\upsilon}^{k+1} & u_{N-1}^{k} & \cdots & u_{\Delta}^{k} \end{bmatrix}. \tag{3.3}$$

Note that because of the (time-invariant) FIR filtering structure in our model, matrix $\mathcal{U}^k$ is Toeplitz and it is completely defined by the specification of its entries along the first column and the first row. Since the true echo channel $\mathbf{h}$ is unknown, the echo canceller has to model and estimate the parameters of the echo channel. In practice, the echo channel is modeled by means of an FIR filter, with weight vector $\mathbf{w}^k$ of size T_e. Hence, a finite impulse response of the length T_e is assumed with $T_e \leq N$, and zero-padding is used.

The emulated echo can be calculated using the estimate of the echo channel,

$$\hat{\mathbf{y}}_e^k = \mathcal{U}^k \, \mathbf{M} \, \mathbf{w}^k \tag{3.4}$$

where the $N \times T_e$ matrix $\mathbf{M} \triangleq [\mathcal{I}_{T_e} | \mathcal{O}_{T_e \times (N-T_e)}]^T$ is used to pad $\mathbf{w}^k$ with zeros. The emulated echo (3.4) can be subtracted from the received signal, resulting in an error

signal vector expressed by

$$\mathbf{e}^k = \mathbf{y}^k - \mathcal{U}^k \, \mathbf{M} \, \mathbf{w}^k. \tag{3.5}$$

The error signal can now be used to update the echo weights, using one of various adaptive filtering methods in the class of interference cancellation, where the received signal serves as the desired response for the adaptive filter [8]. For time-domain echo cancellers, the block least mean square (LMS) method [8] is used, where the weights are updated every symbol time k by

$$\mathbf{w}^{k+1} = \mathbf{w}^k + \mu \, \mathbf{M}^T \, (\mathcal{U}^k)^T \, \mathbf{e}^k, \tag{3.6}$$

where the step-size parameter $\mu > 0$ controls the convergence behaviour. A small value of μ results in accurate estimate of the channel coefficients but slower convergence, while increasing μ speeds up initial convergence at the price of a larger estimation error. Ultimately, if μ is too large the adaptive estimator diverges [8].

The matrix multiplications in (3.4) and (3.6) are computationally expensive. Therefore, this method is usually avoided in practice and, as shown later, other methods with lower complexity are used. However, we present this method here as a baseline for comparison of the convergence and computational complexity of various methods for echo cancellation.

3.3 Circular Echo Synthesis Echo Canceller

The implementation of the echo canceller in the time domain, as discussed earlier, is computationally prohibitive, especially at high sampling rates. In [14], Cioffi and Bingham introduced the idea of implementing the echo canceller partially in the time

domain and partially in the frequency domain. In their proposed data-driven echo canceller, the linear convolution (3.2) is transformed into a circular convolution by employing tail cancellation and cyclic reconstruction. This transformation paved the way for performing the echo weight update on a per tone basis in the frequency domain, with reduced complexity.

In [15], Ho *et al.* improved this method further, where in addition to weight update, most of the echo emulation is also performed in the frequency domain with reduced complexity. As pointed out earlier, the data matrix $\mathcal{U}^k$ (3.3) in the linear convolution (3.4) is a Toeplitz matrix. The ideal case is to have a circulant matrix, representing a circular convolution, which in the frequency domain translates into the multiplication of the Fourier transform of the input vector and the Fourier transform of the echo weights (per tone multiplication). However, when the length of the echo channel exceeds that of the cyclic prefix (i.e., $T_e > \upsilon$), which is usually the case, or when the synchronization delay $\Delta \neq 0$, some cross echoes are caused from adjacent symbols to the k^{th} echo reference symbol. In this case, the non-circulant nature of the matrix $\mathcal{U}^k$ (3.3) needs to be taken into consideration.

In the following subsections, the circular echo synthesis canceller presented in [15] is reviewed, where the Toeplitz matrix $\mathcal{U}^k$ is decomposed into a sum of a circulant and a residual components. We begin with the case of symmetric rates and then extend the discussion to the multirate scenario.

3.3.1 Symmetric rate circular echo synthesis canceller

In [15], Ho *et al.* introduced the circular echo synthesis (CES) canceller, where the Toeplitz matrix $\mathcal{U}^k$ (3.3) is decomposed as a sum:

$$\mathcal{U}^k = \underbrace{\mathcal{X}^k}_{\text{residual part}} + \underbrace{\mathcal{L}^k}_{\text{circulant part}} . \tag{3.7}$$

Here $\mathcal{L}^k$ is a circulant matrix containing the samples from the near-end transmitted signal at the k^{th} period, i.e.,

$$\mathcal{L}^k \triangleq \begin{bmatrix} u_{\Delta}^k & \cdots & u_0^k & u_{N-1}^k & \cdots & u_{\Delta+1}^k \\ \vdots & \ddots & & & \ddots & \vdots \\ u_{N-1}^k & & & & & u_{N-1}^k \\ u_0^k & & & & & u_0^k \\ \vdots & \ddots & & & \ddots & \vdots \\ u_{\Delta-1}^k & \cdots & u_0^k & u_{N-1}^k & \cdots & u_{\Delta}^k \end{bmatrix} . \tag{3.8}$$

The matrix $\mathcal{X}^k$, which is the residual component, is simply given by

$$\mathcal{X}^k \triangleq \mathcal{U}^k - \mathcal{L}^k. \tag{3.9}$$

Matrix $\mathcal{X}^k$ is usually *sparse* with two triangles of non-zero entries at the upper-left and lower-right corners; which take into account the cross echoes from symbols $k-1$ and $k+1$ instead of just the k^{th} symbol [1]. Now, the circulant matrix $\mathcal{L}^k$ can be

[1] Our formulation for the asynchronous case is slightly different from the one given in [15]; for more details see [4].

diagonalized using the DFT and IDFT matrices [82], as given by

$$\mathcal{L}^k = \mathcal{F}_N^{-1} \, \mathrm{diag}\{\mathbf{\Lambda}^k\} \, \mathcal{F}_N \tag{3.10}$$

where the vector $\mathbf{\Lambda}^k$ is obtained as the normalized Fourier transform of the first column of $\mathcal{L}^k$, and $\mathcal{F}_N$ is the $N \times N$ DFT matrix with entries $\mathcal{F}_N(k,l) = \frac{1}{\sqrt{N}} e^{-j2\pi kl/N}$ and $\mathcal{F}_N^{-1} = \mathcal{F}_N^H$. Since the first column of $\mathcal{L}^k$ contains only samples from symbol k, the vector $\mathbf{\Lambda}^k$ is the frequency-domain symbol $\mathbf{U}^k$ corrected with a phase rotation vector to compensate for the misalignment Δ, i.e.,

$$\mathbf{\Lambda}^k = \mathbf{U}^k \odot \mathbf{p}, \tag{3.11}$$

where $\mathbf{p} = [1, \cdots, e^{j2\pi\Delta i/N}, \cdots, e^{j2\pi\Delta(N-1)/N}]^T$, and $\odot$ denotes the component-wise multiplication [2]. Therefore, the echo emulation can be done partially in the time domain to cancel the cross echoes and partially in the frequency domain to cancel the circulant part.

Let $\mathbf{W}^k$ denote the frequency-domain weight vector at time k, which is going to be updated adaptively. The associated time-domain weight vector is given by

$$\mathbf{w}^k = \mathbf{M}^T \, \mathcal{F}_N^{-1} \, \mathbf{W}^k, \tag{3.12}$$

which is derived from $\mathbf{W}^k$ by means of IDFT and shortening to the length T_e. The

[2]The IDFT relationship in (2.1) is based on the standard definition of the DFT [48]. If the normalized DFT with $1/\sqrt{N}$ is used instead, the right-hand side of (3.11) must be scaled by an appropriate factor.

exact representation of the echo estimate in the frequency domain is

$$\begin{aligned} \hat{\mathbf{Y}}_e^k &= \mathcal{F}_N\, \hat{\mathbf{y}}_e^k \\ &= \mathcal{F}_N\, (\mathcal{U}^k\, \mathbf{M}\, \mathbf{w}^k) \\ &= \mathcal{F}_N \mathcal{X}^k\, \mathbf{M}\, \mathbf{w}^k + \mathcal{F}_N \mathcal{L}^k\, \mathbf{M}\, \mathbf{w}^k \\ &= \mathcal{F}_N(\mathcal{X}^k\, \mathbf{M}\, \mathbf{w}^k) + \mathbf{\Lambda}^k\ \odot\ (\mathcal{F}_N\, \mathbf{M}\, \mathbf{w}^k) \end{aligned} \tag{3.13}$$

In [15], this is approximated by

$$\mathbf{E}^k = \mathcal{F}_N(\mathbf{y}^k\ -\ \mathcal{X}^k\, \mathbf{M}\, \mathbf{w}^k) - \mathbf{\Lambda}^k\ \odot\ \mathbf{W}^k. \tag{3.14}$$

Since the residual matrix $\mathcal{X}^k$ is sparse, the computational complexity of the echo emulation is reduced significantly compared to the time-domain canceller.

The complete LMS update in the frequency domain for this canceller based on the error signal in (3.14) is given by

$$\mathbf{W}^{k+1} \quad = \quad \mathbf{W}^k\ +\ \mu\, \mathcal{F}_N\, \mathbf{M}\, \mathbf{M}^T\, (\mathcal{X}^k)^T\, \mathcal{F}_N^{-1}\, \mathbf{E}^k\ +\ \mu\, (\mathbf{\Lambda}^k)^*\ \odot\ \mathbf{E}^k \tag{3.15}$$

with μ denoting the step-size. In [15], (3.15) is approximated by a per tone update of $\mathbf{W}^k$, given by

$$\mathbf{W}^{k+1} = \mathbf{W}^k\ +\ \mu\, (\mathbf{\Lambda}^k)^*\ \odot\ \mathbf{E}^k. \tag{3.16}$$

Finally, the time-domain weights used in the emulation part can be calculated using (3.12), which can be performed infrequently. The main steps of the resulting algorithm are illustrated in Fig. 3.3

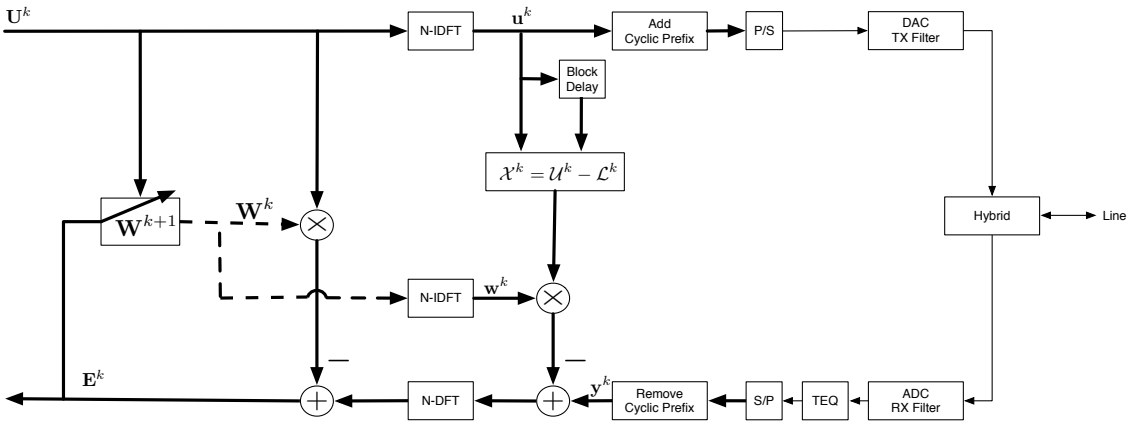

Fig. 3.3 Symmetric rate CES-based Echo Canceller

From (3.16), it is easy to see that if any element of $\mathbf{\Lambda}^k$ is equal to zero, the corresponding frequency-domain weight is not updated. This lack of excitation happens actually often in DSL systems, since tones are divided between upstream and downstream and also, power mask or bit allocation algorithms may require that some of the tones remain unused. To compensate this insufficient excitation, Cioffi and Bingham, in [14], proposed to send dummy data with reduced power on the unused tones. However, this solution is not desirable because of the extra interference it generates.

3.3.2 Multirate circular echo synthesis canceller

So far, we have assumed similar sampling rates at the transmitter and the receiver. In practical DSL systems, different sampling rates are used for the downstream and the upstream. Therefore, in the case of equal symbol rate in both directions, more samples are received at the remote terminal (RT) where higher data rates are required than at the central office (CO). Consequently, echo cancellers are modified to function in the multirate set-up by using data interpolation at the RT side and decimation at

the CO side. These modifications are explained below for the multitone CES echo canceller given in [15].

Interpolated echo canceller

At the RT transceiver, the transmitted signal data rate is κ times smaller than that of the received signal. Hence, because of the non-ideal reconstruction filter at the DAC, the higher frequencies of the transmitted signal leak into the received signal. This aliasing is modeled by the interpolation of the transmitted signal, which in the time domain corresponds to padding $\kappa - 1$ zeros between adjacent samples before the convolution with the FIR echo weights $\mathbf{w}^k$. Thus, the error signal in (3.14) is modified as follows:

$$\mathbf{E}^k = \mathcal{F}_{\kappa N}\left(\mathbf{y}^k \; - \; \mathcal{X}^k_{\text{int}}\,\mathbf{M}\,\mathbf{w}^k\right) \; - \; (\mathbf{R}\,\mathbf{\Lambda}^k) \; \odot \; \mathbf{W}^k \tag{3.17}$$

where the $\kappa N \times \kappa N$ matrix $\mathcal{X}^k_{\text{int}}$ is defined as in the previous section with the difference that here, it is constructed from the interpolated (i.e., zero-padded) data. In the frequency domain, the interpolation is performed by the use of a matrix $\mathbf{R}$ which is the vertical concatenation of κ identity matrices of order N, i.e., $\mathbf{R} = [\mathcal{I}_N|\cdots|\mathcal{I}_N]^T$. Note that in (3.17), the DFT matrix is of size κN, the weight vector $\mathbf{W}^k$ is of length κN and the zero-padding matrix $\mathbf{M} \triangleq [\mathcal{I}_{T_e}|\mathcal{O}_{T_e\times(\kappa N - T_e)}]^T$. It should be noted that the length T_e weight vector $\mathbf{w}^k$ in the time domain is based on the higher data rate. The echo channel weight is subsequently updated by

$$\mathbf{W}^{k+1} = \mathbf{W}^k + \mu\,(\mathbf{R}\,(\mathbf{\Lambda}^k)^*) \; \odot \; \mathbf{E}^k. \tag{3.18}$$

Decimated echo canceller

At the CO transceiver, the transmitted signal bandwidth is κ times larger than that of the received signal and aliasing occurs because of the non-ideal anti-aliasing filter at the ADC. In order to model the effect of this aliasing in the echo canceller, the time-domain portion of the synthesized echo signal is decimated, i.e., downsampled by a factor of κ. The effect of aliasing in the frequency-domain portion of the echo is reproduced via a block and add operation, i.e., pre-multiplication by $\mathbf{R}^T$. Thus, the error signal is given by

$$\mathbf{E}^k = \mathcal{F}_N \left(\mathbf{y}^k - \mathcal{X}^k_{\text{dec}} \, \mathbf{M} \, \mathbf{w}^k \right) - \frac{1}{\kappa} \mathbf{R}^T \left(\mathbf{\Lambda}^k \odot \mathbf{W}^k \right) \tag{3.19}$$

where the $N \times \kappa N$ matrix $\mathcal{X}^k_{\text{dec}}$ contains the decimated data in the time domain. Note that in (3.19), the weight vector $\mathbf{W}^k$ is of length κN and the zero-padding matrix $\mathbf{M}$ is defined as above. For this canceller, the weights are updated via

$$\mathbf{W}^{k+1} = \mathbf{W}^k + \mu \, (\mathbf{\Lambda}^k)^* \; \odot \; (\mathbf{R} \, \mathbf{E}^k). \tag{3.20}$$

where matrix $\mathbf{R}$ is used to replicate the error vector $\mathbf{E}^k$ (an operation equivalent to the time-domain upsampling).

3.4 Circulant Decomposition Echo Canceller

As discussed earlier, the CES canceller has a low implementation complexity, but in order to achieve an acceptable convergence rate, it requires the transmission of dummy data with reduced power on the unused tones. This approach results in

several undesirable effects, e.g., increase of the transmit power and extra interference. To overcome the extra interference caused by dummy data near the edges of the front-end transmit filter, a more complex equalizer at the receiver is required along with a high order front-end receiver filter, which in turn makes the echo channel longer [4].

In [17], Ysebaert *et al.* introduce the circulant decomposition canceller (CDC), which does not require the transmission of dummy data. In this canceller, the data Toeplitz matrix $\mathcal{U}^k$ is decomposed as a sum of a circulant and skew-circulant matrices. Similar to the CES canceller, the echo is emulated mixed in the time and frequency domains; however, the tap-input vector used in the weight update step usually has sufficient excitation on all tones. The main features of the CDC method are reviewed below for both the symmetric and multirate cases.

3.4.1 Symmetric rate circulant decomposition echo canceller

The time-domain linear convolution involved in the echo emulation step (3.4) can be performed by means of a $2N$-point circular convolution and using the overlap-save procedure. As shown in [83], using this procedure the estimated echo is given by

$$\hat{\mathbf{y}}_e^k = \left[\begin{array}{c|c} \mathcal{I}_N & \mathcal{O}_N \end{array}\right] \underbrace{\left[\begin{array}{c|c} \mathcal{U}^k & \mathcal{V}^k \\ \hline \mathcal{V}^k & \mathcal{U}^k \end{array}\right]}_{\tilde{\mathcal{L}}^k} \left[\begin{array}{c} \mathbf{M}\,\mathbf{w}^k \\ \hline \mathcal{O}_N \end{array}\right] \tag{3.21}$$

where $\tilde{\mathcal{L}}^k$ is a $2N \times 2N$ circulant matrix, and the $N \times N$ Toeplitz matrix $\mathcal{V}^k$ is constructed in the following way:

$$\mathcal{V}^k \triangleq \begin{bmatrix} u_{\Delta+\upsilon}^{k-1} & u_{\Delta-\upsilon-2}^{k+1} & \cdots & u_0^{k+1} & u_{N-1}^{k+1} & \cdots & u_{N-\upsilon}^{k+1} & u_{N-1}^{k} & \cdots & u_{\Delta+1}^{k} \\ \vdots & \ddots & & & & & & & \ddots & \vdots \\ u_{N-1}^{k-1} & & & & & & & & & u_{N-1}^{k} \\ u_{N-\upsilon}^{k} & & & & & & & & & u_{N-\upsilon}^{k+1} \\ \vdots & & & & & & & & & \vdots \\ u_{N-1}^{k} & & & & & & & & & u_{N-1}^{k+1} \\ u_0^k & & & & & & & & & u_0^{k+1} \\ \vdots & \ddots & & & & & & & \ddots & \vdots \\ u_{\Delta-1}^{k} & \cdots & u_0^k & u_{N-1}^{k} & \cdots & \cdots & u_{N-\upsilon}^{k} & u_{N-1}^{k-1} & \cdots & u_{\upsilon+\Delta}^{k-1} \end{bmatrix}. \quad (3.22)$$

It can be seen that all the elements of the matrix $\mathcal{V}^k$ are determined from the matrix $\mathcal{U}^k$ except for the element on the main diagonal which in this case, it is chosen to be equal to $u_{\upsilon+\Delta}^{k-1}$ [4]. The circulant matrix $\tilde{\mathcal{L}}^k$ can now be diagonalized using a $2N$-point Fourier transform, as expressed by

$$\tilde{\mathcal{L}}^k = \mathcal{F}_{2N}^{-1} \, \mathrm{diag}\{\tilde{\mathbf{\Lambda}}^k\} \, \mathcal{F}_{2N} \quad (3.23)$$

where the diagonal elements $\tilde{\mathbf{\Lambda}}^k$ are obtained as the Fourier transform of the first column of the matrix $\tilde{\mathcal{L}}^k$.

Using (3.21) and (3.23), the Toeplitz matrix $\mathcal{U}^k$ can be written as (for more details see [4])

$$\mathcal{U}^k = \frac{1}{2} \mathcal{F}_N^{-1} \, \mathrm{diag}\{\tilde{\mathbf{\Lambda}}_{\mathrm{even}}^k\} \, \mathcal{F}_N \; + \; \frac{1}{2} \mathbf{Q}^H \mathcal{F}_N^{-1} \, \mathrm{diag}\{\tilde{\mathbf{\Lambda}}_{\mathrm{odd}}^k\} \, \mathcal{F}_N \, \mathbf{Q} \quad (3.24)$$

where $\tilde{\mathbf{\Lambda}}^k_{\text{even}}$ and $\tilde{\mathbf{\Lambda}}^k_{\text{odd}}$ are obtained from the even and odd numbered elements of $\tilde{\mathbf{\Lambda}}^k$, respectively, and $\mathbf{Q} = \text{diag}\{[1, \cdots, e^{-j\pi(i-1)/N}, \cdots, e^{-j\pi(N-1)/N}]^T\}$. Consequently, the emulated echo is given by

$$\hat{\mathbf{y}}^k_e = \frac{1}{2}\,\mathcal{F}_N^{-1}\,\text{diag}\{\tilde{\mathbf{\Lambda}}^k_{\text{even}}\}\,\mathcal{F}_N\,\mathbf{M}\,\mathbf{w}^k \;+\; \frac{1}{2}\,\mathbf{Q}^H\,\mathcal{F}_N^{-1}\,\text{diag}\{\tilde{\mathbf{\Lambda}}^k_{\text{odd}}\}\,\mathcal{F}_N\,\mathbf{Q}\,\mathbf{M}\,\mathbf{w}^k. \tag{3.25}$$

It should be noted that in this method, the Toeplitz matrix $\mathcal{U}^k$ is basically decomposed as the sum of a circulant and a skew-circulant matrix[3], i.e.,

$$\mathcal{U}^k = \frac{1}{2}\overbrace{(\mathcal{U}^k + \mathcal{V}^k)}^{\text{circulant part}} + \frac{1}{2}\overbrace{(\mathcal{U}^k - \mathcal{V}^k)}^{\text{skew-circulant part}} \tag{3.26}$$

where matrices $\mathcal{U}^k$ and $\mathcal{V}^k$ are as defined above. In [4], Ysebaert *et al.* showed that the two terms in (3.24) are indeed the diagonalization of the circulant and skew-circulant components of the matrix $\mathcal{U}^k$, and the diagonal elements for these transformations are obtained from the diagonalization of the matrix $\tilde{\mathcal{L}}^k$.

Using the same approach as in the CES canceller, the echo emulation is performed partially in the time domain and partially in the frequency domain. Therefore, the error signal for this canceller in the frequency domain is given by

$$\mathbf{E}^k = \mathcal{F}_N\left(\mathbf{y}^k - \frac{1}{2}\mathbf{Q}^H\,\mathcal{F}_N^{-1}\,(\tilde{\mathbf{\Lambda}}^k_{\text{odd}} \odot \breve{\mathbf{W}}^k)\right) \;-\; \frac{1}{2}\tilde{\mathbf{\Lambda}}^k_{\text{even}} \;\odot\; \mathbf{W}^k \tag{3.27}$$

where $\mathbf{W}^k = \mathcal{F}_N\,\mathbf{M}\,\mathbf{w}^k$ is the echo weight vector in the frequency domain, and $\breve{\mathbf{W}}^k = \mathcal{F}_N\,\mathbf{Q}\,\mathbf{M}\,\mathbf{w}^k$. The block LMS method can be used to update the weight vector in the

[3] A matrix is skew-circulant if and only if it is both circulant and skew-symmetric, can consult Appendix A for more details

frequency domain. As shown in [4], the complete update of $\mathbf{W}^k$ is given by

$$\begin{aligned}\mathbf{W}^{k+1} &= \mathbf{W}^k + \mu\,\mathcal{F}_N\,\mathbf{M}\,\mathbf{M}^T\,\mathcal{F}_N^{-1}\,\mathrm{diag}\{(\tilde{\mathbf{\Lambda}}^k_{\mathrm{even}})^*\}\,\mathbf{E}^k \\ &+ \mu\,\mathcal{F}_N\,\mathbf{M}\,\mathbf{M}^T\,\mathbf{Q}^H\,\mathcal{F}_N^{-1}\,\mathrm{diag}\{(\tilde{\mathbf{\Lambda}}^k_{\mathrm{odd}})^*\}\,\mathcal{F}_N\,\mathbf{Q}\,\mathbf{e}^k \qquad (3.28)\end{aligned}$$

where $\mathbf{e}^k = \mathcal{F}_N^{-1}\,\mathbf{E}^k$. Using a similar approximation to the one used in the CES canceller, the per tone update can be expressed as

$$\mathbf{W}^{k+1} = \mathbf{W}^k + \mu\,\mathcal{F}_N\,\mathbf{M}\,\mathbf{M}^T\,\mathcal{F}_N^{-1}\,((\tilde{\mathbf{\Lambda}}^k_{\mathrm{even}})^* \odot \mathbf{E}^k) \qquad (3.29)$$

where the term $\mathcal{F}_N\,\mathbf{M}\,\mathbf{M}^T\,\mathcal{F}_N^{-1}$ is a gradient constraint to ensure that the time-domain weight vector $\mathbf{w}^k$ has only T_e non-zero taps. As shown in [17], the update can be simplified with an acceptable loss of performance, as

$$\mathbf{W}^{k+1} = \mathbf{W}^k + \mu\,(\tilde{\mathbf{\Lambda}}^k_{\mathrm{even}})^* \odot \mathbf{E}^k, \qquad (3.30)$$

and $\breve{\mathbf{W}}^{k+1}$ can be updated infrequently, given by

$$\breve{\mathbf{W}}^{k+1} = \mathcal{F}_N\,\mathbf{Q}\,\mathbf{M}\,\mathbf{M}^T\,\mathcal{F}_N^{-1}\,\mathbf{W}^{k+1}. \qquad (3.31)$$

The structure for the CDC algorithm is illustrated in Fig. 3.4.

The convergence of the CDC method does not require the transmission of dummy data as in the CES canceller, due to the fact that the proposed tap-input vector in (3.30), i.e., $\tilde{\mathbf{\Lambda}}^k_{\mathrm{even}}$, does not have zero elements generally. Indeed, the elements of $\tilde{\mathbf{\Lambda}}^k_{\mathrm{even}}$ are obtained as the N-point DFT of the first column of the matrix sum $\mathcal{U}^k + \mathcal{V}^k$. It can be verified that if the first column of any of these matrices contains

entries from more than one symbol, $\tilde{\mathbf{\Lambda}}^k_{\text{even}}$ will not have zero elements on the unused tones. However, for the special case $\Delta = -\upsilon$, the above condition is not satisfied, and therefore $\tilde{\mathbf{\Lambda}}^k_{\text{even}}$ will have zero entries on the unused tones. Accordingly, a slight modification in the delay definition is suggested in [17] to solve this deficiency.

3.4.2 Multirate circulant decomposition echo canceller

As discussed earlier, in practice the downstream and upstream directions have different sampling rates. Therefore, any practical echo canceller has to be implemented for multirate cases also. In [4], Ysebaert showed that decimated and interpolated echo cancellers can be designed either by using a method like the one used previously for the CES canceller, or by using polyphase decomposition. In the following, we briefly discuss the multirate CDC echo canceller based on the polyphase decomposition.

Interpolated echo canceller

Using (3.21), the interpolated echo estimate is given by

$$\hat{\mathbf{y}}^k_e = [\mathcal{I}_{\kappa N} \mid \mathcal{O}_{\kappa N}]\ \tilde{\mathcal{L}}^k_{\text{int}}\ \tilde{\mathbf{w}}^k \tag{3.32}$$

where

$$\tilde{\mathbf{w}}^k \triangleq \left[\begin{array}{c} \mathbf{M}\,\mathbf{w}^k \\ \hline \mathcal{O}_{\kappa N\times 1} \end{array}\right] \tag{3.33}$$

and the $2\kappa N \times 2\kappa N$ matrix $\tilde{\mathcal{L}}^k_{\text{int}}$ is the interpolated circulant matrix generated from upsampled input data based on (3.21), and the $\kappa N \times T_e$ matrix $\mathbf{M} \triangleq [\mathcal{I}_{T_e} | \mathcal{O}_{T_e\times(\kappa N - T_e)}]^T$. Note that as in Section 3.3.2, T_e is chosen based on higher rate. The $2N \times 2N$ submatrices of $\tilde{\mathcal{L}}^k_{\text{int}}$ given by $\tilde{\mathcal{L}}^k_{\text{int}}[l : \kappa : 2\kappa N\ ,\ l : \kappa : 2\kappa N]$ for $l = 1 \cdots \kappa$ are all circulant and

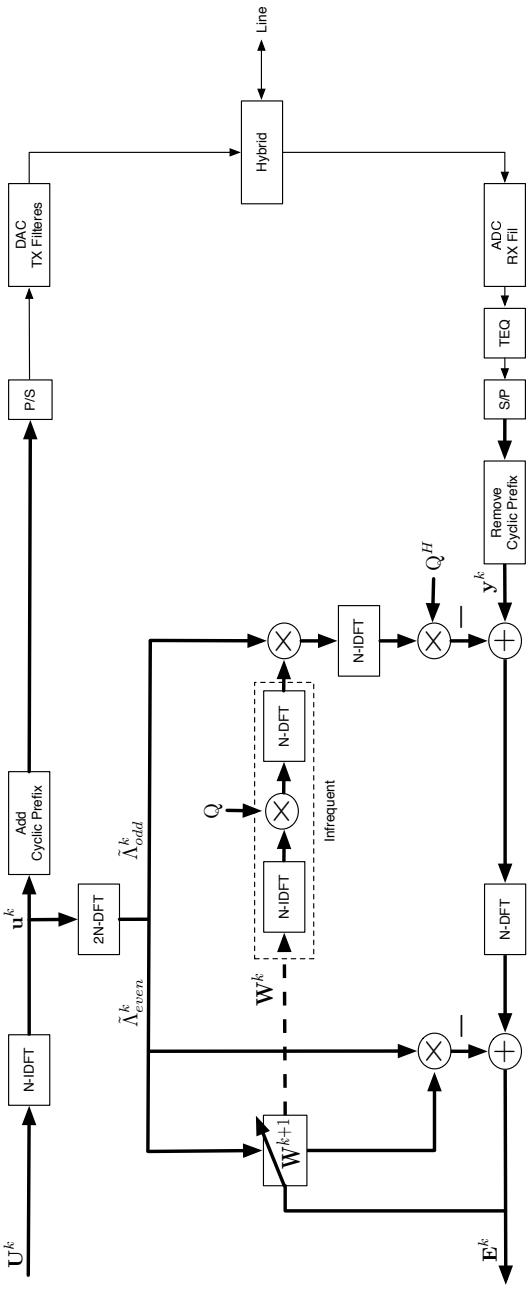

Fig. 3.4 Symmetric rate CDC Echo Canceller

equal to $\tilde{\mathcal{L}}^k$, which is the circulant matrix generated by low rate input data before the interpolation, as defined in Section 3.4.1. The vector $\tilde{\mathbf{w}}^k$ can be decomposed in its polyphase components, i.e., $\tilde{\mathbf{w}}_l^k = \tilde{\mathbf{w}}^k[l : \kappa : 2\kappa N]$ for $l = 1 \cdots \kappa$. Using this polyphase decomposition, the emulated echo is expressed as

$$\hat{\mathbf{y}}_e^k = \sum_{l=1}^{\kappa} [\mathcal{I}_{\kappa N} | \mathcal{O}_{\kappa N}] \, \mathbf{D}_{2\kappa N,l} \, \tilde{\mathcal{L}}^k \, \tilde{\mathbf{w}}_l^k \tag{3.34}$$

where $\mathbf{D}_{2\kappa N,l} \triangleq \mathcal{I}_{2\kappa N}[:\ ,\ l : \kappa : 2\kappa N]$. Using this notation, the error signal for the interpolated echo canceller can be expressed

$$\mathbf{E}^k = \mathcal{F}_{\kappa N} \left(\mathbf{y}^k - \frac{1}{2} \sum_{l=1}^{\kappa} \mathbf{D}_{\kappa N,l} \mathbf{Q}^H \, \mathcal{F}_N^{-1} \, (\tilde{\mathbf{\Lambda}}_{\text{odd}}^k \odot \breve{\mathbf{W}}_l^k) \right) \, - \, \frac{1}{2} (\mathbf{R} \tilde{\mathbf{\Lambda}}_{\text{even}}^k) \, \odot \, \mathbf{W}^k \tag{3.35}$$

where $\breve{\mathbf{W}}_l^k = \mathcal{F}_N \, \mathbf{Q} \tilde{\mathbf{w}}_l^k$, $\mathbf{W}^k = \mathcal{F} \tilde{\mathbf{w}}^k$, $\mathbf{R}$ is defined in Section 3.3.2 and $\tilde{\mathbf{\Lambda}}_{\text{even}}^k$ and $\tilde{\mathbf{\Lambda}}_{\text{odd}}^k$ are obtained as before form the diagonalization of $\tilde{\mathcal{L}}^k$. In deriving (3.35), the identity $[\mathcal{I}_{\kappa N} \mid \mathcal{O}_{\kappa N}] \mathbf{D}_{2\kappa N,l} = \mathbf{D}_{\kappa N,l} [\mathcal{I}_N \mid \mathcal{O}_N]$ has been employed. The approximate weight update corresponding to (3.30) is given by

$$\mathbf{W}^{k+1} = \mathbf{W}^k \, + \, \mu \left(\mathbf{R} (\tilde{\mathbf{\Lambda}}_{\text{even}}^k)^* \right) \, \odot \, \mathbf{E}^k. \tag{3.36}$$

Finally, $\breve{\mathbf{W}}_l^k$ is updated infrequently by

$$\breve{\mathbf{W}}_l^k = \mathcal{F}_N \, \mathbf{Q} \tilde{\mathbf{w}}_l^k. \tag{3.37}$$

Decimated echo canceller

Using (3.21), the decimated version of the emulated echo is given by

$$\begin{aligned}\hat{\mathbf{y}}_e^k &= [\mathcal{I}_N \mid \mathcal{O}_{\kappa N}] \left[\begin{array}{c|c} \mathbf{D}\mathcal{U}^k & \mathbf{D}\mathcal{V}^k \\ \hline \mathbf{D}\mathcal{V}^k & \mathbf{D}\mathcal{U}^k \end{array}\right] \left[\begin{array}{c} \mathbf{M}\,\mathbf{w}^k \\ \hline \mathcal{O}_N \end{array}\right] \\ &= [\mathcal{I}_N \mid \mathcal{O}_{\kappa N}]\, \tilde{\mathcal{L}}_{\text{dec}}^k \tilde{\mathbf{w}}^k \end{aligned} \tag{3.38}$$

where the decimation matrix $\mathbf{D} \triangleq \mathcal{I}_{\kappa N}[1:\kappa:\kappa N,:]$, and matrices $\mathcal{U}^k$ and $\mathcal{V}^k$ contain the high rate data. It can be seen that for the circulant matrix $\tilde{\mathcal{L}}_{\text{dec}}^k$, every submatrix given by $\tilde{\mathcal{L}}_{\text{dec},l}^k \triangleq \tilde{\mathcal{L}}_{\text{dec}}^k[:,\ l:\kappa:2\kappa N]$ for $l = 1 \cdots \kappa$ is circulant and can be diagonalized individually. Therefore, by using the polyphase decomposition of $\tilde{\mathbf{w}}^k$ as in the previous sub-section, the emulated echo is expressed as

$$\hat{\mathbf{y}}_e^k = [\mathcal{I}_N \mid \mathcal{O}_N] \sum_{l=1}^{\kappa} \tilde{\mathcal{L}}_{\text{dec},l}^k \tilde{\mathbf{w}}_l^k, \tag{3.39}$$

and the error signal for the decimated CDC canceller is given by

$$\mathbf{E}^k = \mathcal{F}_N \left(\mathbf{y}^k - \frac{1}{2}\mathbf{Q}^H \mathcal{F}_N^{-1} \left(\sum_{l=1}^{\kappa} \tilde{\mathbf{\Lambda}}_{\text{odd},l}^k \odot \breve{\mathbf{W}}_l^k \right) \right) - \frac{1}{2} \left(\sum_{l=1}^{\kappa} \tilde{\mathbf{\Lambda}}_{\text{even},l}^k \odot \mathbf{W}_l^k \right) \tag{3.40}$$

where $\breve{\mathbf{W}}_l^k = \mathcal{F}_N\, \mathbf{Q}\tilde{\mathbf{w}}_l^k$, $\mathbf{W}^k = \mathcal{F}_N\, \tilde{\mathbf{w}}_l^k$ and $\tilde{\mathbf{\Lambda}}_{\text{odd},l}^k$ and $\tilde{\mathbf{\Lambda}}_{\text{even},l}^k$ are the odd and even entries of the diagonal matrix $\tilde{\mathbf{\Lambda}}_l^k$ that results from the diagonalization of the submatrix $\tilde{\mathcal{L}}_{\text{dec},l}^k$. The echo canceller weight vectors are then updated as

$$\mathbf{W}_l^{k+1} = \mathbf{W}_l^k \ + \ \mu\, (\tilde{\mathbf{\Lambda}}_{\text{even},l}^k)^* \ \odot \ \mathbf{E}^k \tag{3.41}$$

where $\mathbf{W}_l^k = \mathcal{F}_N \, \tilde{\mathbf{w}}_l^k$. The updated values of $\mathbf{W}_l^k$ can be used to update $\breve{\mathbf{W}}_l^k$ infrequently.

This method, which requires the application of κ times of $2N-$point DFT's for calculating the matrices $\tilde{\mathbf{\Lambda}}_l^k$'s, is less complex than direct downsampling of the emulated echo after being calculated at the high rate, which would instead require one $2\kappa N$-points DFT.

3.5 Symmetric Decomposition Echo Canceller

In [18], Pisoni and Bonaventura proposed a symmetric decomposition canceller (SDC), which provides a reduced complexity implementation of the CDC algorithm. The symmetric decomposition of the Toeplitz matrix $\mathcal{U}^k$ (3.3) used in this method is based on [84], where Potts and Steidl presented the optimal trigonometric preconditioners for nonsymmetric Toeplitz systems. They proved that any combination (addition or subtraction) of a symmetric Toeplitz matrix with a persymmetric Hankel matrix (or anti-symmetric Toeplitz with anti-persymmetric Hankel matrix) can be transformed into either a diagonal matrix or a matrix with non-zero elements only on either sub-diagonal or super-diagonal using discrete trigonometric transformations[4].

It is known that the sum of a Toeplitz matrix with its conjugate transpose results in a symmetric Toeplitz matrix while their difference results in an anti-symmetric Toeplitz matrix, i.e.,

$$\begin{aligned} 2\,\mathcal{U}^k &= \underbrace{(\mathcal{U}^k + (\mathcal{U}^k)^H)}_{\text{Symmetric Toeplitz}} + \underbrace{(\mathcal{U}^k - (\mathcal{U}^k)^H)}_{\text{anti-symmetric Toeplitz}} \\ &= \mathcal{T}_S^k - \mathcal{T}_A^k \end{aligned} \tag{3.42}$$

[4]Reader may consult Appendix A for a brief review of the matrix terminology used here.

where $\mathcal{T}_S^k$ is a symmetric Toeplitz matrix with its first row given by the vector $\mathbf{a}^k$, with i$^{\text{th}}$ entry $\mathbf{a}^k(i) = \mathcal{U}^k(0,i) + (\mathcal{U}^k(i,0))^*$ for $i = 0, \cdots, N-1$, and $\mathcal{T}_A^k$ is an anti-symmetric Toeplitz matrix with its first row given by the vector $\mathbf{b}^k$, with $\mathbf{b}^k(i) = \mathcal{U}^k(0,i) - (\mathcal{U}^k(i,0))^*$ for $i = 0, \cdots, N-1$. In order to obtain the desired symmetric decomposition in [84], the authors add to and subtract from (3.42) a persymmetric Hankel matrix $\mathcal{H}_S^k$ with its first row given as $[\mathbf{a}^k(i), \cdots, \mathbf{a}^k(N-1), 0]$ and an anti-persymmetric Hankel matrix $\mathcal{H}_A^k$ with first row $[\mathbf{b}^k(1), \cdots, \mathbf{b}^k(N-1), 0]$.

Therefore, the original Toeplitz matrix $\mathcal{U}^k$ can be rewritten as a combination of the above matrices, i.e.,

$$\begin{aligned} 2\,\mathcal{U}^k &= \frac{1}{2}(\mathcal{T}_S^k + \mathcal{H}_S^k) + \frac{1}{2}(\mathcal{T}_S^k - \mathcal{H}_S^k) \\ &\quad - \frac{1}{2}(\mathcal{T}_A^k + \mathcal{H}_A^k) - \frac{1}{2}(\mathcal{T}_A^k - \mathcal{H}_A^k). \end{aligned} \tag{3.43}$$

Using the discrete cosine transform (DCT) and discrete sine transform (DST), each term in (3.43) can be individually diagonalized, yielding

$$\begin{aligned} \mathcal{U}^k &= (\mathcal{C}^{\text{II}})^T \tilde{\mathcal{Z}}^T \mathcal{D}^k \tilde{\mathcal{Z}} \mathcal{C}^{\text{II}} + (\mathcal{S}^{\text{II}})^T \mathcal{Z}^T \mathcal{D}^k \mathcal{Z} \mathcal{S}^{\text{II}} \\ &\quad + (\mathcal{C}^{\text{II}})^T \tilde{\mathcal{Z}}^T \tilde{\mathcal{D}}^k \mathcal{Z} \mathcal{S}^{\text{II}} - (\mathcal{S}^{\text{II}})^T \mathcal{Z}^T \tilde{\mathcal{D}}^k \tilde{\mathcal{Z}} \mathcal{C}^{\text{II}} \end{aligned} \tag{3.44}$$

where $\mathcal{C}^{\text{II}}$ and $\mathcal{S}^{\text{II}}$ are $N \times N$ Type-II DCT and DST matrices [85], with entries:

$$\mathcal{C}^{\text{II}}(i,k) = \epsilon_i \sqrt{2/N} \cos[\frac{i(2k+1)\pi}{2N}] \qquad i,k \in \{0, \cdots, N-1\} \tag{3.45}$$

$$\mathcal{S}^{\text{II}}(i,k) = \epsilon_{i+1} \sqrt{2/N} \sin[\frac{(i+1)(2k+1)\pi}{2N}] \qquad i,k \in \{0, \cdots, N-1\} \tag{3.46}$$

and $\epsilon_i = 1/\sqrt{2}$ for $i = 0, N$ and $\epsilon_i = 1$ otherwise[5]. In (3.44), the $(N+1)\times N$ matrices $\mathcal{Z} = [\mathbf{0}_{N\times 1}|\mathcal{I}_N]^T$ and $\tilde{\mathcal{Z}} = [\mathcal{I}_N|\mathbf{0}_{N\times 1}]^T$ which are shift matrices. The $(N+1)\times(N+1)$ matrices $\mathcal{D}^k$ and $\tilde{\mathcal{D}}^k$ are defined as follows

$$\mathcal{D}^k = \frac{1}{2}\text{diag}\{\mathbf{d}^k\} \tag{3.47}$$

$$\tilde{\mathcal{D}}^k = \frac{1}{2}\text{diag}\{[0, (\tilde{\mathbf{d}}^k)^T, 0]^T\} \tag{3.48}$$

where the vectors $\mathbf{d}^k$ and $\tilde{\mathbf{d}}^k$ are defined as

$$\mathbf{d}^k = \tilde{\mathcal{C}}^{\text{I}}\,[\mathbf{a}^k(0), \cdots, \mathbf{a}^k(N-1), 0]^T \tag{3.49}$$

$$\tilde{\mathbf{d}}^k = \tilde{\mathcal{S}}^{\text{I}}\,[\mathbf{b}^k(1), \cdots, \mathbf{b}^k(N-1)]^T. \tag{3.50}$$

and the non-normalized $(N+1)\times(N+1)$ DCT-I matrix $\tilde{\mathcal{C}}^{\text{I}}$ and $(N-1)\times(N-1)$ DST-I matrix $\tilde{\mathcal{S}}^{\text{I}}$are defined as [85],

$$\tilde{\mathcal{C}}^{\text{I}}(i,k) = \epsilon_i^2 \cos(\frac{ik\pi}{N}) \qquad i,k \in \{0,\cdots,N\} \tag{3.51}$$

$$\tilde{\mathcal{S}}^{\text{I}}(i,k) = \sin(\frac{ik\pi}{N}) \qquad i,k \in \{1,\cdots,N-1\}, \tag{3.52}$$

In the SDC [18], the echo emulation is performed using the decomposition in (3.44). For updating the weights, the connection between CDC and SDC is derived, showing that the elements of the vector $\tilde{\mathbf{\Lambda}}^k_{\text{even}}$ used in the CDC update (3.30) can be written in terms of diagonal elements of the matrices $\mathcal{D}^k$ and $\tilde{\mathcal{D}}^k$, i.e.,

$$\tilde{\mathbf{\Lambda}}^k_{\text{even}}(i) = 2\,\mathcal{D}^k(2i,2i) + \tilde{\mathcal{L}}^k(i,0) - 2\,j\,\tilde{\mathcal{D}}^k(2i,2i) \tag{3.53}$$

[5]In [18] and this work, the discrete trigonometric transforms are mainly used for diagonalization of the involved matrices and their energy compaction properties have not been used directly.

with $i = 0, \cdots, \frac{N}{2} - 1$ and $\tilde{\mathcal{L}}^k$ is defined in (3.23). Thus, the vector $\tilde{\mathbf{\Lambda}}^k_{\text{even}}$ is calculated directly from SDC elements and (3.30) is employed to update the weights in the frequency domain using (3.27).

Despite the intricate nature of the above construction, the use of the trigonometric transformations in [18] provides a more cost efficient implementation of CDC than in [17]. Yet both algorithms have similar convergence, since they use the same weight update formula (3.30). The SDC algorithm is depicted in Fig. 3.5, where it can be seen that echo emulation is done in the time domain and the adaptive part is done in the frequency domain.

3.6 Improved Frame Asynchronous Echo Canceller

In the previous sections, we assume a general asynchronous case, in other words that there is a general misalignment of Δ samples between the echo and far-end frames. In a real DSL system, we have control over the misalignment at only one side, which is if a specific value is chosen for the misalignment at one side, and the misalignment at the other side is dictated by the propagation delay of the far end channel. One can choose $\Delta = 0$ which results in synchronous operation; however, at least at one side of the transmission the echo is cancelled asynchronously.

The value of the misalignment between the frames can affect some aspects of the echo canceller; e.g., its computational complexity and the ability to be easily combined with double talk canceller. Considering the computational complexity of the echo canceller, in [20], Jones examined the complexity of the CES algorithm as a function of the misalignment value. He showed that there is a certain misalignment value for which the CES algorithm achieves its minimum required number of operations.

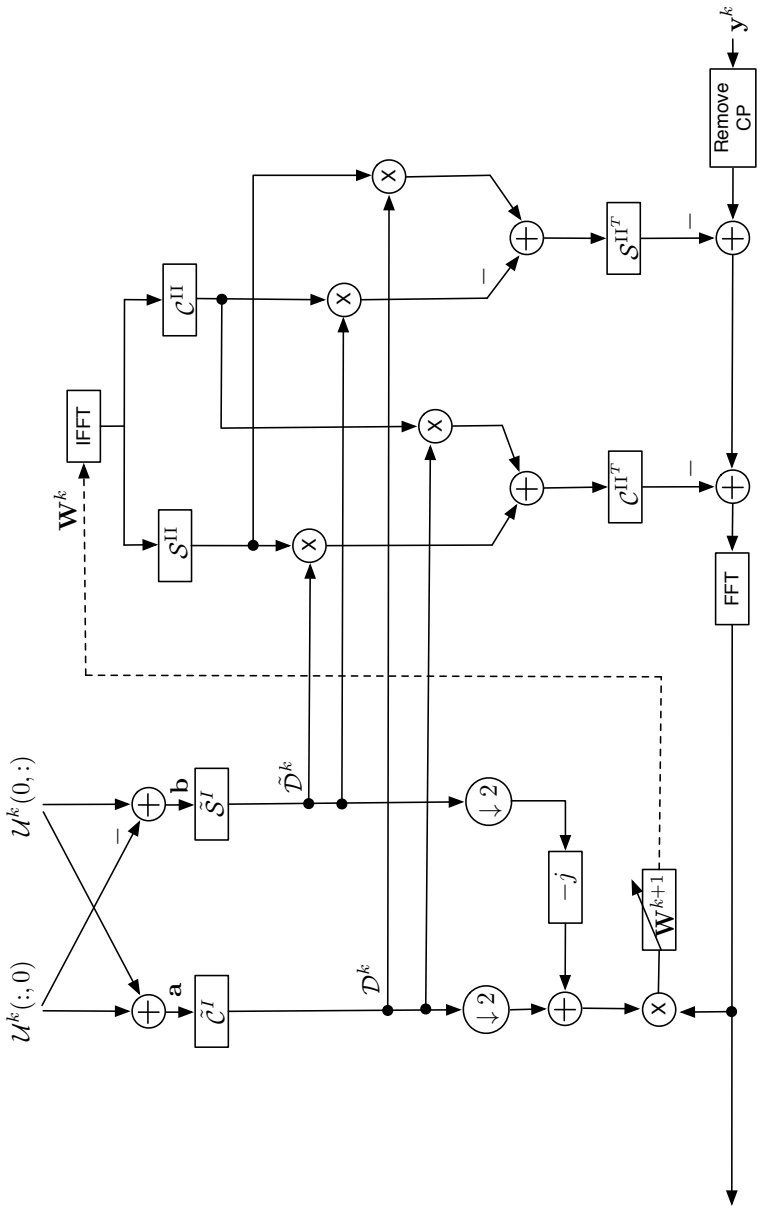

Fig. 3.5 Symmetric rate SDC Echo Canceller

However, as noted earlier, this specific optimal value can be guaranteed only at one side of the transmission system. In order to achieve the minimal complexity for CES algorithm at the other side, the use of an extra set of DFT/IDFT is suggested. This enables the echo canceller to choose the proper block of data with the specific misalignment regardless of the actual value of the delay and perform the echo cancelling in the time domain.

The structures proposed for asynchronous echo cancellation in [20, 16], both result in a structure where the echo canceller and the far end signal demodulator do not share the receiver's DFT. As shown in [21, 76], if the echo canceller and the demodulator share the DFT, a cheaper implementation of double talk canceller is attainable, which results in a better tracking capability for the echo canceller while the far end channel is active.

In [22], Ysebaert *et al.* proposed the structure where the extra DFT is added in the transmitter instead of the extra pair of DFT/IDFT in the receiver as in the Jones' method [20]. The extra DFT at the transmitter side is used to diagonalize a modified circulant matrix for the CES echo canceller, which in this case can include elements from two different symbols. Using the proposed structure the complexity of the CES canceller can be reduced without requiring a specific misalignment and the DFT at the receiver is shared between the modulator and the echo canceller facilitating the implementation of the double talk canceller.

3.7 Final Remarks

In design of echo cancellers there are some practical issues that need to be considered, namely the increased dynamic range, system non-linearities and the fixed-point

implementation. In DSL transmission, the received far-end signal can be attenuated over the channel by as much as 60 to 70 dB, while the echo signal caused by the hybrid faces only 10-20 dB of attenuation. For FDD based systems, the echo is attenuated by means of an analog filter, which reduces its power considerably. However, in echo canceller based systems, high dynamic ranges of the received signal are experienced which requires an increased number of bits in ADC [86]. In addition, some non-linearity can be expected, e.g., because of the saturation caused by the high peak-to-average power rate of the DMT signals. Finally, for any designed canceller, its performance under the fixed-pinot implementation would be of importance for practical applications.

Chapter 4

Linearly Constrained Adaptive Echo Canceller

In this chapter, the problem of mixed time- and frequency-domain echo cancellation for DMT-based systems is remodeled as one of linearly constrained optimization. A preliminary motivational discussion for this approach is provided in Section 4.1. In Section 4.2, we explain how the linearly constrained optimization can be introduced in the echo cancellation context, by considering an extended weight vector combining both the time-domain and frequency-domain filtering weight vectors. The application of this new concept to the mixed time- and frequency-domain echo cancellers, e.g., CES algorithm, is presented in detail in Section 4.3. Finally, in Section 4.4, appending of supplementary linear constraints to the canceller in order to improve its performance is discussed.

4.1 Motivation

As discussed in the previous chapter, various echo cancellation algorithms for DMT-based systems are established based on the mixed filtering in the time and frequency domains. In such cancellers, the adaptive weight update is done mostly in the frequency domain and the time-domain weight vector, used in conjunction with the frequency-domain one for the echo emulation, is acquired by means of inverse Fourier transform.

In this chapter, we propose that such mixed time- and frequency-domain filtering can be regarded as a constrained optimization problem, where a cost function is minimized over an extended linear space. This extended linear space contains the weights of the FIR filter modeling the echo channel both in the time and frequency domains. In this extended space, the mapping between the time- and frequency-domain weights is regarded as a linear constraint on the extended set of weights. Finally, this linear constraint is enforced during the optimization process over the extended linear space.

Based on this constrained optimization interpretation, we introduce a linearly constrained adaptive (LCA) echo cancellation structure for DMT-based systems. We shall examine two possible approaches for introducing the linear constraints within the structure of echo canceller: the first one is based on the work by Frost in [25] and the second one is based on the generalized sidelobe canceller (GSC) structure by Griffiths and Jim in [26].

Since, the new LCA cancellers are developed based on a general mixed time- and frequency-domain error signal and a general set of constraints, the existing cancellers, presented in Chapter 3 based on these two domains, can be considered as special

realizations within this framework. These realizations can be derived by defining the error signal, used in LCA cancellers, based on different existing algorithms. In this work, we discuss the LCA canceller based the CES algorithm, and examine its performance using different choice of constraints.

In addition to providing a constrained representation for the existing echo cancellers, the proposed structure allows a new generalization by adding the capability to incorporate additional processing constraints in a more systematic way. For instance, supplementary constraints can be applied in the time and/or frequency domains to the echo canceller to improve the performance of the system. One such application, discussed in this work, is echo cancellation in the presence of radio frequency interference (RFI). It is shown that the constrained echo cancellers with additional linear constraints have improved robustness against the RFI.

4.2 Linearly Constrained Adaptive Echo Cancellation

As discussed earlier, the echo cancellation in DMT-modulated DSL systems relies on the joint filtering in the time and frequency domains. In this section, we propose a novel formulation of the echo cancellation problem as a constrained optimization problem in an extended linear space containing both the time- and frequency-domain weights. In this approach, the desired cost function is minimized, while satisfying certain constraints, which primarily can be used to ensure the proper mapping of the weights from the frequency domain into the time domain or vice versa. The proposed linearly constrained canceller is made inclusive by assuming a general form of the error signal and a general set of linear constraints. In the following, we explain two approaches for developing the linearly constrained canceller framework: one based

on the work of Frost in [25] and another based on the generalized sidelobe canceller (GSC) by Griffiths and Jim in [26].

4.2.1 LCA echo canceller based on constrained LMS algorithm

Let us consider a frame synchronous system with equal rates at the transmitter and the receiver. We want to represent the echo cancellation for DMT-based systems as a constrained optimization problem, where a cost function is minimized under certain constraints. The optimization is performed over an extended linear space, which is spanned by the extended weight vector, containing the weight vectors both in the time domain $\mathbf{w}^k$ (length T_e) and in the frequency domain $\mathbf{W}^k$ (length N), as given by

$$\boldsymbol{\omega}^k = \left[\begin{array}{c} \mathbf{w}^k \\ \hline \mathbf{W}^k \end{array}\right] \tag{4.1}$$

where $\boldsymbol{\omega}^k$ is a vector of length $N + T_e$.

As seen in the previous chapter, the weights are updated adaptively using the error signal. In a general case, we can assume that the error signal in the frequency domain has the form of

$$\begin{aligned} \mathbf{E}^k &= \mathbf{Y}^k - \hat{\mathbf{Y}}_e^k & (4.2) \\ &= \mathbf{Y}^k - (\boldsymbol{\Psi}^k)^H \boldsymbol{\omega}^k & (4.3) \end{aligned}$$

where the received signal in the frequency domain is denoted by $\mathbf{Y}^k = \mathcal{F}_N \mathbf{y}^k$. In addition, the extended reference matrix $\boldsymbol{\Psi}^k$of size $(N + T_e) \times N$ contains the echo reference symbols both in the time and frequency domains. The exact definition of

the matrix $\mathbf{\Psi}^k$ depends on the underlying algorithm used for the echo emulation, as discussed in the next section.

Using this extended notation, the design problem for the echo cancellation can be expressed as a constrained optimization, where the error power is minimized subject to a linear constraint on $\boldsymbol{\omega}^k$. This can be formulated as

$$\min_{\boldsymbol{\omega}^k} \mathrm{E}[\|\mathbf{E}^k\|^2] \quad \text{s.t. } \mathcal{C}^H \boldsymbol{\omega}^k = \mathbf{g} \tag{4.4}$$

where E[.] denotes the statistical expectation. In our derivation, we assume a general set of l_c linear constraints described by the constraint matrix $\mathcal{C}$ of size $(N + T_e) \times l_c$ and vector $\mathbf{g}$ of length l_c, where $l_c < N + T_e$ and the matrix $\mathcal{C}$ is full column rank. The constraint matrix is primarily used to ensure the Fourier transform relation between the weights in the time and frequency domains. However, additional constraints can be added to improve the system performance, as discussed later.

Using the method of Lagrange multipliers [8], this specific constrained optimization problem can be transformed into an unconstrained one. Therefore, the constraint can be appended to the cost function, as given by

$$J = \mathrm{E}[\|\mathbf{E}^k\|^2] + \left((\boldsymbol{\omega}^k)^H \mathcal{C} - \mathbf{g}^H\right) \boldsymbol{\lambda} + \boldsymbol{\lambda}^H \left(\mathcal{C}^H \boldsymbol{\omega}^k - \mathbf{g}\right). \tag{4.5}$$

where $\boldsymbol{\lambda}$ is the Lagrange multipliers vector of length l_c. Complying with the method in [25], constrained gradient-descent optimization is used where the weight vector is adaptively updated by the gradient of the constrained cost function, as follows (calculated based on [87])

$$\boldsymbol{\omega}^{k+1} = \boldsymbol{\omega}^k - \mu \nabla_{\boldsymbol{\omega}^H} J \tag{4.6}$$

where,

$$\nabla_{\boldsymbol{\omega}^H} J = \mathcal{R}\,\boldsymbol{\omega}^k \;-\; \mathbf{P} \;+\; \mathcal{C}\,\boldsymbol{\lambda}. \tag{4.7}$$

The matrix $\mathcal{R}$ and the vector $\mathbf{P}$ are the correlation matrix and cross correlation vector, respectively, defined by

$$\mathcal{R} = \mathrm{E}[\boldsymbol{\Psi}^k\,(\boldsymbol{\Psi}^k)^H], \tag{4.8}$$

$$\mathbf{P} = \mathrm{E}[\boldsymbol{\Psi}^k\,\mathbf{Y}^k]. \tag{4.9}$$

The Lagrange multipliers $\boldsymbol{\lambda}$ is found by forcing $\boldsymbol{\omega}^{k+1}$ to satisfy the constraint. Replacing the obtained value of $\boldsymbol{\lambda}$ in (4.6), the iterative weight update is given by

$$\boldsymbol{\omega}^{k+1} = \boldsymbol{\omega}_q \;+\; \left(\mathcal{I}_{(N+T_e)} \;-\; \mathcal{C}(\mathcal{C}^H\mathcal{C})^{-1}\mathcal{C}^H\right)\left(\boldsymbol{\omega}^k - \mu\left(\mathcal{R}\,\boldsymbol{\omega}^k - \mathbf{P}\right)\right) \tag{4.10}$$

where $\boldsymbol{\omega}_q = \mathcal{C}(\mathcal{C}^H\mathcal{C})^{-1}\mathbf{g}$ is the quiescent term and depends only on the constraint. The term $\mathcal{C}(\mathcal{C}^H\mathcal{C})^{-1}\mathcal{C}^H$ represents the projection operator onto the subspace spanned by the constraint matrix $\mathcal{C}$ (denoted by $\mathcal{P}_c$), and the matrix

$$\mathcal{P}_c^{\perp} = \mathcal{I}_{(N+T_e)} - \mathcal{P}_c \tag{4.11}$$

is the projection onto its orthogonal complement. Hence, (4.10) can be rewritten as

$$\boldsymbol{\omega}^{k+1} = \boldsymbol{\omega}_q \;+\; \mathcal{P}_c^{\perp}\left(\boldsymbol{\omega}^k \;-\; \mu\left(\mathcal{R}\,\boldsymbol{\omega}^k - \mathbf{P}\right)\right). \tag{4.12}$$

The adaptive update in (4.12) requires the knowledge of the correlation matrix $\mathcal{R}$ and the vector $\mathbf{P}$, which is unavailable *a priori*. However, for a LMS style approach,

these quantities can be approximated by their instantaneous values given by:

$$\mathcal{R}^k = \mathbf{\Psi}^k \, (\mathbf{\Psi}^k)^H, \tag{4.13}$$

$$\mathbf{P}^k = \mathbf{\Psi}^k \, \mathbf{Y}^k. \tag{4.14}$$

Using the instantaneous approximations, the iterative update of the extended weight vector $\boldsymbol{\omega}^{k+1}$ based on the constrained LMS algorithm is given by

$$\boldsymbol{\omega}^{k+1} \; = \; \boldsymbol{\omega}_q \; + \; \mathcal{P}_c^{\perp} \left(\boldsymbol{\omega}^k \; + \; \mu \, \mathbf{\Psi}^k \, \mathbf{E}^k \right) \tag{4.15}$$

where $\mathbf{E}^k$ is given in (4.3). As shown in [25], this algorithm converges in the mean if

$$0 < \mu < 1/\lambda_{max} \tag{4.16}$$

where λ_{max} is the largest eigenvalue of the matrix $\mathcal{P}_c^{\perp} \, \mathcal{R} \, \mathcal{P}_c^{\perp}$.

The adaptive weight update in (4.15) together with (4.3) define a linearly constrained echo canceller. As mentioned earlier, the exact implementation of the algorithm and the definition of the matrices involved depend on the underlying echo emulation algorithm and the chosen set of constraints. In the next section, we investigate the LCA echo canceller based on the GSC approach in [26].

4.2.2 LCA echo canceller based on generalized sidelobe canceller

One of the efficient implementations for adaptive constrained optimization is proposed by Griffiths and Jim in [26]. In this method, known as generalized sidelobe canceller (GSC), the weight vector space is decomposed into two orthogonal subspaces, the

constraint subspace spanned by the columns of the constraint matrix $\mathcal{C}$ and its orthogonal complement subspace. Originally, this adaptive processor was introduced in the context of beamforming applications, where it is partitioned into two processing paths. One path processes the signal from the desired direction, often subject to some constraints, and the other one filters out (blocks) the interference and the noise.

Employing this method, the $(N+T_e)$-dimensional extended weight vector $\boldsymbol{\omega}^k$ can be written as the sum of two components resulting from the projection onto the two orthogonal subspaces. That is,

$$\boldsymbol{\omega}^k = \boldsymbol{\omega}_c^k + \boldsymbol{\omega}_b^k \tag{4.17}$$

where $\boldsymbol{\omega}_c^k$ is the projection of $\boldsymbol{\omega}^k$ onto the constraint subspace and $\boldsymbol{\omega}_b^k$ is the projection onto the orthogonal subspace. If the constraint subspace is spanned by the columns of matrix $\mathcal{C}$ of size $(N+T_e)\times l_c$, the orthogonal subspace is spanned by the columns of a so-called blocking matrix $\mathcal{B}$ of size $(N+T_e)\times(N+T_e-l_c)$. The blocking matrix can be any full column rank matrix with columns orthogonal to the columns of $\mathcal{C}$, i.e.,

$$\mathcal{B}^H\,\mathcal{C} = \mathcal{O}_{(N+T_e-l_c)\times l_c}. \tag{4.18}$$

It is often convenient but not necessary to choose matrix $\mathcal{B}$ such that $\mathcal{B}^H\,\mathcal{B} = \mathcal{I}_{(N+T_e-l_c)}$.

The projection of $\boldsymbol{\omega}^k$ onto the constraint subspace is performed by its left multiplication with the projection matrix $\mathcal{P}_c = \mathcal{C}(\mathcal{C}^H\mathcal{C})^{-1}\mathcal{C}^H$. Thus, from the constraint in (4.4) it can be seen that

$$\boldsymbol{\omega}_c^k = \mathcal{C}(\mathcal{C}^H\mathcal{C})^{-1}\,\mathbf{g} = \boldsymbol{\omega}_q. \tag{4.19}$$

As noted in the previous section, $\boldsymbol{\omega}_q$ depends only on the constraint and is not adaptive. Similarly, the projection of $\boldsymbol{\omega}^k$ onto the orthogonal subspace can be derived via left multiplication with the projection matrix onto the orthogonal subspace $\mathcal{P}_c^{\perp}$, which in terms of the blocking matrix is given as follows

$$\mathcal{P}_c^{\perp} = \mathcal{B}(\mathcal{B}^H\mathcal{B})^{-1}\mathcal{B}^H. \tag{4.20}$$

It can be shown that $\boldsymbol{\omega}_b^k$ is given by

$$\boldsymbol{\omega}_b^k = \mathcal{B}\,\boldsymbol{\omega}_a^k \tag{4.21}$$

where length $(N + T_e - l_c)$ vector $\boldsymbol{\omega}_a^k$ is the unconstrained solution of

$$\min \mathrm{E}[\|\mathbf{Y}^k - (\boldsymbol{\Psi}^k)^H\,\boldsymbol{\omega}_q - (\boldsymbol{\Psi}^k)^H\,\mathcal{B}\,\boldsymbol{\omega}_a^k\|^2], \tag{4.22}$$

where $\boldsymbol{\omega}_a^k$ is now unconstrained. Thus, $\boldsymbol{\omega}_a^k$ can be adaptively updated by the gradient of (4.22), as

$$\boldsymbol{\omega}_a^{k+1} \;=\; \boldsymbol{\omega}_a^k \;+\; \mu\,\mathcal{B}^H\left(\mathbf{P} \;-\; \mathcal{R}\,\boldsymbol{\omega}_q \;-\; \mathcal{R}\,\mathcal{B}\,\boldsymbol{\omega}_a^k\right) \tag{4.23}$$

where the matrix $\mathcal{R}$ and the vector $\mathbf{P}$ are defined in (4.8) and (4.9), respectively. The decomposition of $\boldsymbol{\omega}^k$ as in (4.17) makes it possible to transform the constrained optimization over $\boldsymbol{\omega}^k$ into an equivalent unconstrained one over $\boldsymbol{\omega}_a^k$. In addition, the term $\boldsymbol{\omega}_c^k = \boldsymbol{\omega}_q$ ensures that the constraint is satisfied at all times, independent of the choice of $\boldsymbol{\omega}_a^k$.

The iterative update for $\boldsymbol{\omega}_a^k$ in (4.23) requires the knowledge of the correlation matrix $\mathcal{R}$ and the vector $\mathbf{P}$. Similar to the previous section, these values can be

approximated by their instantaneous values given by (4.13) and (4.14), respectively. Consequently, the iterative update for the extended weight vector based on the GSC algorithm is given by:

$$\boldsymbol{\omega}_a^{k+1} \;=\; \boldsymbol{\omega}_a^k \;+\; \mu\, \boldsymbol{\Psi}_b^k \left(\mathbf{Y}^k \;-\; (\boldsymbol{\Psi}^k)^H\, \boldsymbol{\omega}_q \;-\; (\boldsymbol{\Psi}_b^k)^H\, \boldsymbol{\omega}_a^k\right) \tag{4.24}$$

where the $(N + T_e - l_c) \times N$ matrix $\boldsymbol{\Psi}_b^k = \mathcal{B}^H\, \boldsymbol{\Psi}^k$ is the projection of the extended echo reference matrix onto the subspace spanned by the matrix $\mathcal{B}$. Using (4.24), a compact implementation of the GSC-based LCA echo canceller is shown in Fig. 4.1. It can also be seen that the adaptive update is equivalent to

$$\boldsymbol{\omega}_a^{k+1} = \boldsymbol{\omega}_a^k \;+\; \mu\, \boldsymbol{\Psi}_b^k\, \mathbf{E}^k \tag{4.25}$$

where $\mathbf{E}^k$ is the error signal in (4.3). It is notable that this algorithm converges in the mean if

$$0 < \mu < 1/\lambda_{max} \tag{4.26}$$

where λ_{max} is the largest eigenvalue of the matrix $\mathcal{B}^H\, \mathcal{R}\, \mathcal{B}$.

4.3 LCA Cancellers Based on Mixed Time- and Frequency-Domain Processing

In the previous section, we have developed two structures for LCA echo cancellers. As discussed earlier, variants of the LCA cancellers can be realized based on different choices of echo emulation technique and the constraint matrix. In this section, we focus on the CES-based implementation of the LCA canceller as a representative

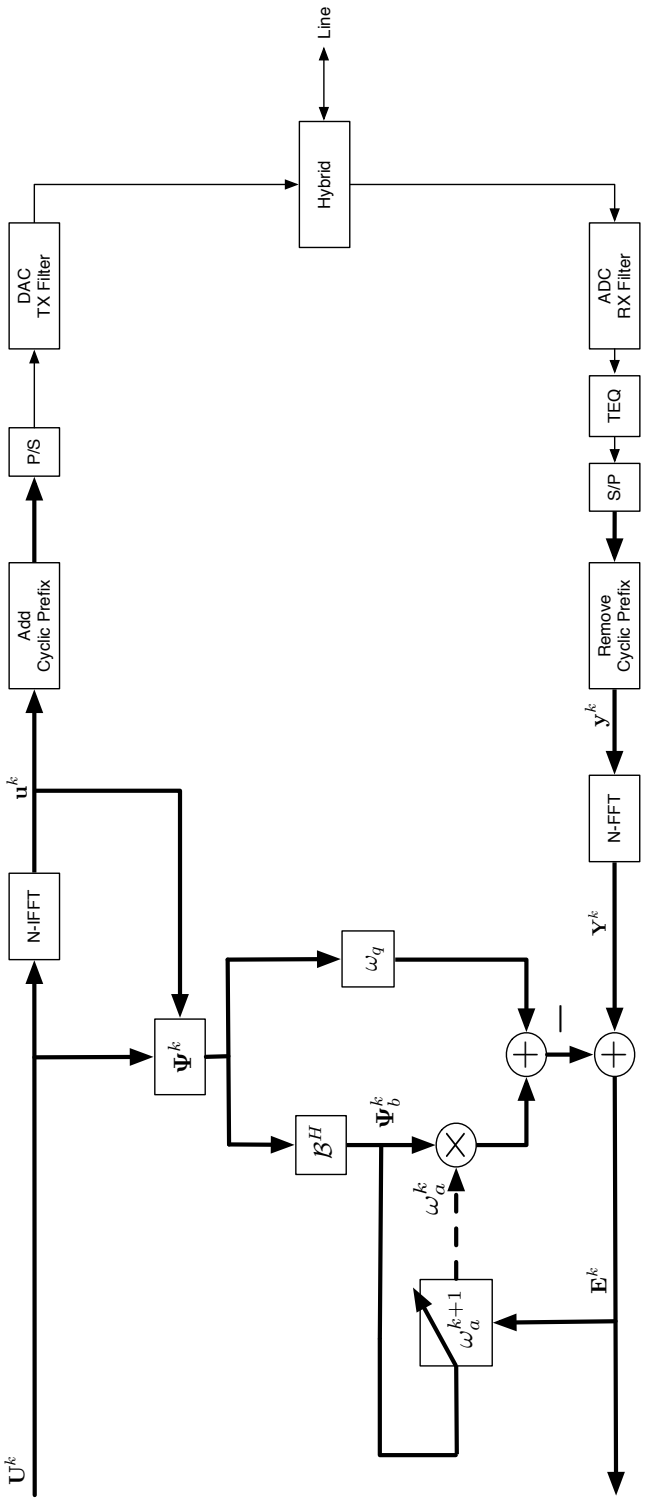

Fig. 4.1 Block diagram for GSC-based LCA echo canceller

member of the group of mixed time- and frequency-domain cancellers.

To achieve the realization of the LCA canceller based on the CES method, it is required to define the extended echo reference matrix $\mathbf{\Psi}^k$ in (4.3) and also the constraint matrix $\mathcal{C}$ in (4.4) and the blocking matrix $\mathcal{B}$ in (4.18). These definitions are covered in Section 4.3.1, which includes the symmetric and multirate CES-based cancellers. In Section 4.3.2, the computational complexity of the time-domain LMS canceller and CES echo canceller is compared with the CES-based realization of the LCA echo cancellers.

4.3.1 LCA echo cancellers based on CES method

Formation of the extended echo reference matrix

One of the key elements in the LCA canceller is the extended echo reference matrix $\mathbf{\Psi}^k$ whose definition depends on the technique used for the echo emulation. In the following, the representation of this matrix is defined for the CES-based approach, including the symmetric and multirate cancellers.

The extended echo reference matrix $\mathbf{\Psi}^k$ can be defined by considering its function in the echo emulation step described in (4.3). Consequently, for a symmetric rate canceller, it can be formulated by comparing (4.3) and the representation for the frequency-domain echo estimate in the CES canceller as given by (3.14). This immediately results into the following definition of the $(N + T_e) \times N$ extended echo reference matrix $\mathbf{\Psi}^k$ given by

$$\mathbf{\Psi}^k = \begin{bmatrix} \mathbf{M}^T \left(\mathcal{X}^k\right)^H \mathcal{F}_N^{-1} \\ \hline \operatorname{diag}\{(\mathbf{\Lambda}^k)^*\} \end{bmatrix}, \tag{4.27}$$

where the matrices $\mathcal{X}^k$ and $\mathbf{M}$ and the vector $\mathbf{\Lambda}^k$ are as defined in Section 3.3.1.

In practical systems, different data rates are used in the upstream and downstream directions. Hence, as discussed in Section 3.3.2, the relating emulated echo signal is interpolated or decimated in order to consider the effect of the non-ideal filters at the DAC or ADC, respectively. The LCA echo cancellers can be easily applied to multirate cases. This extension is simply achieved by modifying the definition of the extended echo reference matrix $\mathbf{\Psi}^k$ in (4.3).

For the *interpolated* echo cancellation, the same methods for constrained echo cancellation can be used where the error vector $\mathbf{E}^k$ of length κN in (4.3) is now calculated based on the modified $\mathbf{\Psi}^k$ as follows

$$\mathbf{\Psi}^k = \left[\frac{\mathbf{M}^T \left(\mathcal{X}^k_{\text{int}}\right)^H \mathcal{F}^{-1}_{\kappa N}}{\text{diag}\{(\mathbf{R}\,\mathbf{\Lambda}^k)^*\}} \right] \tag{4.28}$$

and $\mathbf{Y}^k$ is obtained from $\mathbf{y}^k$ via κN-point DFT as

$$\mathbf{Y}^k = \mathcal{F}_{\kappa N}\,\mathbf{y}^k. \tag{4.29}$$

In the above equation, the matrix $\mathcal{X}^k_{\text{int}}$ containing the interpolated data, the vector $\mathbf{\Lambda}^k$, the matrix $\mathbf{R}$ are defined as noted in Section 3.3.2, and as before, matrix $\mathbf{M} \triangleq [\mathcal{I}_{T_e} | \mathcal{O}_{T_e \times (\kappa N - T_e)}]^T$ is used for the purpose of zero-padding.

For the decimated echo cancellation, it is only required to modify the extended echo reference matrix as follows

$$\mathbf{\Psi}^k = \left[\frac{\mathbf{M}^T \left(\mathcal{X}^k_{\text{dec}}\right)^H \mathcal{F}^{-1}_{N}}{\text{diag}\{(\mathbf{\Lambda}^k)^*\}\,\mathbf{R}} \right] \tag{4.30}$$

where the matrix $\mathcal{X}_{\text{dec}}^k$ containing the decimated data and the vector $\mathbf{\Lambda}^k$ are defined in Section 3.3.2.

Formation of the constraint matrix

In order to fully implement the LCA canceller, besides the extended echo reference matrix $\mathbf{\Psi}^k$, the constraint and blocking matrices should also be determined. As discussed earlier, in the mixed time- and frequency-domain echo cancellers, the weight vectors in the time and frequency domains are related via a Fourier transform. This relationship between the weight vectors can be imposed in either of the domains, which results in two different constraint matrices.

In Case I, the constraint is applied in the frequency domain, where the frequency-domain weight vector is calculated in terms of the time-domain weight vector, i.e., $\mathbf{W}^k = \mathcal{F}_N \mathbf{M} \mathbf{w}^k$. Using the form in (4.4), the $(N + T_e) \times N$ constraint matrix for this case is given by

$$\mathcal{C} = [-\mathcal{F}_N \mathbf{M} \,|\, \mathcal{I}_N]^H \tag{4.31}$$

and the vector $\mathbf{g} = \mathcal{O}_{N\times 1}$. The corresponding equation $\mathcal{C}^H \boldsymbol{\omega}^k = \mathbf{g}$ in (4.4) now denotes N linear constraints ($l_c = N$).

In Case II, the constraint is applied in the time domain, where the time-domain weight vector is calculated in terms of the frequency-domain weight vector, i.e., $\mathbf{w}^k = \mathbf{M}^T \mathcal{F}_N^{-1} \mathbf{W}^k$. Similarly, the $(N + T_e) \times T_e$ constraint matrix for this case is given by

$$\mathcal{C} = [\mathcal{I}_{T_e} \,|\, -\mathbf{M}^T \mathcal{F}_N^{-1}]^H \tag{4.32}$$

where the vector $\mathbf{g} = \mathcal{O}_{T_e\times 1}$. The corresponding equation $\mathcal{C}^H \boldsymbol{\omega}^k = \mathbf{g}$ in (4.4) now

denotes T_e linear constraints ($l_c = T_e$).

As it can be seen, the two formulations result in different number of constraints, which in the context of linearly adaptive filtering, relates to different degrees of freedom. As discussed in [88], the reduced degrees of freedom, which corresponds to having more constraints, result in faster convergence to the steady state conditions. As will be shown later in Section 6.2, the constrained cancellers based on these two constraint matrices perform differently, in compliance with the above statement.

The projection matrix $\mathcal{P}_c^{\perp}$ required for the LCA echo cancellers can be derived based on the constraint matrix. For both aforementioned cases, the projection matrix $\mathcal{P}_c = \mathcal{C}(\mathcal{C}^H\mathcal{C})^{-1}\mathcal{C}^H$ and the corresponding orthogonal projection matrix $\mathcal{P}_c^{\perp}$ can be calculated based on (4.11).

Formation of the blocking matrix

For simple constraint matrices, the blocking matrix $\mathcal{B}$ of size $(N+T_e)\times(N+T_e-l_c)$ can be found using (4.18). For instance, for the Case I, where the constraint matrix is given in (4.31), the blocking matrix $\mathcal{B}$ is as follows

$$\mathcal{B} = \frac{1}{\sqrt{2}}\,[\mathcal{I}_{T_e}\,|\,\mathbf{M}^T\mathcal{F}_N^{-1}]^H. \tag{4.33}$$

For the Case II, where the constraint matrix is given in (4.32), the blocking matrix $\mathcal{B}$ can be obtained as follows

$$\mathcal{B} = \frac{1}{\sqrt{2}}\,[\mathcal{F}_N\mathbf{M}\,|\,\mathcal{I}_N]^H, \tag{4.34}$$

where the normalization factor $\frac{1}{\sqrt{2}}$ is introduced to ensure that $\mathcal{B}^H\,\mathcal{B} = \mathcal{I}_{(N+T_e-l_c)}$. For a more complicated constraint matrix, methods such as Gram-Schmidt or QR-

factorization can be used to find a corresponding blocking matrix [89]. In addition, the above definitions for the constraint and the blocking matrices can be directly expanded for the multirate echo cancellers.

As it can be seen, the extended weight vector $\boldsymbol{\omega}^k$ and the extended echo reference matrix $\boldsymbol{\Psi}^k$ provide a unifying representation of the various realizations of the CES echo canceller. Similar derivations can be used to implement constrained echo cancellers based on the other mixed time- and frequency-domain algorithms. In the next chapter, we will show that most of the existing echo cancellers, e.g., CES, CDC and SDC, can be unified and represented in terms of a general matrix decomposition, which is then used to develop a more general form of LCA echo canceller.

4.3.2 Complexity Analysis of LCA Echo Cancellers

In this section, the computational complexity of the LCA canceller based on the CES algorithm is calculated and compared with the complexity of the time-domain LMS canceller and the CES algorithm echo cancellers. The complexity, in this work, is expressed as the number of real multiplications at the symbol rate. It is assumed that both transmitter and receiver use the same data rate and is frame synchronous. As noted earlier, T_e is the number of the time-domain echo canceller taps, and N and υ are the symbol length and cyclic prefix length, respectively. Regarding the FFT complexity, the use of the split-radix FFT algorithm is assumed.

In Table 4.1, the computational complexity of the time-domain echo canceller based on LMS method and the CES echo canceller are compared with the LCA canceller. The studied LCA echo canceller is based on the CES technique for the echo emulation and utilizes the GSC-based approach for adaptive part, which is referred

Table 4.1 Complexity comparison between time-domain LMS and CES echo cancellers with GSC-based LCA canceller

Application	Echo Emulation	Adaptive Update	Total
LMS	T_eN	T_eN	$2T_eN$
CES	$\frac{(T_e-\upsilon)^2}{2}+2N$	$N\log_2 N-N+4$	$N\log_2 N+\frac{(T_e-\upsilon)^2}{2}+N+4$
GSC EC	$\frac{(T_e-\upsilon)^2}{2}+N\log_2 N-N+4$	$T_eN+N\log_2 N-3N+4$	$2N\log_2 N+\frac{(T_e-\upsilon)^2}{2}+T_eN-4N+4$

to as GSC EC.

For this realization the adaptive update for the constrained algorithm translates into performing the LMS update in the time domain, where $\mathbf{E}^k$ is transformed into the time domain using IDFT. As it can be seen from Table 4.1, the constrained algorithm GSC EC has decreased complexity compared to the time-domain canceller but increased complexity compared to the CES one. On the other hand, as the simulation results in Chapter 6 will show, the constrained algorithm has a convergence behaviour similar to the time-domain LMS method which is faster that the CES canceller. In the constrained canceller, an additional step is used to ensure the proper mapping of the weights between the two-domain, which is responsible for the added complexity but improves the convergence rate of the canceller.

For a general linear constraint matrix, the complexity of the LCA echo canceller increases, which is mainly caused by the additional projection operation involved in this algorithm. The first LCA implementation, given in (4.12), requires the orthogonal projection by matrix $\mathcal{P}_c^{\perp}$, which is uniquely defined. In the second implementation based on the GSC algorithm, the input signal is divided using the blocking matrix $\mathcal{B}$, which is only required to be orthogonal to the constraint matrix $\mathcal{C}$ and full rank. Therefore, the complexity of the GSC-based constrained echo canceller can be further reduced by the proper formation of matrix $\mathcal{B}$ (e.g., using the method proposed in [90]).

4.4 Constrained Adaptive Echo Cancellation in the Presence of Radio Frequency Interference

The constrained echo canceller developed in this work provides a general framework for studying the mixed time- and frequency-domain echo cancellers. It also provides

a framework to append supplementary constraints to the canceller, where these constraints can be employed to improve the performance of the system. For instance, when the transmission is degraded by the radio frequency interference, the constrained echo canceller can be utilized to improve the robustness of the system.

As discussed earlier, in DSL systems, the twisted-pair lines act as an antenna for the RF transmissions, resulting in RF interference (RFI). Predominantly, this RFI consists of the ingress from the AM radio broadcasts and amateur radio transmissions. Both of these interferences can be modeled as a narrowband noise (NBN), which is a signal with narrowband and high amplitude over a short period of time. For the ingress caused from the AM radio transmission, the frequencies are known and do not change during the transmission. In contrast, the carrier frequencies of the amateur radio transmissions change constantly every few minutes. The level of the ingress from both of these sources, at the receiver, is higher than the level of the crosstalk and the background noise.

In the presence of RFI, the weights of the echo canceller corresponding to the tones affected by the noise may increase substantially. Therefore, even after the termination of the radio transmission, the echo canceller needs to compensate for the large error on these tones. This phenomenon is known as the drifting problem. In the following, the constrained echo canceller is used in the presence of RFI and the linear constraints are proposed to restrain the drifting problem.

4.4.1 Linearly Constrained adaptive echo canceller in the presence of RFI

Utilizing the developed framework, we are able to apply desired constraints to the weights of the echo canceller. Therefore, in the presence of the RFI, which cause the

deteriorating error on the affected tones, the proper constraint can be used to prevent this problem. For the case of linear constraints, the weights of the affected tones, i.e., specific components of the frequency-domain weight vector $\mathbf{W}^k$, can be forced to zero during the period that RFI is present. This can be obtained by extending the constraint matrix $\mathcal{C}$ in (4.31) as follows,

$$\mathcal{C} = \left[\begin{array}{c|c} -\mathcal{F}_N \mathbf{M} & \mathcal{I}_N \\ \hline \mathcal{O}_{l_a \times T_e} & \mathcal{T}_{l_a \times N} \end{array}\right]^H \tag{4.35}$$

where l_a is the number of affected tones, and $\mathcal{T}$ is a submatrix of the identity matrix used to incorporate the affected tones into the constraint. That is, if the affected tones have indices $n_1, n_2, \cdots, n_{l_a}$, then matrix $\mathcal{T} = [\mathbf{e}_{n_1}, \mathbf{e}_{n_2}, \cdots, \mathbf{e}_{n_{l_a}}]^T$, where $\mathbf{e}_{n_i}$ denotes the $\mathrm{n}_i^{\mathrm{th}}$ column of identity matrix. It should be noted that, due to the extended formulation, the effect of the constraint in the frequency domain will correctly be mapped onto the weights in the time domain by the constrained canceller structure.

This approach requires that the existence of the RFI can be detected on the reserved tones [91]. As a result, it is best suited for the cases where the RF ingress is continuous e.g., AM ingress. The simulation results using these constraints, given in Section 6.2.2, show a major improvement in terms of the error on the affected tones.

It should be noted that in cases where it is not possible to detect the noise, other method such as adding additional quadratic inequality constraints, as in [92], can be used to improve the robustness of the system. An example for adding additional quadratic constraints has also been discussed in Section 6.2.2. Finally, we note that it is possible to extend this approach so as to constrain certain components of the time-domain weight vector $\mathbf{w}^k$. This might be desirable if *a priori* information about

the true echo channel is available.

4.5 Summary

In this chapter, we have introduced linearly constrained adaptive echo cancellers for DMT-based systems. Utilizing the extended weight vector containing the weights in the time and frequency domains, we show that the echo cancellation, in such extended linear space, can be reformulated as a constrained optimization. Two implementations for the LCA echo canceller have been discussed based on the constrained LMS method [25] and the generalized sidelobe canceller method [26]. These LCA cancellers can result several different cancellers, depending on the choice of the specific technique used for echo emulation and the chosen set of constraints. For instance, in this chapter we discussed the realization of LCA canceller based on the CES algorithm and certain linear constraints to ensure the proper mapping of the weights between the time and frequency domains. In addition, supplementary constraints can be added to the constrained echo canceller to improve the performance of the system. For illustration, it was shown how additional linear constraints can be introduced into the canceller in order to improve the robustness of the system in the presence of radio frequency interference.

Chapter 5

Dual Transform Domain Echo Canceller

In Chapter 4, a constrained optimization framework to study the echo cancellation problem in the time and frequency domains has been established. In this chapter, a more generalized framework is investigated where the echo cancellation is studied in a general dual domain, whose definition is based on a pair of arbitrary unitary transformations. After an introductory discussion in Section 5.1, the general form for the decomposition of the Toeplitz data matrix is introduced in Section 5.2. Based on this general form, a two-step design procedure for echo cancellers is proposed and used to derive a new dual domain echo cancellation method in Section 5.3. Next, the constrained echo cancellation in the dual domain is presented in Section 5.4. Later, by properly combining the unconstrained and constrained forms of the dual domain echo cancellation, a new combined dual domain echo canceller is proposed, and its computational complexity and convergence behaviour are examined in Section 5.5.

Finally, the extension of these dual domain cancellers to multirate cases is discussed in Section 5.6.

5.1 Motivation

The comprehensive study of the existing echo cancellers in Chapter 3 reveals a common general structure between these cancellers. In these methods, the design of the echo canceller is initiated by choosing a technique to decompose the Toeplitz data matrix, and then the rest of the conception follows this decomposition.

This order of design procedure has the disadvantage that the choice of the employed decomposition imposes some limitations on the canceller which directly affects its performance. The choice of the decomposition explicitly implies the domains in which the echo emulation and the adaptive weight update are performed and also defines the transformation matrices involved, therefore this decision has a direct impact; on the complexity and the convergence of the algorithm.

In this chapter, we propose to reverse the order of echo canceller design procedure. This is done by *first*, assuming a generic dual domain decomposition of the Toeplitz data matrix and designing a general dual domain echo canceller and *second*, choosing the decomposition to be used in this canceller. The proposed design order has the advantage that the structure of the echo canceller can be optimized without having any limitations imposed by the choice of the decomposition.

Following the aforementioned two-step design procedure, a new dual transform domain canceller (DTDC) is proposed. In this canceller, the time-domain signals and weight vectors are mapped into a dual domain defined by a pair of generic unitary matrices. This canceller employs an LMS weight update in the dual domain with low

computational complexity. Based upon this structure, the conditions for an appropriate decomposition, i.e., with reduced computational complexity of the algorithm, are determined. For the proposed DTDC structure, the symmetric decomposition performed by discrete trigonometric transformations satisfies the conditions of an appropriate decomposition. Consequently, the proposed dual domain canceller can be implemented using the above decomposition, which is referred to as dual trigonometric canceller (DTC).

As it is shown later, the decompositions used in the existing cancellers can be regarded as special cases of the proposed general decomposition of the Toeplitz data matrix. Therefore, the proposed DTDC structure provides a unified representation of these cancellers in a general dual domain framework. The existing cancellers comply with the dual domain operation in the echo emulation part but perform the adaptive weight update in a single domain to reduce the complexity of the algorithm. As a result, the DTDC structure establishes an analytical tool to study the existing cancellers from a unified prospective and, as shown in this chapter, provides an infrastructure to design new cancellers with better performance and/or lower complexity.

As discussed in Chapter 4, any a priori information about the weights modeling the echo channel can be translated into linear constraints, which can be used to improve the performance of the canceller. Accordingly, we develop linearly constrained dual domain cancellers where linear constraints are added to the canceller to ensure the proper mapping of the weight vectors in the dual domain. These dual domain constrained cancellers are indeed the generalized form of the cancellers developed in Chapter 4, since in these cancellers the signals are assumed to be mapped in any dual domain rather than being constrained to the time and frequency domains.

The comprehensive study of the constrained and unconstrained dual domain cancellers shows that the constrained canceller has a faster convergence rate which is similar to the convergence behaviour of the time-domain LMS canceller. This improved convergence rate is achieved at the expense of increased computational complexity compared with that of the unconstrained canceller. Therefore, we propose a combined dual domain canceller which is based on the unconstrained dual domain canceller, while infrequently the constrained adaptive weight update is used. As it is shown later, the proposed combined dual domain canceller has a convergence rate very close to that of the time-domain LMS canceller with the computational complexity similar to those of the existing cancellers.

Finally, we examine the dual domain cancellers for the practical DSL systems where echo cancellers must operate in multirate scenarios. Two approaches for implementing dual domain cancellers are studied: the direct approach and the polyphase approach. Furthermore, it is shown that the latter provides a more efficient implementation in terms of the complexity of the resulting algorithm.

5.2 General Decomposition of the Toeplitz Data Matrix

In Chapter 3, the emulated echo (3.4) is calculated based on the Toeplitz matrix $\mathcal{U}^k$, which is made up of the input data samples. As discussed earlier, various echo cancellation algorithms benefit from different decompositions of this Toeplitz data matrix in order to decrease their computational complexity.

In general, the Toeplitz input data matrix $\mathcal{U}^k$ can be decomposed in the dual

domain as follows

$$\mathcal{U}^k = [\mathcal{G}_1^H \quad \mathcal{G}_2^H] \begin{bmatrix} \mathcal{S}_{11}^k & \mathcal{S}_{12}^k \\ \mathcal{S}_{21}^k & \mathcal{S}_{22}^k \end{bmatrix} \begin{bmatrix} \mathcal{G}_1 \\ \mathcal{G}_2 \end{bmatrix} \tag{5.1}$$

or

$$\mathcal{U}^k = \mathcal{G}_1^H \mathcal{S}_{11}^k \mathcal{G}_1 + \mathcal{G}_2^H \mathcal{S}_{21}^k \mathcal{G}_1 + \mathcal{G}_1^H \mathcal{S}_{12}^k \mathcal{G}_2 + \mathcal{G}_2^H \mathcal{S}_{22}^k \mathcal{G}_2. \tag{5.2}$$

where $\mathcal{G}_i$ $(i = 1, 2)$ are $N \times N$ unitary matrices which are constant for all symbol periods, and $\mathcal{S}_{i,j}^k$ $(i, j = 1, 2)$ are $N \times N$ matrices where their elements are calculated based on the transmitted symbols. This general form provides a proper structure to incorporate the decompositions used in the existing echo cancellers, as represented in Chapter 3.

In the CES echo canceller presented by Ho *et al.* in [15], the matrix $\mathcal{U}^k$ is decomposed as

$$\mathcal{U}^k = \mathcal{X}^k + \mathcal{F}_N^{-1} \operatorname{diag}\{\mathbf{\Lambda}^k\} \mathcal{F}_N. \tag{5.3}$$

Therefore, it can be represented in the general form as

$$\mathcal{U}^k = \begin{bmatrix} \mathcal{F}_N^{-1} & \mathcal{I}_N \end{bmatrix} \begin{bmatrix} \operatorname{diag}\{\mathbf{\Lambda}^k\} & \mathcal{O}_N \\ \mathcal{O}_N & \mathcal{X}^k \end{bmatrix} \begin{bmatrix} \mathcal{F}_N \\ \mathcal{I}_N \end{bmatrix} \tag{5.4}$$

where the vector $\mathbf{\Lambda}^k$ and the matrix $\mathcal{X}^k$ are defined as in Section 3.3.1, and the unitary matrices $\mathcal{G}_1 = \mathcal{F}_N$ and $\mathcal{G}_2 = \mathcal{I}_N$.

Similarly, in the decomposition used in the CDC algorithm [17], the matrix $\mathcal{U}^k$ is decomposed as

$$\mathcal{U}^k = \frac{1}{2} \mathcal{F}_N^{-1} \operatorname{diag}\{\tilde{\mathbf{\Lambda}}_{\text{even}}^k\} \mathcal{F}_N \; + \; \frac{1}{2} \mathbf{Q}^H \mathcal{F}_N^{-1} \operatorname{diag}\{\tilde{\mathbf{\Lambda}}_{\text{odd}}^k\} \mathcal{F}_N \mathbf{Q}. \tag{5.5}$$

Expressed in terms of the general format (5.1), matrix $\mathcal{U}^k$ can be rewritten as

$$\mathcal{U}^k = \begin{bmatrix} \mathcal{F}_N^{-1} & \mathcal{Q}^H \mathcal{F}_N^{-1} \end{bmatrix} \begin{bmatrix} \frac{1}{2}\text{diag}\{\tilde{\mathbf{\Lambda}}^k_{\text{even}}\} & \mathcal{O}_N \\ \mathcal{O}_N & \frac{1}{2}\text{diag}\{\tilde{\mathbf{\Lambda}}^k_{\text{odd}}\} \end{bmatrix} \begin{bmatrix} \mathcal{F}_N \\ \mathcal{F}_N \mathbf{Q} \end{bmatrix} \tag{5.6}$$

where the vectors $\tilde{\mathbf{\Lambda}}^k_{\text{even}}$ and $\tilde{\mathbf{\Lambda}}^k_{\text{odd}}$ and the matrix $\mathbf{Q}$ are defined as in Section 3.4.1, and $\mathcal{G}_1 = \mathcal{F}_N$ and $\mathcal{G}_2 = \mathcal{F}_N \mathbf{Q}$.

Finally, in the symmetric decomposition used in the SDC algorithm [18], the matrix $\mathcal{U}^k$ is decomposed as

$$\mathcal{U}^k = (\mathcal{C}^{\text{II}})^T \tilde{\mathcal{Z}}^T \mathcal{D}^k \tilde{\mathcal{Z}} \mathcal{C}^{\text{II}} + (\mathcal{S}^{\text{II}})^T \mathcal{Z}^T \mathcal{D}^k \mathcal{Z} \mathcal{S}^{\text{II}} + (\mathcal{C}^{\text{II}})^T \tilde{\mathcal{Z}}^T \tilde{\mathcal{D}}^k \mathcal{Z} \mathcal{S}^{\text{II}} - (\mathcal{S}^{\text{II}})^T \mathcal{Z}^T \tilde{\mathcal{D}}^k \tilde{\mathcal{Z}} \mathcal{C}^{\text{II}} \tag{5.7}$$

which can similarly be expressed as

$$\mathcal{U}^k = \begin{bmatrix} (\mathcal{C}^{\text{II}})^T & (\mathcal{S}^{\text{II}})^T \end{bmatrix} \begin{bmatrix} \tilde{\mathcal{Z}}^T \mathcal{D}^k \tilde{\mathcal{Z}} & \tilde{\mathcal{Z}}^T \tilde{\mathcal{D}}^k \mathcal{Z} \\ -\mathcal{Z}^T \tilde{\mathcal{D}}^k \tilde{\mathcal{Z}} & \mathcal{Z}^T \mathcal{D}^k \mathcal{Z} \end{bmatrix} \begin{bmatrix} \mathcal{C}^{\text{II}} \\ \mathcal{S}^{\text{II}} \end{bmatrix} \tag{5.8}$$

where the involved $\mathcal{D}^k$, $\tilde{\mathcal{D}}^k$, $\mathcal{Z}$ and $\tilde{\mathcal{Z}}$ matrices are introduced as in Section 3.5, and $\mathcal{G}_1 = \mathcal{C}^{\text{II}}$ and $\mathcal{G}_2 = \mathcal{S}^{\text{II}}$ are the type-II discrete cosine and sine transformations, respectively. In this decomposition, the corresponding $\mathcal{S}^k_{11} = \tilde{\mathcal{Z}}^T \mathcal{D}^k \tilde{\mathcal{Z}}$ and $\mathcal{S}^k_{22} = \mathcal{Z}^T \mathcal{D}^k \mathcal{Z}$ submatrices are diagonal, since $\mathcal{D}^k$ and $\tilde{\mathcal{D}}^k$ are diagonal matrices, and $\mathcal{Z}$ and $\tilde{\mathcal{Z}}$ are only shift matrices. Also, it can be easily verified that the submatrix $\mathcal{S}^k_{12}$ has non-zero elements only on the super-diagonal and the submatrix $\mathcal{S}^k_{21}$ has non-zero elements only on the sub-diagonal[1].

[1]Super- and sub-diagonal refers to the first diagonal above and below the main diagonal, respectively.

As shown above, the general decomposition in (5.1) provides a unified representation for the previously used decompositions of the matrix $\mathcal{U}^k$. In the rest of this chapter, the short form of the decomposition in (5.1) is used, noted by

$$\mathcal{U}^k = \mathcal{G}^H \mathcal{S}^k \mathcal{G} \tag{5.9}$$

where $2N \times N$ matrix $\mathcal{G} \triangleq \begin{bmatrix} \mathcal{G}_1 \\ \mathcal{G}_2 \end{bmatrix}$ and $2N \times 2N$ matrix $\mathcal{S}^k \triangleq \begin{bmatrix} \mathcal{S}^k_{11} & \mathcal{S}^k_{12} \\ \mathcal{S}^k_{21} & \mathcal{S}^k_{22} \end{bmatrix}$. In the following section, we utilize this general form to propose a two-step design procedure for the echo cancellation in the dual domain.

5.3 General Dual Domain Echo Cancellation

As discussed earlier, different echo cancellers are designed based on different decompositions of the Toeplitz data matrix. The utilized decomposition has a decisive effect on the convergence behaviour and the computational complexity of the canceller, since it explicitly defines the transformation matrices available for mapping the time-domain signals and weight vectors. Therefore, this decomposition defines the domains available for the echo emulation and adaptive weight update. Consequently, the choice of the domains to perform the adaptive weight update affects the convergence of the canceller, and the computational cost for performing the involved transformations has a direct impact on the complexity of the canceller.

As discussed above, the choice of the employed decomposition restrains the possible structures for the echo cancellers. Therefore, in this section, we propose to initially assume a generic decomposition of the Toeplitz data matrix and perform the echo canceller design procedure in the following two steps. In the first step, a proper structure

based on the general decomposition is developed and the criteria for an *appropriate* decomposition are defined. Next, in the second step, an appropriate decomposition based on these criteria is selected. This division has the benefit that it outlines the limitations forced by each step on the overall structure independently. As a result, the effect of each step on the performance of the canceller in terms of the convergence rate and computational complexity can be studied separately. In addition, the structure of the canceller can be optimized without having any limitations imposed by the choice of the decomposition.

In Section 5.3.1, we discuss the first step, where a new dual transform domain canceller (DTDC) is proposed. This canceller is based on the general decomposition form, and uses the unitary submatrices of $\mathcal{G}$ to transform the time-domain signals and weight vectors into the dual domain. The goal for this step is to perform an LMS adaptive weight update in the dual domain with low computational complexity. Based on the proposed structure, the criteria for an *appropriate* decomposition are described, where appropriate is interpreted in the sense of reducing the complexity of the resulting algorithm. In Section 5.3.2, we show that these conditions are satisfied by the symmetric decomposition, which is based on the discrete trigonometric transformations. Finally, using this decomposition, an implementation of the DTDC algorithm is presented which is referred to as the dual trigonometric canceller (DTC).

5.3.1 Dual transform domain canceller

As discussed in Section 3.2, the emulated echo in the time domain is given by

$$\hat{\mathbf{y}}_e^k = \mathcal{U}^k \, \mathbf{M} \, \mathbf{w}^k. \tag{5.10}$$

where the length of the weight vector $\mathbf{w}^k$ is smaller than the frame size, and as before, the matrix $\mathbf{M}$ is used for zero-padding. Substituting the matrix $\mathcal{U}^k$ with its general decomposition form in (5.9), the emulated echo can be rewritten as

$$\hat{\mathbf{y}}_e^k = \mathcal{G}^H \mathcal{S}^k \mathcal{G} \mathbf{M} \mathbf{w}^k. \tag{5.11}$$

As discussed before, the separation dictates the available transformation matrices, where for the general case, the transformations are performed by the submatrices of $\mathcal{G}$. The emulated echo can be mapped into the dual domain, using the transformation matrix $\mathcal{G}$, i.e.,

$$\begin{aligned} \hat{\mathbf{Y}}_e^k &\triangleq \mathcal{G} \hat{\mathbf{y}}_e^k \\ &= \mathcal{G} \mathcal{G}^H \mathcal{S}^k \mathcal{G} \mathbf{M} \mathbf{w}^k. \end{aligned} \tag{5.12}$$

Based on (5.12), the transformed input data matrix is defined as

$$\mathbf{\Phi}^k = (\mathcal{S}^k)^H \mathcal{G} \mathcal{G}^H \tag{5.13}$$

and the mapped weight vector into the dual domain using $\mathcal{G}$ is expressed by

$$\boldsymbol{\omega}^k = \mathcal{G} \mathbf{M} \mathbf{w}^k. \tag{5.14}$$

Therefore, the estimated echo in the transform domain is given by

$$\hat{\mathbf{Y}}_e^k = (\mathbf{\Phi}^k)^H \boldsymbol{\omega}^k. \tag{5.15}$$

In order to use adaptive methods, e.g., LMS algorithm, for updating the weight vector, the error signal must be calculated. In the dual domain, the error signal is calculated by

$$\mathbf{E}^k = \mathbf{Y}^k - (\mathbf{\Phi}^k)^H \boldsymbol{\omega}^k \tag{5.16}$$

where $\mathbf{Y}^k$ is the transformed received signal $\mathbf{Y}^k = \mathcal{G}\,\mathbf{y}^k$. Using the LMS algorithm, the echo weights are updated by

$$\boldsymbol{\omega}^{k+1} = \boldsymbol{\omega}^k + \mu\,\mathbf{\Phi}^k\,\mathbf{E}^k. \tag{5.17}$$

Equations (5.16) and (5.17) jointly describe an adaptive dual domain echo canceller, where (5.17) performs an adaptation of the weight vector using the LMS method.

In the existing echo cancellers, the dual domain calculations are partially used in the echo emulation step but not in the weight update step in order to decrease the complexity. In these cancellers, a per-tone frequency-domain weight update is performed, using an approximate representation of the data matrix in order to reduce the complexity. The use of this approximation deteriorates the convergence of the adaptive algorithms and in some cancellers, e.g., CES canceller, makes it sensitive to the lack of excitation on the unused tones. However, as shown in the following, a computationally efficient weight update is achievable by the proposed dual domain structure.

The adaptive update in (5.17) is computationally costly because of the calculation involved for determining the matrix $\mathbf{\Phi}^k$. However, by substituting the value of $\mathbf{\Phi}^k$ from (5.13) and using the definition of the error signal in (5.16), the adaptive update

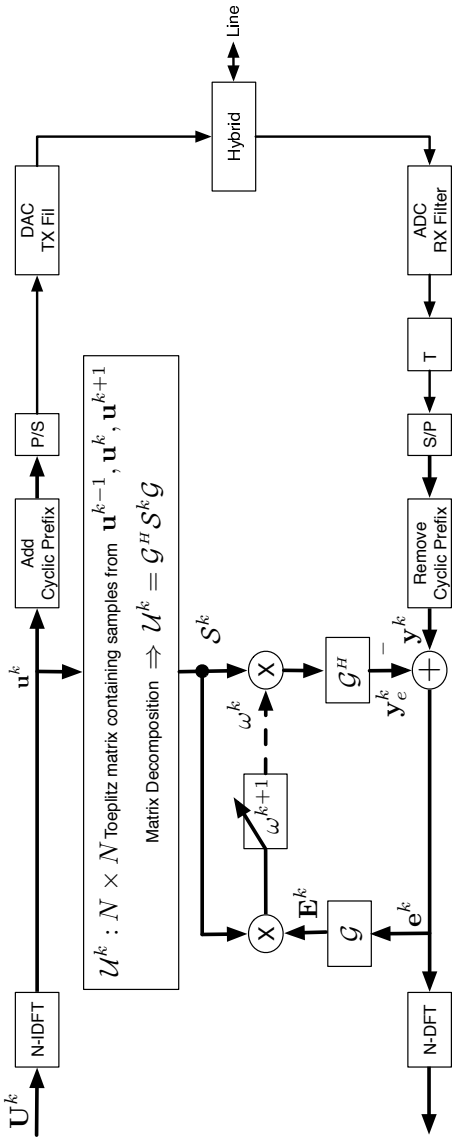

Fig. 5.1 Block diagram of the dual transform domain canceller (DTDC).

in (5.17) can be rewritten as

$$\boldsymbol{\omega}^{k+1} \;=\; \boldsymbol{\omega}^{k} + \mu\,(\mathcal{S}^{k})^{H}\,\mathcal{G}\,\mathcal{G}^{H}\left(\mathcal{G}\,\mathbf{y}^{k} \;-\; \mathcal{G}\,\mathcal{G}^{H}\,\mathcal{S}^{k}\,\boldsymbol{\omega}^{k}\right). \tag{5.18}$$

Since, the submatrices of $\mathcal{G}$ are unitary matrices, $\mathcal{G}^{H}\mathcal{G} = 2\mathcal{I}_{N}$. Therefore, the weight update can be written as

$$\begin{aligned}\boldsymbol{\omega}^{k+1} &= \boldsymbol{\omega}^{k} + \bar{\mu}\,(\mathcal{S}^{k})^{H}\mathcal{G}\,\left(\mathbf{y}^{k} \;-\; \mathcal{G}^{H}\,\mathcal{S}^{k}\,\boldsymbol{\omega}^{k}\right)\\ &= \boldsymbol{\omega}^{k} + \bar{\mu}\,(\mathcal{S}^{k})^{H}\mathbf{E}^{k}.\end{aligned} \tag{5.19}$$

Equations (5.16) and (5.19) jointly describe an adaptive algorithm which we refer to as dual transform domain canceller (DTDC), and the block diagram for this structure is shown in Fig. 5.1. In this canceller, in order to avoid the calculations of the matrix $\boldsymbol{\Phi}^{k}$ in the emulation step, we note that the error signal is equivalent to:

$$\mathbf{E}^{k} = \mathbf{Y}^{k} - (\boldsymbol{\Phi}^{k})^{H}\,\boldsymbol{\omega}^{k} = \mathcal{G}\,\left(\mathbf{y}^{k} \;-\; \mathcal{G}^{H}\,\mathcal{S}^{k}\,\boldsymbol{\omega}^{k}\right). \tag{5.20}$$

Therefore, the estimated echo is calculated in the dual domain yet subtracted from the received signal in the time domain, which requires only one set of transformations. Then, the error signal is mapped into the dual domain, and the weights are updated in the dual domain entirely.

It should be noted that the DTDC structure provides a uniform representation of echo cancellers in the dual domain, and as a result establishes an analytical tool to study these algorithms from a unified prospective. Based on the DTDC structure, the criteria for an *appropriate* decomposition, in the sense of reducing the complexity,

can be determined. As it can be seen from (5.19), for a decomposition where the submatrices of $\mathcal{S}^k_{i,j}$ $(i,j=1,2)$ are diagonal or at most tridiagonal, the echo canceller weights can be updated without using any approximation and with low computational complexity. In addition, a decomposition is preferred where the transformations (defined by the submatrices of $\mathcal{G}$) can be implemented efficiently. As discussed in the next section, these conditions are satisfied by the symmetric decomposition, where the data matrix is decomposed as in (5.8).

5.3.2 Dual trigonometric canceller

As discussed above, for the proposed DTDC structure, the preferred decomposition should have at most tridiagonal $\mathcal{S}^k$ submatrices and the involved transformations must have an efficient implementation. The symmetric decomposition defined in (5.8), which is based on the discrete trigonometric transformations, satisfies both of these conditions. In this decomposition, the $\mathcal{S}^k$ submatrices have non-zero elements only on the main diagonal, on the sub-diagonal or on the super-diagonal. In addition, the required transformations for implementing this decomposition are discrete trigonometric transformers for which efficient algorithms are available [85].

We refer to this implementation of the DTDC structure using the symmetric decomposition as dual trigonometric canceller (DTC). The block diagram for this canceller is given in Fig. 5.2. In this canceller, the decomposition of the Toeplitz matrix is done by the DCT-I and DST-I defined in (3.51) and (3.52), respectively [85]. The estimated echo is calculated in the dual domain and afterwards mapped into the time domain using the inverse DCT-II and inverse DST-II defined in (3.45) and (3.46), respectively, to be subtracted from the received signal. The error signal is mapped

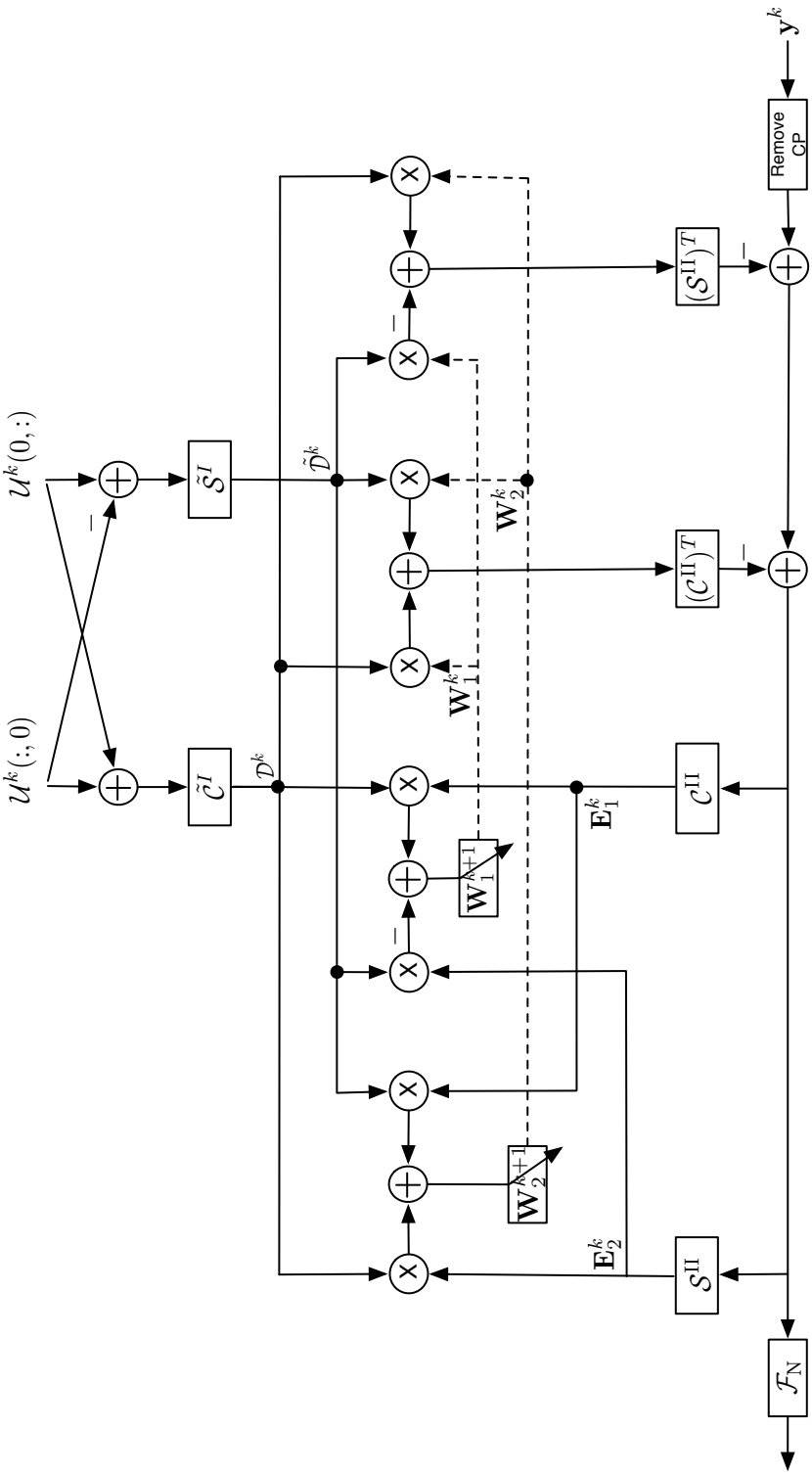

Fig. 5.2 Block diagram of the dual trigonometric canceller (DTC).

into the dual domain using the DCT-II and DST-II, and the weights are updated based on (5.19) in the dual domain. It should be noted that shift by the matrices $\mathcal{Z}$ and $\tilde{\mathcal{Z}}$ and conjugation is not shown in the block diagram, for readability.

In the next section, we show that the general decomposition framework and the dual domain canceller discussed in this section can be combined with the linear constrained structures discussed in Chapter 4.

5.4 Linearly Constrained Dual Domain Echo Cancellation

In the previous section, we have developed a general framework for echo cancellation in the dual domain. In addition, by using this structure, the DTC algorithm was proposed which is capable of performing an LMS adaptive weight update in the dual domain with reduced complexity. The DTDC structure, and as a result the DTC algorithm, perform an unconstrained optimization in the dual domain. However, for these algorithms, additional information is available because of the dual mapping of the weight vector. Therefore, it is of interest to develop a configuration which can benefit from this information towards improving the convergence of the canceller. This can be realized by establishing linearly constrained cancellers in the dual domain, where the relation between the weight vectors in the two domains is translated into linear constraints, which then can be included in the optimization of the weights.

In Chapter 4, we have developed linearly constrained cancellers based on mixed time- and frequency-domain filtering. In Section 5.4.1, a more generalized form of the linearly constrained cancellers is developed, where the weight vectors and signals can be in any dual transform domains. In Section 5.4.2, we examine a specific implementation of these constrained dual domain cancellers where the corresponding constraint

matrix ensures the proper relation between the weight vectors in the dual domain.

Later, in Section 5.5, the convergence behaviour and the computational complexity of the unconstrained and constrained dual domain cancellers are examined. In addition, it is shown that the combination of these two algorithms can provide a canceller with a faster convergence rate compared with those of the existing algorithms with similar computational complexity.

5.4.1 Linearly constrained dual transform domain canceller

In Chapter 4, we have shown that the echo cancellation can be formulated as a constrained optimization where the cost function, which is equal to the error signal, is minimized under certain constraints. Let us consider the error signal for the DTDC structure in the dual domain, given by

$$\mathbf{E}^k = \mathbf{Y}^k - (\mathbf{\Phi}^k)^H \boldsymbol{\omega}^k \tag{5.21}$$

where $\mathbf{Y}^k = \mathcal{G}\,\mathbf{y}^k$ and $\mathbf{\Phi}^k$ and $\boldsymbol{\omega}^k$are given by (5.13) and (5.14), respectively. The echo cancellation problem can be described by the following constrained optimization:

$$\min_{\boldsymbol{\omega}^k} \mathrm{E}[\|\mathbf{E}^k\|^2] \quad \text{s.t. } \mathcal{C}^H \boldsymbol{\omega}^k = \mathbf{g}. \tag{5.22}$$

In (5.22), $\boldsymbol{\omega}^k$ is the weight vector in the dual domain, the constraint matrix $\mathcal{C}$ is of size $(2N) \times l_c$ and the vector $\mathbf{g}$ is of length l_c, where l_c is the number of constraints.

Following similar justifications as in Section 4.2.1, the linearly constrained echo canceller based on the Frost method presented in [25] can be derived for the DTDC structure in the dual domain. For this constrained canceller, the adaptive weight

update equivalent to (4.15) is given by

$$\boldsymbol{\omega}^{k+1} \;=\; \boldsymbol{\omega}_q \;+\; \mathcal{P}_c^{\perp}\left(\boldsymbol{\omega}^k \;+\; \mu\,\boldsymbol{\Phi}^k\,\mathbf{E}^k\right) \tag{5.23}$$

where $\boldsymbol{\omega}_q = \mathcal{C}(\mathcal{C}^H\mathcal{C})^{-1}\mathbf{g}$ and $\mathcal{P}_c^{\perp}$ is defined as in (4.11) based on the matrix $\mathcal{C}$ and the vector $\mathbf{g}$.

It should be noted that the main difference between the constrained dual domain canceller described in this section and the constrained canceller developed in Section 4.2.1 is the domains in which the signals and weight vectors are represented. In the latter, the signals and weight vectors are either in the time or frequency domain, while in the constrained dual domain canceller, the weight vectors and signals can belong to any domain defined by the submatrices of $\mathcal{G}$. Therefore, different realizations of the constrained dual domain canceller can be obtained by choosing different decompositions of the Toeplitz data matrix, which results in different transform submatrices of $\mathcal{G}$.

Likewise, the constrained dual domain canceller based on the GSC approach presented in [26] can be derived, as in Section 4.2.2. For this canceller the weight vector in the dual domain can be written as a sum of two components, i.e.,

$$\boldsymbol{\omega}^k = \boldsymbol{\omega}_c^k + \boldsymbol{\omega}_b^k \tag{5.24}$$

where $\boldsymbol{\omega}_c^k = \mathcal{C}(\mathcal{C}^H\mathcal{C})^{-1}\mathbf{g} = \boldsymbol{\omega}_q$ is the projection of $\boldsymbol{\omega}^k$ onto the constraint subspace and $\boldsymbol{\omega}_b^k = \mathcal{B}\,\boldsymbol{\omega}_a^k$ is the projection onto the orthogonal subspace. For this canceller, the blocking matrix $\mathcal{B}$ can be any $(2N-l_c)\times 2N$ full-rank matrix with columns orthogonal to the columns of the constraint matrix $\mathcal{C}$, i.e., $\mathcal{B}^H\,\mathcal{C} = \mathcal{O}_{(2N-l_c)\times l_c}$.

Similar to the development in the previous chapter, the adaptive component of $\boldsymbol{\omega}^k$ for the constrained dual domain canceller based on the GSC approach can be updated in a similar way to (4.25) by

$$\boldsymbol{\omega}_a^{k+1} = \boldsymbol{\omega}_a^k + \mu \, \boldsymbol{\Phi}_b^k \, \mathbf{E}^k \tag{5.25}$$

where $\boldsymbol{\Phi}_b^k = \mathcal{B}^H \, \boldsymbol{\Phi}^k$. As noted earlier, the above dual domain canceller differs from its counterpart in Section 4.2.2 in terms of the domains where the computations are performed.

5.4.2 Implementation of the linearly constrained dual transform domain canceller

In the previous section, we have developed a linearly constrained canceller based on the DTDC structure. Different realizations of this canceller can be obtained by adopting different decompositions of the Toeplitz data matrix and different choices of the constraint matrix. For example, by employing the symmetric decomposition, a linearly constrained canceller based on the DTC algorithm is obtained. A complete description of the constrained canceller also requires defining a set of constraints. In the following, we discuss a set of linear constraints proper for the dual domain implementation and derive the constrained canceller based on the Frost method using these constraints.

In the dual domain, the weight vector has two components $\boldsymbol{\omega}_1^k$ and $\boldsymbol{\omega}_2^k$ which are the transformations of the time-domain weight vector $\mathbf{w}^k$ by the submatrices of $\mathcal{G}$, $\mathcal{G}_1$

and $\mathcal{G}_2$, respectively, i.e.,

$$\boldsymbol{\omega}^k = \begin{bmatrix} \boldsymbol{\omega}_1^k \\ \boldsymbol{\omega}_2^k \end{bmatrix} = \begin{bmatrix} \mathcal{G}_1 \\ \mathcal{G}_2 \end{bmatrix} \mathbf{M}\, \mathbf{w}^k. \tag{5.26}$$

The proposed constraint matrix includes constraints to ensure the proper relationship between the mapped weight vectors $\boldsymbol{\omega}_1^k$ and $\boldsymbol{\omega}_2^k$ in the dual domain. In addition, it includes constraints for the practical cases where the length of the FIR filter modeling the echo channel is smaller than the frame size, i.e., $T_e < N$. For these cases, the last $N - T_e$ weights of the inverse transformations of $\boldsymbol{\omega}_1^k$ and $\boldsymbol{\omega}_2^k$ into the time domain (tail weights of the impulse response) are forced to zero.

The weight vectors $\boldsymbol{\omega}_1^k$ and $\boldsymbol{\omega}_2^k$ are related, since they should have equal inverse transformations in the time domain. This association can be conveyed into linear constraints where the first T_e weights of the inverse transformations of the vectors $\boldsymbol{\omega}_1^k$ and $\boldsymbol{\omega}_2^k$ into the time domain are forced to be equal, as expressed by

$$\mathbf{M}^T\, \mathcal{G}_1^H\, \boldsymbol{\omega}_1^k = \mathbf{M}^T\, \mathcal{G}_2^H\, \boldsymbol{\omega}_2^k \tag{5.27}$$

which yields T_e constraints.

To ensure that the $N - T_e$ tail weights of the inverse transformations of the vectors $\boldsymbol{\omega}_1^k$ and $\boldsymbol{\omega}_2^k$ into the time domain are equal to zero, the following constraints are used:

$$\tilde{\mathbf{M}}^T\, \mathcal{G}_1^H\, \boldsymbol{\omega}_1^k \;\; = \;\; \mathcal{O}_{N-T_e \times 1} \tag{5.28}$$

and

$$\tilde{\mathbf{M}}^T \mathcal{G}_1^H \boldsymbol{\omega}_2^k = \mathcal{O}_{N-T_e \times 1} \tag{5.29}$$

where the $N \times (N - T_e)$ matrix $\tilde{\mathbf{M}} \triangleq [\mathcal{O}_{(N-T_e)\times T_e} | \mathcal{I}_{(N-T_e)}]^T$ extracts the last $N - T_e$ tail weights in the time domain.

Incorporating these constraints into a single constraint matrix, the $2N \times (2N - T_e)$ full-rank constraint matrix $\mathcal{C}$ is given by:

$$\mathcal{C} = \begin{bmatrix} \mathcal{G}_1 \tilde{\mathbf{M}} & \mathcal{G}_1 \mathbf{M} & \mathcal{O}_{N \times N - T_e} \\ \mathcal{O}_{N \times N - T_e} & -\mathcal{G}_2 \mathbf{M} & \mathcal{G}_2 \tilde{\mathbf{M}} \end{bmatrix}. \tag{5.30}$$

In addition, considering the form in (5.22), the vector $\mathbf{g} = \mathcal{O}_{(2N-T_e)\times 1}$.

Using the above constraint matrix, we can develop a linearly constrained dual domain canceller based on the constrained LMS approach in (5.23). For this approach, we need to calculate the projection matrices $\mathcal{P}_c$ and $\mathcal{P}_c^{\perp}$ and the quiescent term $\boldsymbol{\omega}_q$, based on the given constraint matrix $\mathcal{C}$. Considering the constraint matrix $\mathcal{C}$ as in (5.30) and the relation between $\mathbf{M}$ and $\tilde{\mathbf{M}}$, where $\tilde{\mathbf{M}}\,\tilde{\mathbf{M}}^T + \mathbf{M}\,\mathbf{M}^T = \mathcal{I}_N$, the projection matrices $\mathcal{P}_c$ and $\mathcal{P}_c^{\perp}$ are as follows (The details are discussed in Appendix B.1):

$$\mathcal{P}_c = \begin{bmatrix} \mathcal{I}_N - \frac{1}{2}\mathcal{G}_1 \mathbf{M}\mathbf{M}^T \mathcal{G}_1^H & -\frac{1}{2}\mathcal{G}_1 \mathbf{M}\mathbf{M}^T \mathcal{G}_2^H \\ -\frac{1}{2}\mathcal{G}_2 \mathbf{M}\mathbf{M}^T \mathcal{G}_1^H & \mathcal{I}_N - \frac{1}{2}\mathcal{G}_2 \mathbf{M}\mathbf{M}^T \mathcal{G}_2^H \end{bmatrix}, \tag{5.31}$$

$$\mathcal{P}_c^{\perp} = \frac{1}{2} \begin{bmatrix} \mathcal{G}_1 \mathbf{M}\mathbf{M}^T \mathcal{G}_1^H & \mathcal{G}_1 \mathbf{M}\mathbf{M}^T \mathcal{G}_2^H \\ \mathcal{G}_2 \mathbf{M}\mathbf{M}^T \mathcal{G}_1^H & \mathcal{G}_2 \mathbf{M}\mathbf{M}^T \mathcal{G}_2^H \end{bmatrix} = \frac{1}{2} \mathcal{G} \mathbf{M}\mathbf{M}^T \mathcal{G}^H, \tag{5.32}$$

with $\boldsymbol{\omega}_q = \mathcal{O}_{2N\times 1}$, which can be easily verified using the definition of $\boldsymbol{\omega}_q$based on the constraint matrix $\mathcal{C}$ and the vector $\mathbf{g}$.

By substituting the values for $\mathcal{P}_c^{\perp}$ and $\boldsymbol{\omega}_q$ in (5.23), the adaptive weight update formula for the constrained dual transform domain canceller for the given constraint matrix is obtained as

$$\boldsymbol{\omega}^{k+1} = \frac{1}{2}\,\mathcal{G}\mathbf{M}\mathbf{M}^T\mathcal{G}^H\,(\boldsymbol{\omega}^k + \,\mu\,\boldsymbol{\Phi}^k\,\mathbf{E}^k). \tag{5.33}$$

Similar argument as in Section 5.3.1 can be used to show that (5.33) is equivalent to

$$\boldsymbol{\omega}^{k+1} = \frac{1}{2}\,\mathcal{G}\mathbf{M}\mathbf{M}^T\mathcal{G}^H\,(\boldsymbol{\omega}^k + \,\bar{\mu}\,(\mathcal{S}^k)^H\mathbf{E}^k). \tag{5.34}$$

The adaptive weight update in (5.34) expresses the constrained version of the DTDC algorithm for the chosen constraint matrix in (5.30). Like the unconstrained DTDC structure, the constrained one can also be implemented using the symmetric decomposition, resulting in a constrained DTC algorithm.

5.5 Computational Complexity and Convergence Behaviour of the Dual Domain Echo Cancellers

In Section 5.3, we have developed the general dual domain echo canceller structure, referred to as DTDC and its realization using the symmetric decomposition, referred to as DTC algorithm. In Section 5.4, we have shown that linear constraints can be added to these cancellers and the constrained versions of the DTDC and DTC algorithms based on the given constraint matrix in the dual domain were derived. In

this section, we study the performance of these dual domain cancellers and propose a new combined dual domain canceller.

In Section 5.5.1, a summary of the comparisons between the constrained and unconstrained dual domain cancellers in terms of the computational complexity and the convergence behaviour with the existing cancellers is provided and a new combined dual domain cancellers is proposed. The details of the complexity calculations and the discussion on the convergence behaviour of the dual domain cancellers are presented in Sections 5.5.2 and 5.5.3, respectively.

5.5.1 Combined dual transform domain canceller

In the Sections 5.5.2 and 5.5.3, the computational complexity and the convergence behaviour of the constrained and unconstrained DTC algorithms examined and compared with those of the existing echo cancellers. The summary of these comparisons is presented below to motivate a hybrid form of DTC algorithms.

The unconstrained DTC algorithm, as presented in Section 5.3.2, has a lower computational complexity than the time-domain LMS echo canceller and the CDC method. However, this unconstrained algorithm converges at a lower rate than the time-domain LMS canceller and the CDC method, but faster than the CES canceller. On the other hand, the constrained DTC algorithm converges faster than the CES and CDC algorithms and has a similar convergence rate to that of the time-domain LMS canceller. However, the constrained canceller has increased computational complexity compared with those of the CDC and SDC algorithms[2], which is still lower than that of the time-domain LMS canceller.

[2]It should be noted that the proposed SDC algorithm, as in [18], is presented only for symmetric rate cases and the authors claim that its convergence behaviour is similar to the CDC algorithm.

Table 5.1 Complexity calculation for the combined DTC algorithm.

Echo Emulation		**Adaptive Update**	
Operation	Complexity	Operation	Complexity
Decomposition of $\mathcal{U}^k$	$N\log_2 N - 2N + 2$	$\mathcal{G}\ \mathbf{e}^k$	$N\log_2 N$
$\mathcal{S}^k\boldsymbol{\omega}^k$	$4N$	$(\mathcal{S}^k)^H\ \mathbf{E}^k$	$4N$
$\mathcal{G}^H\ \hat{\mathbf{Y}}_e^k$	$N\log_2 N$	$\mathcal{G}\ \mathbf{M}\ \mathbf{M}^T\ \mathcal{G}^H$	$\frac{1}{\phi}(2N\log_2 N)$

Based on the above observations, we propose a *combined* DTC algorithm where the unconstrained and constrained DTC methods are used in combination with each other. In this combined algorithm, the structure of the unconstrained DTC algorithm as in Section 5.3.2 is mainly used, while infrequently the unconstrained adaptive weight update in (5.19) is replaced by the constrained adaptive weight update in (5.34).

For the combined DTC algorithm, the computational complexity of the algorithm is similar to those of the CDC and SDC algorithms, while it has a faster convergence rate which is very close to that of the time-domain LMS canceller. It should be noted that this algorithm is not sensitive to the lack of excitation on the unused tones in the frequency domain, unlike CES and CDC algorithms. This occurs because the proposed dual domain cancellers use the adaptive weight update without any approximation. Moreover, for the symmetric decomposition, the tap-input vectors do not relate to the frequency domain representation of the signal, and therefore, these vectors are not affected by the unused tones directly.

In Section 5.5.2, the computational complexity of the proposed DTC algorithms is compared with those of the existing cancellers. The convergence issues of the constrained and unconstrained dual domain cancellers are discussed in Section 5.5.3.

Table 5.2 Complexity comparison between the combined DTC algorithm and the existing echo cancellers.

Application	Echo Emulation	Adaptive Update	Total
LMS	$T_e\,N$	$T_e\,N$	$2T_e\,N$
CES	$2N + \frac{(T_e-\upsilon-1)^2}{2}$	$N\log_2 N - N + 4$	$N\log_2 N + N + \frac{(T_e-\upsilon-1)^2}{2} + 4$
CDC	$2N\log_2 N + N + 6$	$2N + \frac{1}{\psi}(1.5N\log_2 N - 2.5N + 6)^a$	$2N\log_2 N + 3N + 6$ $+\frac{1}{\psi}(1.5N\log_2 N - 2.5N + 6)$
SDC	$3N\log_2 N + 3N + 8$	$2N$	$3N\log_2 N + 5N + 8$
DTC	$2N\log_2 N + 2N + 2$	$N\log_2 N + 4N + \frac{1}{\phi}(2N\log_2 N)$	$3N\log_2 N + 6N + 2 + \frac{1}{\phi}(2N\log_2 N)$

[a] ψ relates to the infrequent updates of $\breve{\mathbf{W}}^k$ as given in (3.31).

5.5.2 Complexity analysis of dual domain echo cancellers

In this section, we evaluate the computational complexity of the proposed DTC algorithms and compare it with the complexity of the existing cancellers. As before, the complexity is expressed as the number of real multiplications at the symbol rate.

The complexity of each step of the combined DTC algorithm for a symmetric rate system is given in Table 5.1. In this canceller, the weights are updated by (5.19) and infrequently by (5.34), where the intervals between the infrequent constrained update is controlled by the parameter ϕ. Consequently, $\phi = 1$ corresponds to the constrained DTC algorithm and $\phi = \infty$ corresponds to the unconstrained DTC algorithm. In these calculations, the decomposition of the matrix $\mathcal{U}^k$ is done by using a $2N$-point FFT based on the method in [93], and the error signal is derived based on (5.20). For the DFT complexity, the split-radix FFT algorithm is assumed to be used, and for DCT and DST radix-2 fast recursive algorithm is used [94].

The complexity of the combined DTC algorithm is compared with those of the existing methods in Table 5.2. As it can be seen, the time-domain LMS method requires the biggest number of computations and the CES algorithm requires the least, however, the latter is sensitive to the lack of excitation on the unused tones. For large frame sizes, the SDC method is more efficient to implement than the CDC scheme.

The proposed combined DTC algorithm has approximately the same computational cost as the CDC and SDC methods. However, the combined DTC method convergences faster than the CES and CDC methods and does not suffer from the lack of excitation on the tap-input vector used in the update step. In addition, as shown in Section 5.6, the proposed combined DTC canceller also has a very suitable

structure for implementation in multirate systems.

5.5.3 Convergence analysis of dual domain echo cancellers

A comprehensive comparison of convergence rate between the proposed DTC algorithms and the existing cancellers is possible by means of computer simulations, where the results are given in Section 6.3. The simulated results show that the combined DTC algorithm has a convergence rate close to that of the time-domain LMS canceller which is faster than those of the CDC and CES algorithms. In this section, we provide some analytical tools to examine the convergence behaviour of the proposed dual domain algorithms.

The convergence of LMS-based algorithms can be studied by deriving the relating correlation matrix whose eigenvalue spread determines the convergence rate of the algorithm [8]. In this section, the convergence of the unconstrained and constrained dual domain algorithms is examined analytically by deriving their corresponding correlation matrices. In addition, using the DTC implementation, the eigenvalue spread of these correlation matrices is calculated and used as a measure to compare the convergence rate of different cancellers.

For studying the convergence of the proposed dual domain algorithms, we make the same assumptions as in [4, 16], which is generally used for proving the convergence of the LMS-based algorithms. We assume that the received signal can be modeled as the output of an FIR filter with additive white Gaussian noise with the noise uncorrelated to the transmitted echo symbols. In addition, the transmitted echo symbols are uncorrelated with each other and the frequency-domain elements within each symbol are also uncorrelated with each other. This assumption implies that the

samples of time-domain vectors from on sample period to the other are independent (excluding the prefix), which is not always valid in practice, but usually used to prove the convergence of echo cancellers.

To study the convergence of the unconstrained DTDC algorithm we can use the adaptive weight update as given by (5.19),

$$\boldsymbol{\omega}^{k+1} = \boldsymbol{\omega}^k + \bar{\mu}\,(\mathcal{S}^k)^H \mathbf{E}^k. \tag{5.35}$$

Substituting $\mathbf{E}^k$ from (5.16), the weight vector is updated by

$$\begin{aligned} \boldsymbol{\omega}^{k+1} &= \boldsymbol{\omega}^k + \bar{\mu}\,(\mathcal{S}^k)^H\,\mathcal{G}\,\left(\mathbf{y}^k - \mathcal{G}^H\,\mathcal{S}^k\boldsymbol{\omega}^k\right) \\ &= \left(\mathcal{I}_{2N} - \bar{\mu}\,(\mathcal{S}^k)^H\,\mathcal{G}\,\mathcal{G}^H\,\mathcal{S}^k\right)\boldsymbol{\omega}^k + \bar{\mu}\,(\mathcal{S}^k)^H\,\mathcal{G}\,\mathbf{y}^k. \end{aligned} \tag{5.36}$$

If the optimal transformed weight vector $\mathbf{H} \triangleq \mathcal{G}\,\mathbf{h}$ is subtracted from both sides of (5.36), and the resulting weight-error vector $\Delta^k \triangleq \boldsymbol{\omega}^k - \mathbf{H}$ is given by

$$\begin{aligned} \Delta^{k+1} &= \left(\mathcal{I}_{2N} - \bar{\mu}\,(\mathcal{S}^k)^H\,\mathcal{G}\,\mathcal{G}^H\,\mathcal{S}^k\right)\Delta^k \\ &\quad + \bar{\mu}\,(\mathcal{S}^k)^H\,\mathcal{G}\,\underbrace{\left(\mathbf{y}^k - \mathcal{G}^H\,\mathcal{S}^k\,\mathbf{H}\right)}_{\mathbf{n}^k}. \end{aligned} \tag{5.37}$$

When taking the expectation on both sides of the equation, the term on the last line is cancelled, since the received noise $\mathbf{n}^k$ and the input data are uncorrelated. Furthermore, since the data vectors are uncorrelated, the expectation of the product of weight-error vector and transformed input data can be separated, resulting in

$$\mathrm{E}[\Delta^{k+1}] = \mathrm{E}[\mathcal{I}_{2N} - \bar{\mu}\,(\mathcal{S}^k)^H\,\mathcal{G}\,\mathcal{G}^H\,\mathcal{S}^k]\,\mathrm{E}[\Delta^k]. \tag{5.38}$$

Therefore, the convergence rate for the mean weight-error vector of the unconstrained DTDC algorithm is determined by the correlation matrix $\mathcal{R}_{\text{UC}} = \text{E}[(\mathcal{S}^k)^H \mathcal{G}\,\mathcal{G}^H \mathcal{S}^k]$.

For the constrained DTDC algorithm, as shown in [25], if the linearly constrained algorithm based on the Frost method is used, the correlation matrix corresponding to the constrained algorithm can be derived based on the correlation matrix of the unconstrained algorithm. In this case, the correlation matrix of the constrained algorithm denoted by $\mathcal{R}_{\text{C}}$ is given by

$$\mathcal{R}_{\text{C}} = \mathcal{P}_c^{\perp}\, \mathcal{R}_{\text{UC}}\, \mathcal{P}_c^{\perp}, \tag{5.39}$$

where $\mathcal{P}_c^{\perp}$ is the projection matrix and the $\mathcal{R}_{\text{UC}}$ is the correlation matrix of the unconstrained algorithm.

Using the above relationship between the correlation matrix of the constrained algorithm $\mathcal{R}_{\text{C}}$ and the one of the unconstrained algorithm $\mathcal{R}_{\text{UC}}$, we show, in Appendix B.2, that the correlation matrix determining the convergence of the constrained DTDC algorithm has the same non-zero eigenvalues as the correlation matrix corresponding to the time-domain LMS canceller. Therefore, the time-domain LMS canceller and the constrained DTDC algorithms have similar eigenvalue spread and as a result have a similar convergence rate. It should be noted that these results agree with the simulation observations in Section 6.3, where the convergence behaviour of the constrained DTC algorithm is similar to that of the time-domain LMS echo canceller.

The eigenvalue spread can also be evaluated numerically, where the results for different echo cancellation algorithms are given in Table 5.3. These results are based on the simulated sample covariance matrix and are obtained by assuming a symmetric rate at the transmitter and the receiver, equal length of the echo channel with the

Table 5.3 Simulated eigenvalue spread for different echo cancellation algorithms.

LMS EC	CES EC	CDC	Unconstrained DTC	Constrained DTC
3.2	11.9	14.8	15.7	3.2

frame size and having excitation on all tones.

As it can be seen, the time-domain LMS echo canceller and constrained DTC algorithm have the same eigenvalue spread which is in agreement with the discussion above. Comparing the results for the unconstrained DTC, CES and CDC algorithms, at first it may seem that the CES and CDC algorithms will achieve faster convergence as compared to the unconstrained DTC method. However, these results do not reflect the effect of the insufficient excitation caused by unused tones in the frequency domain and also the error caused by the use of an approximate weight vector in the frequency domain in the CES and CDC algorithms. In practice, these factors deteriorate the performance of the CES and CDC algorithms and more realistic comparisons of convergence rate, as noted before, is possible by simulating learning curves which is provided in Section 6.3.

5.6 Multirate Dual Domain Echo Cancellation

In the previous sections, we have discussed the dual domain cancellers for symmetric rate systems, where the frame size at the RT and the CO transceivers are equal. As discussed in Chapter 3, echo cancellers designed for DSL systems are required to operate in multirate scenarios. In this section, we present the expansion of the dual domain cancellers for the multirate systems. Two implementations are presented for the cancellers both at the RT and the CO transceivers: the direct approach and the

polyphase decomposition approach, where we show that the latter results in a more efficient implementation of the dual domain cancellers. It should be noted that the use of the polyphase decomposition in the context of multirate systems was first discussed in [17]; here we approach this aspect from the more general prospective of the dual domain.

In the Section 5.6.1 and 5.6.2, we discuss the decimated DTDC and the interpolated DTDC algorithms, respectively, for both including the direct and the polyphase approaches. Finally, these algorithms are implemented using DTC implementation, and the complexity of the direct and polyphase methods are compared in Section 5.6.3.

In the following, for simplicity, we denote the zero-padded time-domain weight vector as $\tilde{\mathbf{w}}^k \triangleq \mathbf{M}\,\mathbf{w}^k$, and since the filter weights are always defined at the higher data rate, $\tilde{\mathbf{w}}^k$ has the length κN, and the $\kappa N \times T_e$ matrix $\mathbf{M} \triangleq [\mathcal{I}_{T_e}|\mathcal{O}_{T_e\times(\kappa N-T_e)}]^T$.

5.6.1 Decimated Dual Domain Echo Cancellers

Direct approach decimated DTDC

As discussed in Chapter 3, at the CO transceiver, the effect of the aliasing occurred because of the non-ideal anti-aliasing filter at the ADC, which is modeled by decimating the emulated echo calculated at the high data rate. In this case, the emulated echo is expressed in the time domain by

$$\hat{\mathbf{y}}_e^k = \mathbf{D}\,\mathcal{U}^k\,\tilde{\mathbf{w}}^k. \tag{5.40}$$

In (5.40), $\mathcal{U}^k$ and $\tilde{\mathbf{w}}^k$ are the Toeplitz data matrix and the zero-padded time-domain weight vector, respectively at the higher data rate. That is, matrix $\mathcal{U}^k$ has the

dimension $\kappa N \times \kappa N$ and vector $\tilde{\mathbf{w}}^k$ has the length κN, and the $N \times \kappa N$ matrix $\mathbf{D} = \mathcal{I}_{\kappa N}[1 : \kappa : \kappa N\,, :]$ in (5.40) performs the downsampling. The data matrix $\mathcal{U}^k$ can now be decomposed, i.e.,

$$\mathcal{U}^k = \mathcal{G}_{\kappa N}^H \mathcal{S}^k \mathcal{G}_{\kappa N} \tag{5.41}$$

where $\mathcal{G}_{\kappa N}$has dimension $2\kappa N \times \kappa N$, and $\mathcal{S}^k$ matrix has dimension $2\kappa N \times 2\kappa N$. Hence, if the matrix $\mathcal{U}^k$ is replaced by its decomposition in (5.41), the emulated echo in the dual domain is given by

$$\hat{\mathbf{Y}}_e^k = \mathcal{G}_N \, \mathbf{D} \, \mathcal{G}_{\kappa N}^H \, \mathcal{S}^k \, \mathcal{G}_{\kappa N} \tilde{\mathbf{w}}^k \tag{5.42}$$

$$= (\mathbf{\Phi}_{\text{dec}}^k)^H \, \boldsymbol{\omega}^k. \tag{5.43}$$

In (5.42), the mapping into the dual domain, done after the downsampling, is performed at the lower rate, i.e., $\mathcal{G}_N$ has dimension $2N \times N$. As a result, in (5.43), the matrix $\mathbf{\Phi}_{\text{dec}}^k$ has dimension $2\kappa N \times 2N$, and the transformed weight vector $\boldsymbol{\omega}^k = \mathcal{G}_{\kappa N} \tilde{\mathbf{w}}^k$ is of length $2\kappa N$.

The block diagram for the direct approach decimated DTDC algorithm is shown in Fig. 5.3. Since, the weights are updated at the higher rate, the error signal must be upsampled in the time domain $\mathbf{e}_{\text{int}}^k$ and transformed into the dual domain $\mathbf{E}_{\text{int}}^k = \mathcal{G}_{\kappa N} \mathbf{e}_{\text{int}}^k$. Using the interpolated error signal $\mathbf{E}_{\text{int}}^k$, the weights are updated as:

$$\boldsymbol{\omega}^{k+1} = \boldsymbol{\omega}^k + \, \mu \, (\mathcal{S}^k)^H \, \mathbf{E}_{\text{int}}^k. \tag{5.44}$$

As it can be seen, in this implementation, the decomposition of the matrix $\mathcal{U}^k$ and the mapping of error signal are done at the higher data rate. Following, we show that

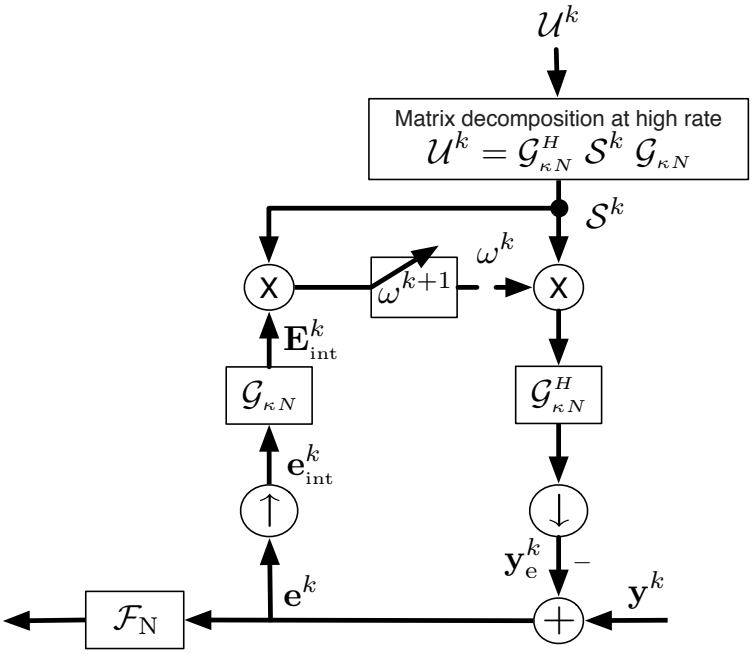

Fig. 5.3 Decimated DTDC structure using direct approach, at CO transceiver

these calculations can be done at the lower rate after proper modifications, which results in reduced complexity.

Decimated DTDC based on polyphase approach

In this approach, the polyphase components of the time-domain signals and weight vectors are used to achieve a more efficient implementation of the cancellers. The decimated emulated echo, in (5.40), can be rewritten in terms of the polyphase components of the input data matrix and those of the weight vector, i.e.,

$$\hat{\mathbf{y}}^k_e = \sum_{l=1}^{\kappa} \mathcal{U}^k_l\, \tilde{\mathbf{w}}^k_l \tag{5.45}$$

where the $N \times N$ polyphase matrices of matrix $\mathcal{U}^k$ are $\mathcal{U}_l^k \triangleq \mathcal{U}^k[1 : \kappa : \kappa N\,,\, l : \kappa : \kappa N]$, and the length N polyphase components of $\mathbf{w}^k$ are $\tilde{\mathbf{w}}_l^k \triangleq \tilde{\mathbf{w}}^k[l : \kappa : \kappa N]$. It can be easily verified that the polyphase matrices $\mathcal{U}_l^k$ are Toeplitz matrices; therefore, each one of them can be decomposed as in (5.9). In this case the decomposition $\mathcal{U}_l^k = \mathcal{G}_N^H \mathcal{S}_l^k \mathcal{G}_N$ is done at the lower data rate. Using these decompositions, (5.45) can be rewritten as

$$\hat{\mathbf{y}}_e^k = \sum_{l=1}^{\kappa} \mathcal{G}_N^H \, \mathcal{S}_l^k \, \mathcal{G}_N \, \tilde{\mathbf{w}}_l^k. \tag{5.46}$$

Therefore, the transformed emulated echo is given by

$$\hat{\mathbf{Y}}_e^k = \mathcal{G}_N \hat{\mathbf{y}}_e^k = \sum_{l=1}^{\kappa} (\mathbf{\Phi}_l^k)^H \boldsymbol{\omega}_l^k, \tag{5.47}$$

where the $2N \times 2N$ matrices $\mathbf{\Phi}_l^k = (\mathcal{S}_l^k)^H \mathcal{G}_N \mathcal{G}_N^H$ and the transformed weight vectors $\boldsymbol{\omega}_l^k = \mathcal{G}_N \tilde{\mathbf{w}}_l^k$ have length $2N$. The $\mathbf{\Phi}_l^k$ matrices can be calculated using only the transformations at the lower data rate, unlike the direct approach.

The error signal, calculated from (5.16), can now be used directly to adaptively update the polyphase weight vectors $\boldsymbol{\omega}_l^k$, i.e.,

$$\boldsymbol{\omega}_l^{k+1} = \boldsymbol{\omega}_l^k + \, \mu \, (\mathcal{S}_l^k)^H \mathbf{E}^k \quad \text{for } l = 1, \cdots, \kappa. \tag{5.48}$$

The block diagram for the resulting canceller is shown in Fig. 5.4, where the polyphase decomposition is used to replace the transformation at the higher data rate with multiple transformations at a lower rate. This approach, as explained later, requires less computations.

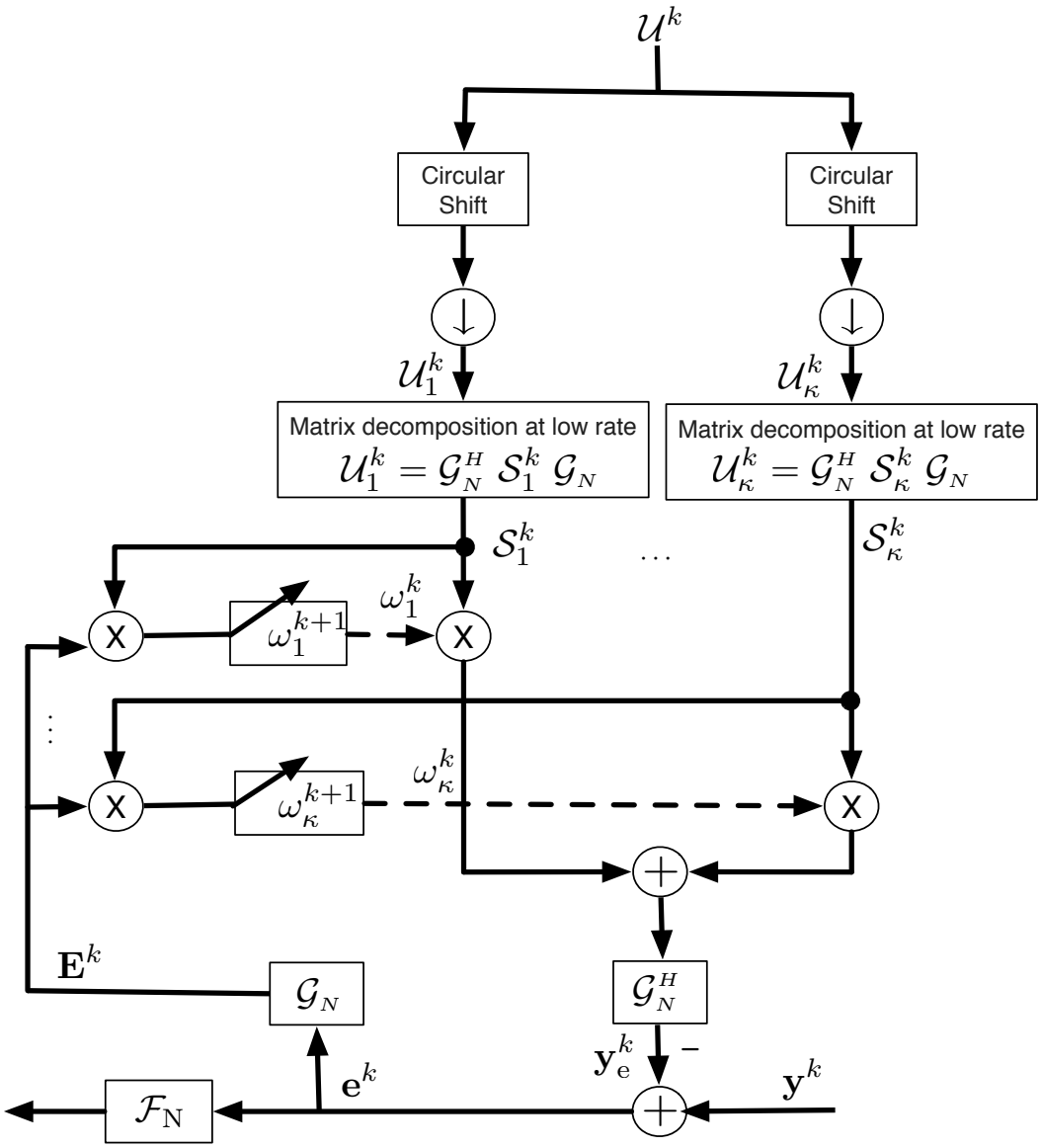

Fig. 5.4 Decimated DTDC structure using polyphase approach, at CO transceiver

5.6.2 Interpolated Dual Domain Echo Cancellers

Direct approach interpolated DTDC

As discussed in Chapter 3, at the RT transceiver, the effect of the aliasing occurred because of the non-ideal reconstruction filter at the DAC, which is modeled by interpolating the transmitted signal before the emulation. Therefore, the emulated echo is given by

$$\hat{\mathbf{y}}_e^k = \mathcal{U}_{\text{int}}^k \, \tilde{\mathbf{w}}^k \tag{5.49}$$

where the $\kappa N \times \kappa N$ matrix $\mathcal{U}_{\text{int}}^k$ contains the upsampled transmitted samples, and vector $\tilde{\mathbf{w}}^k$ is the zero-padded weight vector at the higher data rate. The interpolated data matrix $\mathcal{U}_{\text{int}}^k$ is then decomposed at the higher rate, i.e., $\mathcal{U}_{\text{int}}^k = \mathcal{G}_{\kappa N}^H \mathcal{S}_{\text{int}}^k \mathcal{G}_{\kappa N}$. Based on this decomposition, the transformed emulated echo is given by

$$\begin{aligned} \hat{\mathbf{Y}}_e^k &= \mathcal{G}_{\kappa N} \, \mathcal{G}_{\kappa N}^H \, \mathcal{S}_{\text{int}}^k \, \mathcal{G}_{\kappa N} \, \tilde{\mathbf{w}}^k \\ &= (\mathbf{\Phi}_{\text{int}}^k)^H \, \boldsymbol{\omega}^k, \end{aligned} \tag{5.50}$$

where the $2\kappa N \times 2\kappa N$ matrix $\mathbf{\Phi}_{\text{int}}^k$ is calculated based on the interpolated matrix $\mathcal{S}_{int}^k$, and the transformed weight vector $\boldsymbol{\omega}^k$ is of length $2\kappa N$. The block diagram for the direct approach interpolated DTDC algorithm is shown in Fig. 5.5. In this canceller, the error signal calculated from (5.16) can be used to update the weights by

$$\boldsymbol{\omega}^{k+1} = \boldsymbol{\omega}^k + \, \mu \, (\mathcal{S}_{\text{int}}^k)^H \, \mathbf{E}^k. \tag{5.51}$$

As it can be seen, in the direct approach, the decomposition of the matrix $\mathcal{U}_{\text{int}}^k$ and

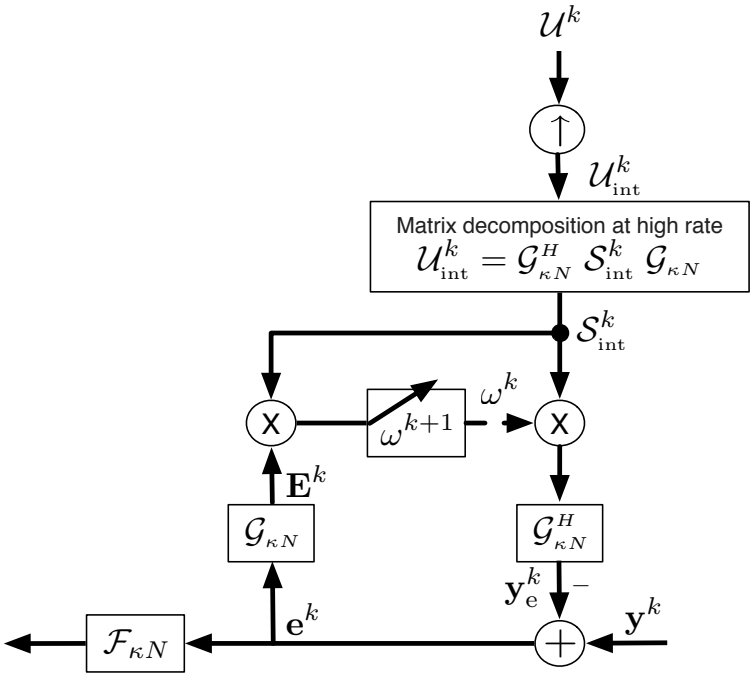

Fig. 5.5 Interpolated DTDC structure using direct approach, at RT transceiver

the mapping involved in $\mathbf{\Phi}^k_{\text{int}}$ need to be done at the higher data rate. Similar to the decimated DTDC, the polyphase decomposition can be used to reduce the computational complexity of this algorithm, as explained below.

Interpolated DTDC based on polyphase approach

At the RT transceiver, the emulated echo, in (5.49), can be expressed in terms of the matrix $\mathcal{U}^k$ which contains the input data before the upsampling, i.e.,

$$\hat{\mathbf{y}}^k_e = \sum_{l=1}^{\kappa} \mathbf{D}_{\kappa N,l}\, \mathcal{U}^k\, \tilde{\mathbf{w}}^k_l, \tag{5.52}$$

where the polyphase component vectors of $\tilde{\mathbf{w}}^k$ are $\tilde{\mathbf{w}}_l^k = \tilde{\mathbf{w}}^k[l : \kappa : \kappa N]$. In (5.52), the $\kappa N \times N$ matrices $\mathbf{D}_{\kappa N,l} \triangleq \mathcal{I}_{\kappa N}[:, l : \kappa : \kappa N]$ are used to upsample the emulated echo properly.

Therefore, the matrix $\mathcal{U}^k$ can now be decomposed at the lower data rate, i.e., $\mathcal{U}^k = \mathcal{G}_N^H \mathcal{S}^k \mathcal{G}_N$. Consequently, the mapped emulated echo in the dual domain is given by

$$\hat{\mathbf{Y}}_e^k = \sum_{l=1}^{\kappa} \mathcal{G}_{\kappa N}\, \mathbf{D}_{\kappa N,l}\, \mathcal{G}_N^H\, \mathcal{S}^k\, \mathcal{G}_N\, \tilde{\mathbf{w}}_l^k \tag{5.53}$$

which can be rewritten as

$$\hat{\mathbf{Y}}_e^k = \sum_{l=1}^{\kappa} (\mathbf{\Phi}_l^k)^H \boldsymbol{\omega}_l^k, \tag{5.54}$$

where the $2N \times 2\kappa N$ matrices $\mathbf{\Phi}_l^k = (\mathcal{S}^k)^H\, \mathcal{G}_N\, (\mathbf{D}_{\kappa N,l})^T\, \mathcal{G}_{\kappa N}^H$, and the transformed weight vectors $\boldsymbol{\omega}_l^k = \mathcal{G}_N \tilde{\mathbf{w}}_l^k$. The error signal at the high rate can be calculated from (5.16); however to reduce the complexity, it is preferable to employ polyphase error vectors $\mathbf{E}_l^k$'s, the latter being defined as

$$\mathbf{E}_l^k = \mathcal{G}_N \mathbf{e}_l^k \quad \text{for } l = 1, \cdots, \kappa. \tag{5.55}$$

which correspond to the dual domain transformation of the polyphase vectors of the error in the time domain $\mathbf{e}_l^k$.

Finally, the polyphase weight vectors can be updated adaptively using the resulting error vectors, as given by

$$\boldsymbol{\omega}_l^{k+1} = \boldsymbol{\omega}_l^k + \mu\, (\mathcal{S}^k)^H \mathbf{E}_l^k \quad \text{for } l = 1, \cdots, \kappa \tag{5.56}$$

where $\mathbf{E}_l^k$ is defined in (5.55). The block diagram for this canceller is shown in Fig. 5.6,

where the polyphase decomposition of the time-domain signals has been used to avoid the high dimensional computations and reduce the complexity of implementation.

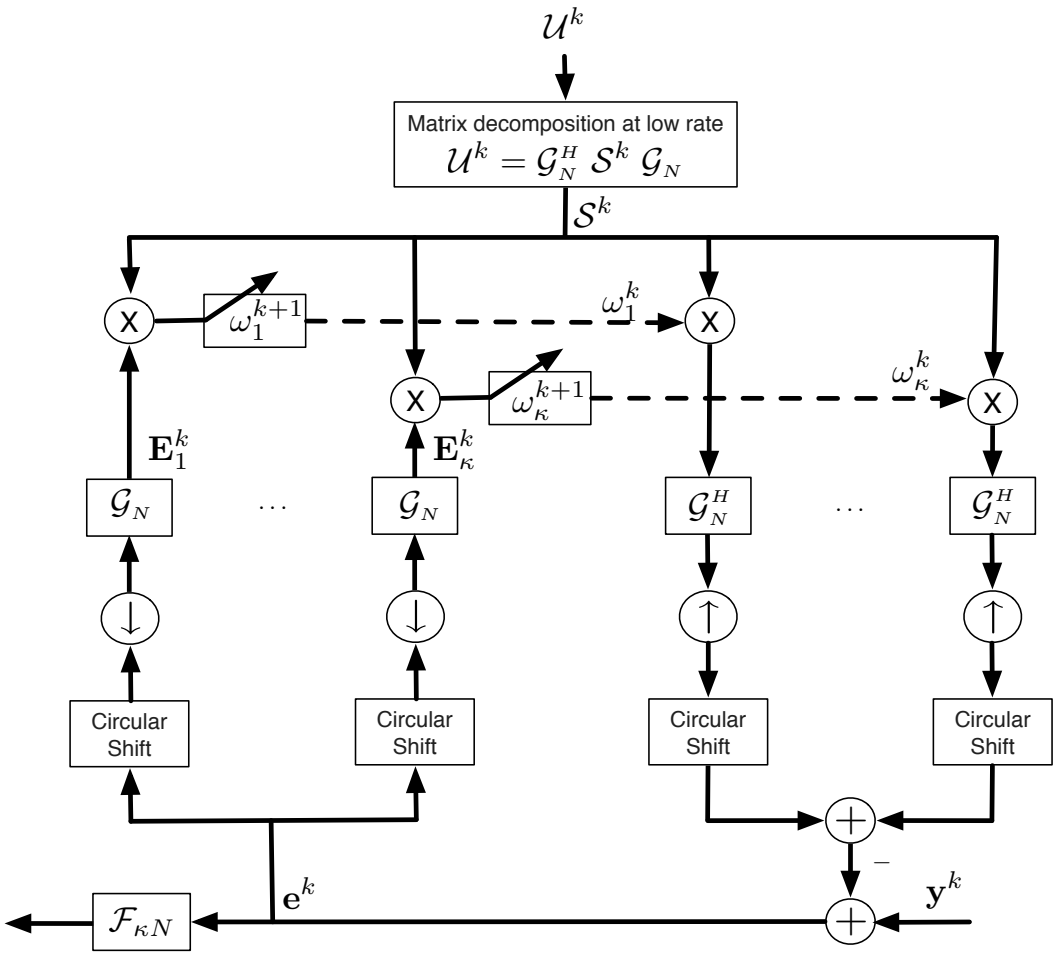

Fig. 5.6 Interpolated DTDC structure using polyphase approach, at RT transceiver

5.6.3 Multirate dual trigonometric canceller

As discussed in Section 5.3, the DTDC structure can be realized efficiently using the symmetric decomposition, which is based on the discrete trigonometric transformations, referred to as DTC algorithm. The algorithms discussed above for multirate

DTDC structure can be used directly for implementing multirate DTC realization as expected. In the DTC method, as discussed in Section 5.3.2, the decomposition of the Toeplitz matrix is done by the DCT-I and DST-I and the mapping into the dual domain is performed by unitary DCT-II and DST-II transformations.

In Table 5.4, the computational complexity of the proposed direct and polyphase approaches for both decimated and interpolated DTC algorithm are computed. The complexity is expressed as the number of real multiplications at symbol rate. For the DCT and DST and for the decomposition of the matrix $\mathcal{U}^k$ the split-radix FFT is used. This comparison shows that by using the polyphase approach, the transformations at the higher data rate can be replaced by multiple transformations at the lower rate, which reduces the complexity considerably. In addition, the polyphase approach does not affect the performance of the canceller, compared with the direct approach.

It should be noted that the discussion in this section is mainly focused on the unconstrained dual domain cancellers. However, it can easily be verified that the constraint gradient applied in (5.34) can also be applied to the polyphase decompositions of the weight vector. Therefore the multirate cancellers based on the polyphase decomposition approach derived in this section can also be used for the constrained dual domain cancellers.

5.7 Summary

In this chapter, we have studied the dual transform domain echo cancellation for DMT-based systems, in detail. We have presented the general form decomposition for the Toeplitz data matrix and shown that this general form provides a uniform description of the decompositions used in the existing echo cancellers. Based on the proposed

two-step design procedure, a new dual transform domain canceller (DTDC) has been proposed. We also showed that for this configuration, the appropriate decomposition is the symmetric decomposition, which results in an implementation referred to as dual trigonometric canceller (DTC).

Later, presented the linear constrained dual domain cancellers, where additional constraints can be added to the system to improve its performance. Using the constrained and unconstrained dual domain infrastructures, we proposed a combined dual domain canceller which has a faster convergence rate, where compared to the existing cancellers with similar computational complexity. This structure is also robust against the lack of excitation on the unused tones and does not require the transmission of dummy data on the unused tones. Finally, we have shown that the proposed structures can be efficiently implemented in multirate systems.

Table 5.4 Complexity comparison between the polyphase approach and the direct approach for the multirate DTC algorithm

Application	Direct approach	Polyphase approach
DTC - CO	$3\kappa N \log_2 \kappa N + 6\kappa N + 2$	$(\kappa N + 2N) \log_2 N + 6\kappa N + 2\kappa$
DTC - RT	$2\kappa N \log_2 \kappa N + N \log_2 N + 8\kappa N - 2N + 2$	$(2\kappa N + N) \log_2 N + 8\kappa N - 2N + 2$

Chapter 6

Simulation Results

This chapter presents and discusses the results of the computer simulation experiments relating to the contributions of this thesis. In Section 6.1, the system model used in the simulations is presented in detail. This discussion covers the modeling of different parts of the system, such as the DSL channel, the echo channel and the various sources of interference. In addition, the structure of the transmitter and receiver, including the digital and analog sub-systems. In Section 6.2, the linearly constrained echo cancellers, proposed in Chapter 4, are implemented and their performance is examined. In Section 6.3, the dual transform domain echo cancellers, established in Chapter 5, are implemented and their performance are compared with that of existing echo cancellers.

6.1 Methodology

As discussed earlier, we utilize an ADSL framework in this thesis. In the following, we discuss the modeling of different parts of an ADSL system, such as test loops, hybrid

circuit and analog and digital parts of the transceiver. Also the techniques to model and simulate various interferences present in this medium, including the Gaussian noise and radio frequency interference is addressed.

6.1.1 ADSL channel modeling

One of the main steps in simulating a communication link is modeling the transmission channel. Because of the wide variety in existing ADSL lines, in simulations, the performance of the echo canceller systems is examined over some standard test loops, known as carrier serving area (CSA). These test loops have various configuration limited to 12 kft, and consisting of non-loaded twisted pairs with or without bridged taps, as illustrated in Fig. 6.1 [45]. As discussed in Section 2.3.2, the transfer function of the line can be derived based on the ABCD modeling [95] by using the primary parameters of line per unit length (including the series and shunt impedances). Using this method the impulse responses for the CSA test loops have been calculated for the downstream and upstream direction, as shown in Fig. 6.2 (a)–(b) and Fig. 6.2 (c)–(d), respectively. [1]

6.1.2 Echo channel modeling

As discussed in Section 2.3.5, in DSL systems, the downstream and the upstream data are sent over a single pair of wires and the hybrid circuit is used to perform the conversion from the two-wire network to the four-wire network. The impedance mismatch in the hybrid circuitry results in a leakage of the transmitted signal into the collocated transceiver, the effect known as echo. In order to calculate the echo at the

[1] The details of the derivation of the impulse response are beyond the scope of this text, for details refer to [45].

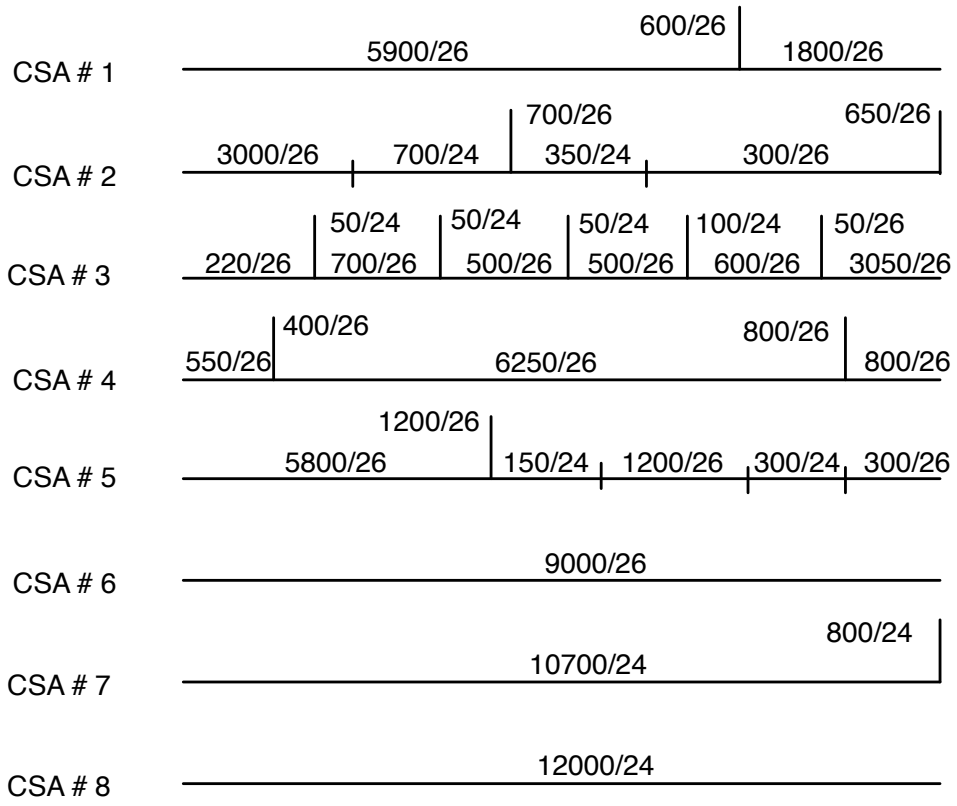

Fig. 6.1 Configuration of CSA test loops, the first number denotes the loop lengths in ft and the second one is the wire gauge in AWG.

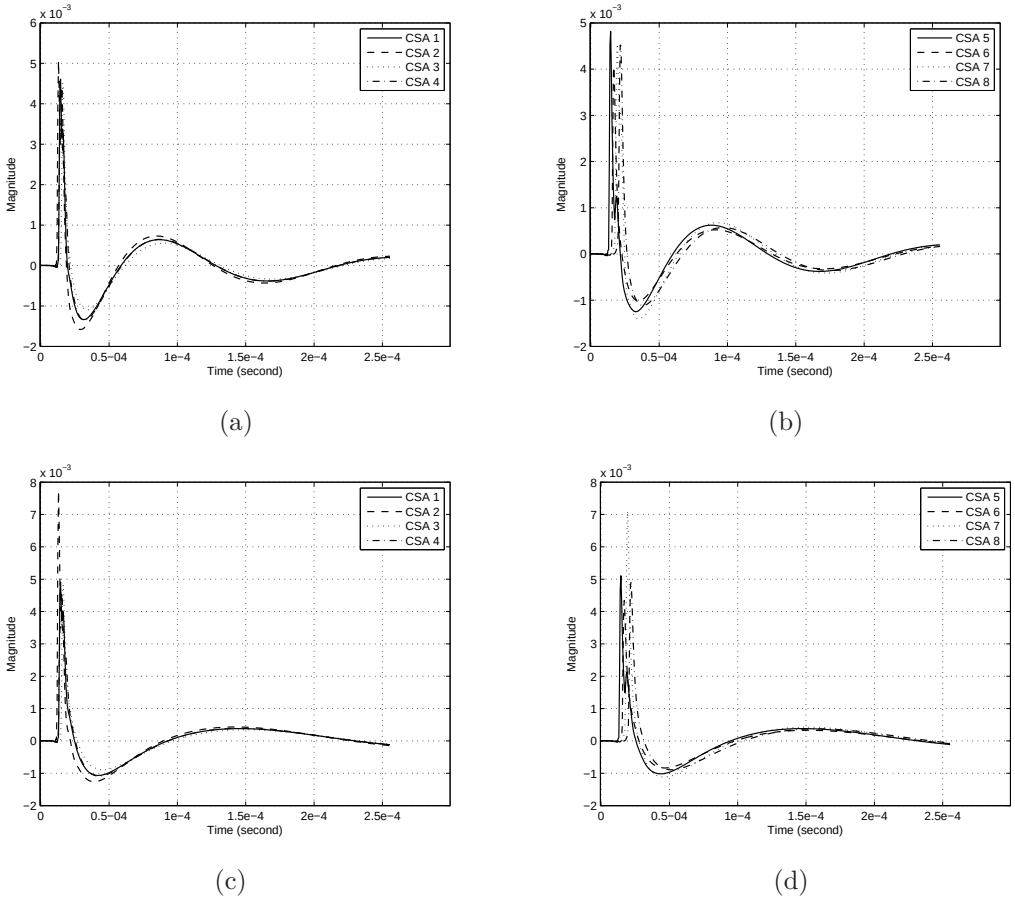

Fig. 6.2 The impulse response of the CSA test loops: (a) and (b) are for downstream and (c) and (d) are for upstream.

receiver, first the echo channel must be modeled, and then the transmitted signal is convolved with the impulse response of the echo channel. Using the method in [45, 96], we have calculated the echo path transfer function based on the input impedance of the line, the impedance of the bridge circuit and the structure of the hybrid circuit. For the hybrid structure discussed in Section 2.3.5, the impulse responses of the echo path experienced in the CSA test loops for the downstream and upstream are shown in Fig. 6.3 (a)–(b) and Fig. 6.3 (c)–(d), respectively.

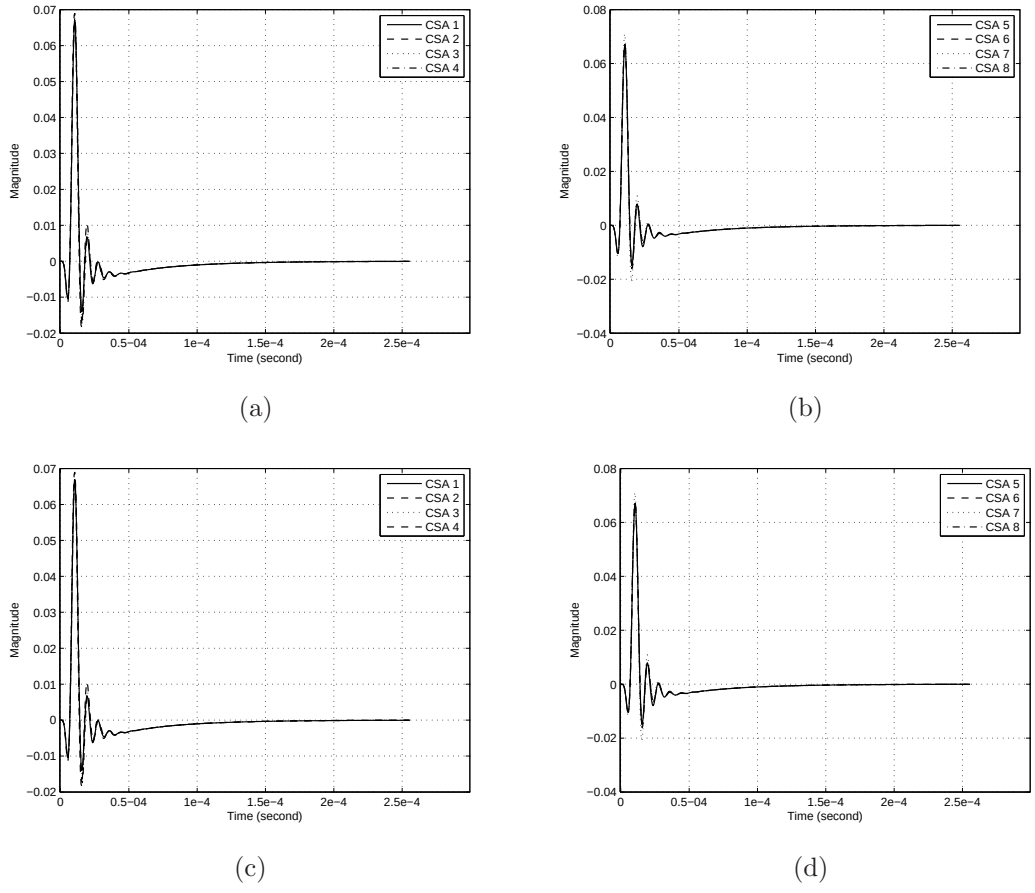

Fig. 6.3 The echo path impulse response of the CSA test loops: (a) and (b) are for downstream and (c) and (d) are for upstream.

6.1.3 Interference modeling

Various interferences are present in the DSL transmission medium. In this section, we briefly review some of these interferences.

Background noise

Background or thermal noise is present in DSL systems, like all transmission systems. This noise is usually modeled as an additive white Gaussian noise (AWGN). The level of AWGN is assumed to be -140 dBm/Hz for DSL systems [45].

Radio frequency interference

As discussed in Section 2.3.4, the RFI in DSL systems originate from two main sources: the AM radio broadcast and the amateur radio transmissions. These interferences can be modeled as narrowband signals. AM radio ingress is caused by continuos narrowband transmission of commercial AM stations on bands spreading from 207 kHz up to 1.6 MHz. Amateur radio transmission also occupies narrow frequency bands in the range from 1.8 MHz up to 29 MHz; however, the carrier frequencies for these transmissions change every few minutes [97]. The level of the ingress from both of these sources at the receiver is higher than the level of the crosstalk and the background noise. For example, the amateur radio transmissions can have a high power peak of 400 W or 56 dBm [98]. In our simulations, we consider AM radio ingress with 10 kHz bandwidth and power of -53 dBm. For an AM radio ingress centered at 603 kHz the power spectrum is shown in Fig. 6.4.

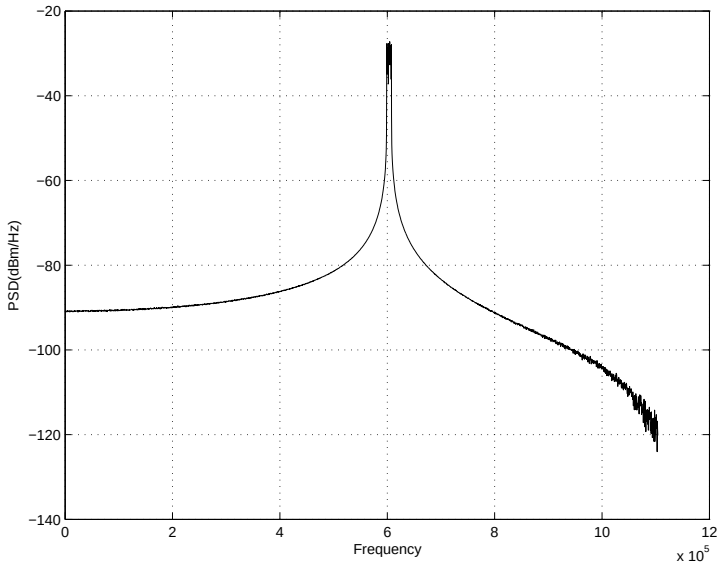

Fig. 6.4 Power Spectral density of AM radio ingress centred at 603 kHz

6.1.4 System model

We implement DMT modulation in this work, which is widely used in DSL standards. The DMT modulation used for ADSL systems has the following parameters: the frequency bandwidth of each tone is 4.3125 kHz, 32 tones are assigned for upstream using 64-point FFT ($N = 64$) and 256 tones are assigned for downstream using 512-point FFT ($\kappa N = 512, \kappa = 8$). From these assigned tones, the upstream uses tones 7-31 and downstream uses tones 33-255. The cyclic prefix contains 5 samples in the upstream and 40 samples in the downstream. Each tone transmits a 4-QAM signal constellation. The downstream and upstream signal power equals -40 dBm/Hz. It should be noted that we used uniform bit loading and no coding technique has been used. The block diagram for this system is as shown in Fig. 3.1.

The test loop used in the simulations is the CSA loop #4. The external additive

noise is white Gaussian noise at -140 dBm/Hz. The true echo channel contains 512 samples at 2.2MHz, including the effect of the hybrid, the transmitter and receiver filters and the TEQ. The front-end receiver filter and the filter involved in DAC are modeled as Butterworth lowpass filters with corner frequencies of 1.104 MHz and 138 kHz, respectively. The TEQ coefficients are calculated using the MATLAB Toolbox developed in [99], using MMSE Unit Tap Constraint method. For the learning curves of the adaptive algorithms presented in the following sections, the ensemble average of square error over 60-70 independent trials of the experiment is simulated.

6.2 Performance of Linearly Constrained Adaptive Echo Cancellers

In this section, we compare the performance of the constrained echo cancellers with those of the existing echo cancellers, where the convergence behaviour of various algorithms are examined using simulated learning curves. In Section 6.2.1, the linearly constrained echo canceller is compared with the time-domain LMS canceller in terms of the convergence rate. The comparison is performed for both cases where the length of the echo canceller is equal to the frame size, and for the case where the length of the echo canceller is smaller than the frame size. In addition, we also discuss the effect of the choice of constraint matrix on the convergence behaviour of constrained algorithms. In Section 6.2.2, we investigate the constrained echo canceller with supplementary constraints in the presence of the radio frequency interference, and show that by appending proper constraints to the system, it can be made more robust against this interference.

6.2.1 Learning curves for linearly constrained echo cancellers

As mentioned earlier, in this section we compare the convergence behaviour of the time-domain LMS echo canceller with those of the linearly constrained echo cancellers. The proposed linearly constrained cancellers are implemented using the approach by Frost, as discussed in Section 4.2.1, denoted by LCA EC, and the generalized sidelobe canceller approach by Griffiths and Jim, as discussed in Section 4.2.2, denoted by GSC EC. In both approaches, the extended weight vector includes the weights in the time and frequency domains, which implements the CES algorithm in the constrained form, as discussed in Section 4.3. Two different constraint matrices are used, denoted as Case I and II, where as discussed in Section 4.3.1, the former, constraint matrix is applied in the frequency domain and defined in (4.31), and the latter, is applied in the time domain and defined in (4.32).

The system setup is as discussed in Section 6.1.4, where the far-end channel is silent, and the interference includes AWGN. This setup is widely used in literature for studying the convergence of echo cancellers such as in [4, 15, 17, 19].

We first consider a scenario where the FIR filter modeling the echo path has an equal number of taps to the frame size, i.e., $T_e = 512$. The results for the frame synchronous system at the RT receiver, where the interpolated echo canceller is used, are presented in Fig. 6.5, while the corresponding results for the CO receiver, where the decimated echo canceller is used, are shown in Fig. 6.6. For these simulations, the value of the step-size parameter μ for each algorithm is chosen to ensure that the cancellers have similar initial convergence slope. For the constrained interpolated cancellers the value of $\mu = 0.3$ and for the decimated cancellers the value of $\mu = 0.003$. For the time-domain LMS canceller at the RT receiver the value of $\mu = 0.7$ and at

the CO receiver the value of $\mu = 0.007$.

It can be seen that both approaches for linearly constrained cancellers, LCA EC and GSC EC, have similar convergence rate, which is the same performance as that of the LMS algorithm, as expected. In addition, the echo cancellers corresponding to the two constraint matrices, Case I and II, also perform similar to each other. The LCA echo cancellers have the same convergence rate as that of the LMS algorithm, but provide additional capability to implement supplementary constraints. It should be noted that unlike the CES echo canceller, the LCA echo cancellers based on CES algorithm are not affected by the lack of excitation on the unused tones in the frequency domain, since the adaptive weight update is done partially in the time domain.

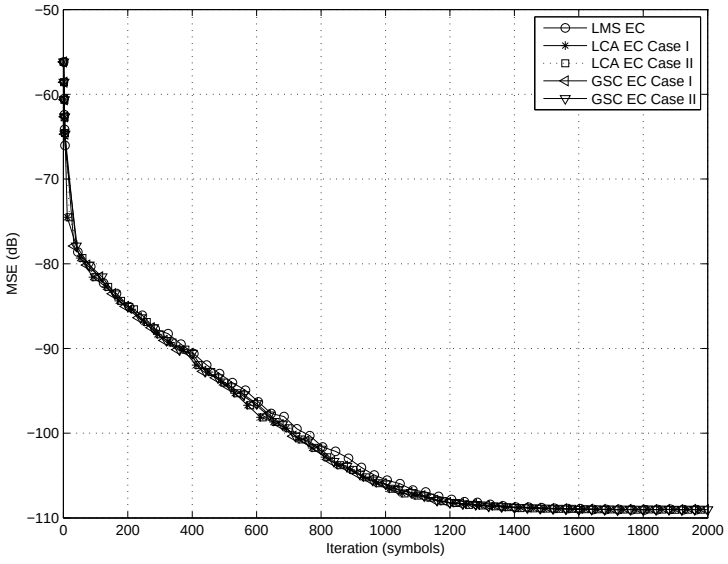

Fig. 6.5 Convergence behaviour of different linearly constrained cancellation methods for synchronous ADSL-RT, $T_e = 512$

We next consider a scenario where the FIR filter modeling the echo path has a

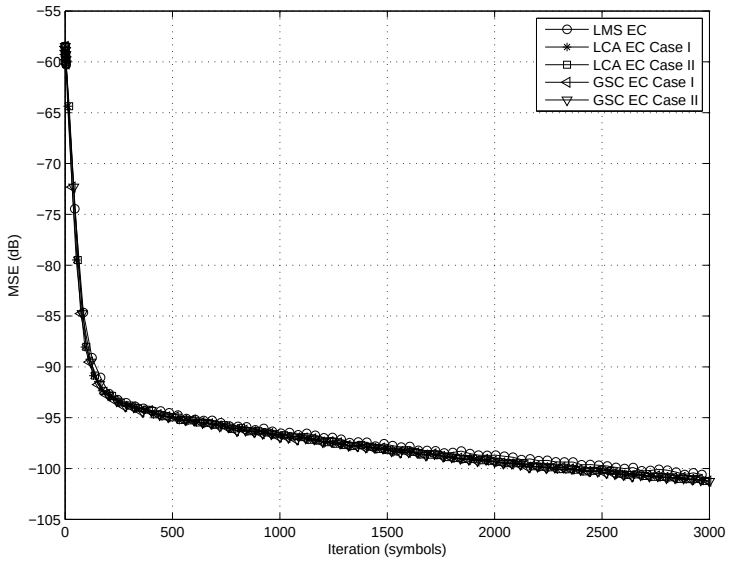

Fig. 6.6 Convergence behaviour of different linearly constrained cancellation methods for synchronous ADSL-CO, $T_e = 512$

smaller number of taps than the frame size, i.e., $T_e = 260$. Similar learning curves have been simulated, and the results for the frame synchronous system at the RT receiver (interpolated echo canceller) and at the CO receiver (decimated echo canceller) are presented in Fig. 6.7 and Fig. 6.8, respectively. For these simulations, as before, the step-size parameter is chosen to ensure that the cancellers have similar initial convergence slope, and for the interpolated cancellers the value of $\mu = 0.7$ and for the decimated cancellers the value of $\mu = 0.005$.

It can be seen, that for this scenario with $T_e = 260$, the echo cancellers corresponding to the two constraint matrices perform differently. Both at the RT and CO receivers, the constrained canceller using Case I constraint matrix, for both approaches, has faster convergence compared with the constrained cancellers using Case II constraint matrix. In addition, the constrained cancellers using Case I constraint

matrix exhibit a similar performance as that of the time-domain LMS canceller.

These results agree with the discussion in Section 4.3.1, where it was explained that due to the reduced degrees of freedom in the canceller with Case I constraint matrix, this canceller is expected to have faster convergence rate. As discussed in [88], the reduction in the degrees of freedom, which results from the additional constraints, results in a faster convergence to the steady state conditions. Here, the constrained cancellers using Case I constraint matrices, have fewer degrees of freedom, and therefore they converge faster. This result can also be justified intuitively, where for the cancellers with the Case I constraint matrix, the frequency-domain weight vector corresponds to the Fourier transform of a vector with the last $(N - T_e)$ tail elements forced to zero. Contrarily, for the cancellers based on the Case II constraint matrix, the frequency-domain weight vector does not correspond to the Fourier transform of a vector with zeroed $(N - T_e)$ tail elements. Therefore, the constrained cancellers with Case I constraint matrix are expected to have lower error-floor.

6.2.2 Constrained echo cancellers in the presence of radio frequency interference

In this section, we examine the effect of the supplementary constraints to improve the robustness of the system in the presence of radio frequency interference. The interference is modeled by narrowband noise (NBN) on the known frequencies affected by AM transmissions as discussed in Section 6.1.3. We investigate two different scenarios, one where additional linear constraints are appended to the system, and another where additional quadratic constraints are used.

In the first scenario, the echo canceller weights are initialized with the true echo

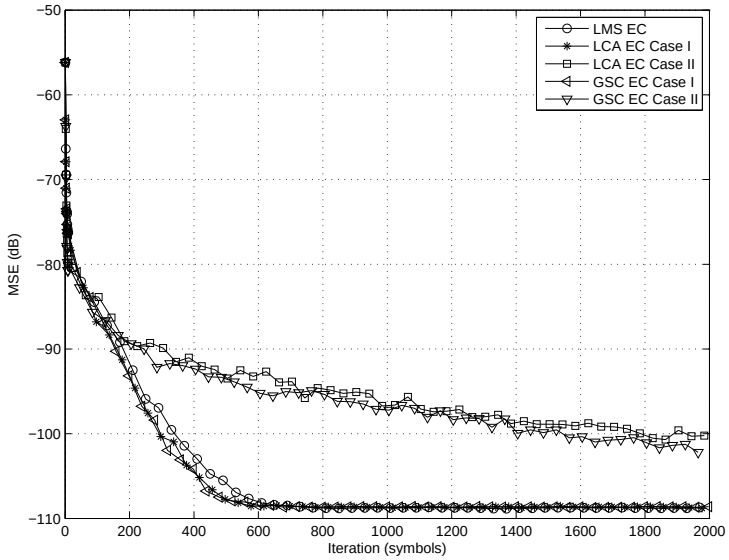

Fig. 6.7 Convergence behaviour of different linearly constrained cancellation methods for synchronous ADSL-RT, $T_e = 260$

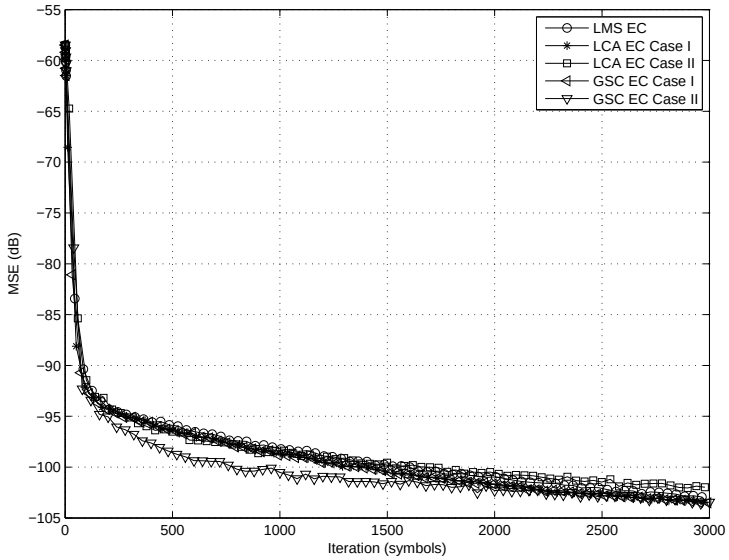

Fig. 6.8 Convergence behaviour of different linearly constrained cancellation methods for synchronous ADSL-CO, $T_e = 260$

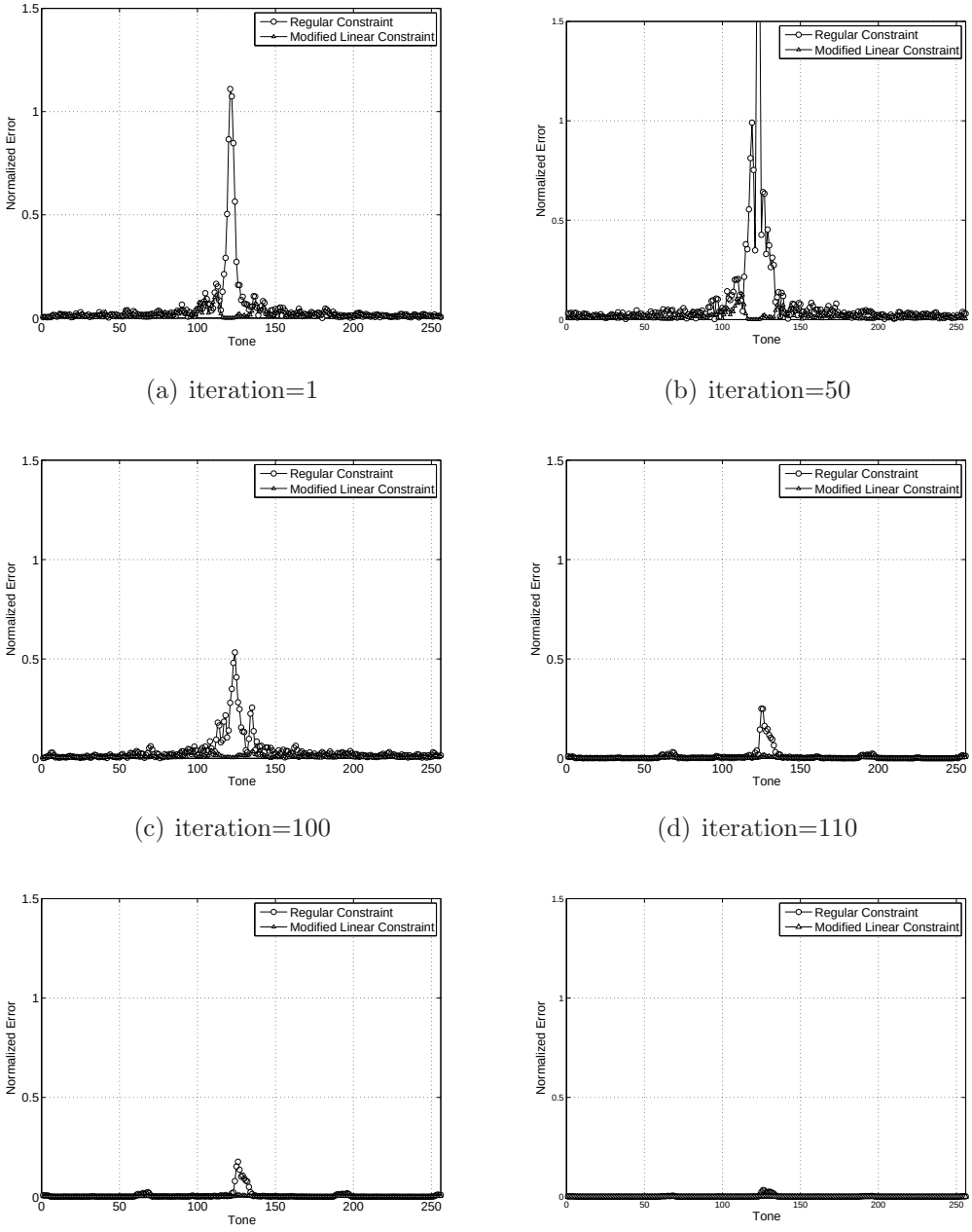

(a) iteration=1

(b) iteration=50

(c) iteration=100

(d) iteration=110

(e) iteration=125

(f) iteration=200

Fig. 6.9 Normalized error of the echo canceller weights for various iterations with regular and modified linear constraints

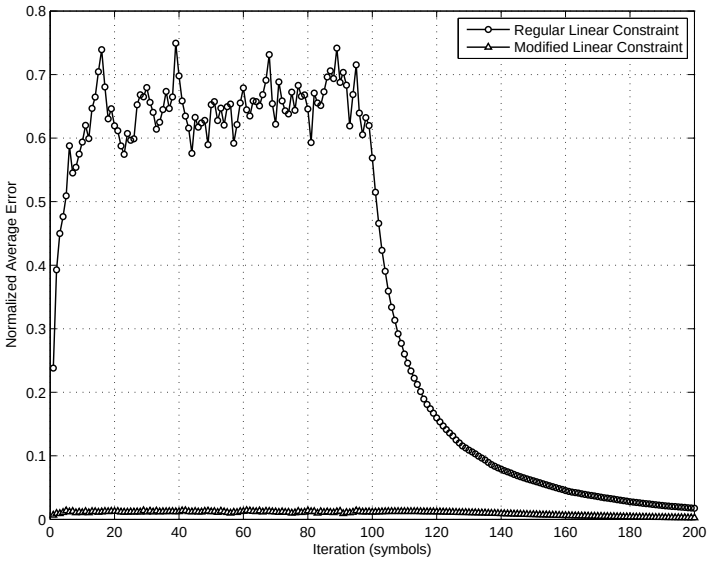

Fig. 6.10 Normalized average error on the weights of the affected tones with regular and modified linear constraints.

channel weights and the NBN is added at frequency 560 kHz corresponding to AM ingress [100]. It is assumed that the noise is present for only 100 frames (iterations), while the adaptive update is continued for next 100 iterations. The normalized error of the echo canceller weights in the frequency domain for various iterations is depicted in Fig. 6.9, and the normalized average error on the echo canceller weights corresponding to the affected tones is depicted in Fig. 6.10.

In these simulations, the regular constraint includes only the Fourier transform relationship between the weights in the time and frequency domains. On the other hand, for the modified linear constraint case, additional linear constraints are added to force the weights of the affected tones to zero in the presence of the noise, as discussed in Section 4.4.1. As it can be seen, the echo canceller with the regular constraint encounters a large increase on the affected tones, while the linearly constrained echo

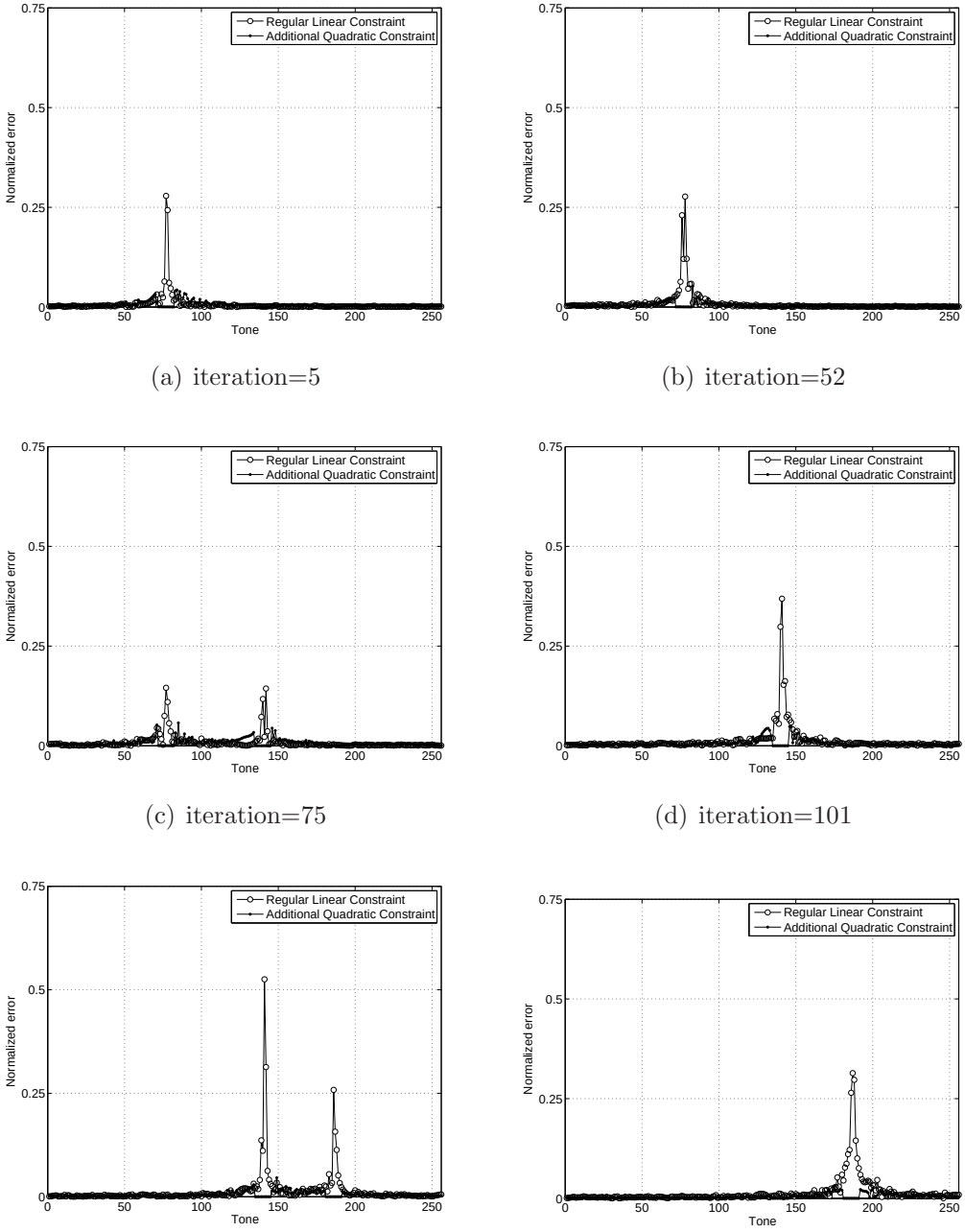

(a) iteration=5

(b) iteration=52

(c) iteration=75

(d) iteration=101

(e) iteration=102

(f) iteration=125

Fig. 6.11 Normalized error of the echo canceller weights for various iterations with regular linear and additional quadratic constraints

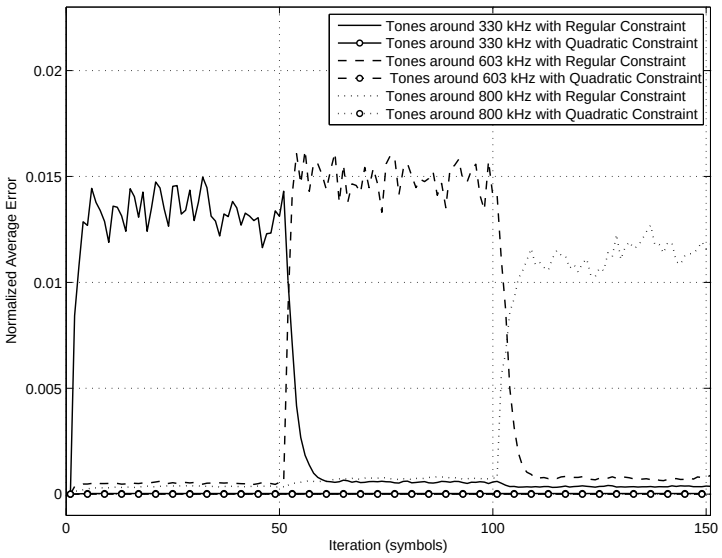

Fig. 6.12 Normalized average error on the weights of the affected tones with regular linear and additional quadratic constraints

canceller with additional zero-forcing constraints is protected, in the presence of the NBN. Additionally, after the removal of the NBN source, the regularly constrained echo canceller needs more than 50 iterations to compensate the error on the affected tones by the noise, while the weights of the canceller with the modified linear constraints are adjusted in few iterations.

As discussed in Section 4.4.1, quadratic inequality constraints can also be used to improve the robustness of constrained adaptive systems in the presence of interferences [92]. Thus, inequality constraints are added to ensure that the energy of the desired tones is limited within a certain threshold. This can be formulated as

$$\| \left[\mathcal{O}_{l_a \times T_e} | \mathcal{T}_{l_a \times N} \right] \boldsymbol{\omega}^k \|^2 \leq \Upsilon \tag{6.1}$$

where matrix $\mathcal{T}$ is used, as discussed in Section 4.4.1, to include the affected tones in

the constraint and leave the weights of the unaffected tones unchanged; the threshold Υ in (6.1) is the limit on the energy of the affected tones.

In the second scenario, the echo canceller weights are initialized with the true echo channel weights and the NBN changes its frequency from 330 kHz to 603 kHz and finally to 800 kHz, in iterations 1, 50 and 100, respectively [100]. In this simulation, regular constrained echo canceller with standard constraints is compared with a constrained canceller where additional quadratic constraints are added, as in (6.1), to limit the weights on the tones suspected to be affected by the NBN. The normalized error of the echo canceller weights in the frequency domain for various iterations is depicted in Fig. 6.11, and the normalized average error on the weights for the echo canceller corresponding to the affected tones with the regular constraints and the one with additional quadratic constraint is depicted in Fig. 6.12. As it can be seen, the regularly constrained echo canceller, not only experiences large error on the affected tones but also requires additional iterations to compensate the error on the previously affected tones even after the change in the frequency of the noise. On the other hand, the echo canceller with additional quadratic constraints shows an improved performance in the presence of the NBN with changing frequencies.

6.3 Performance of Dual Domain Echo Cancellers

In this section, we evaluate the convergence behaviour of the dual domain echo cancellers as presented in Chapter 5. The system setup is as discussed in Section 6.1.4, where the far-end channel is silent, and the interference includes AWGN. The implemented dual domain canceller is the DTC algorithm where unconstrained, constrained and the combination of these two are discussed as proposed in Section 5.5. The per-

formance of these dual domain cancellers is compared with those of the existing echo cancellers, in terms of their convergence rate, using simulated learning curves. It should be noted that for all the multirate simulations in this section, the polyphase approach is implemented as presented in Section 5.6.

We first consider a scenario where the length of the echo canceller is assumed to be equal to the frame size, i.e., $T_e = 512$. The learning curves for the frame synchronous system at the RT receiver (interpolated echo canceller) are depicted in Fig. 6.13, Fig. 6.14 and at the CO receiver (decimated echo canceller) is depicted in Fig. 6.15. For both receivers, the echo channel weights are all initialized to zero, and no dummy data is sent on the unused tones. The DTC algorithm used in these simulations is the constrained DTC (Cons. DTC) algorithm as presented in Section 5.4.2. It should be noted that the SDC algorithm was only presented in [18] for symmetric rate implementations. In this work, in order to make the comparisons with other methods possible, we extended this algorithm so that it can be implemented at the RT receiver using interpolated input data matrix.

In Fig. 6.13, the step-sizes are chosen so that the algorithms have the same error-floor and In Fig. 6.14, the step-sizes are chosen so that the algorithms have a similar slope during the initial convergence. As it can be seen, the time-domain LMS canceller and the proposed constrained DTC method have similar performance and have faster convergence compared with those of the CDC, SDC and CES algorithms. As discussed in [18], the SDC method has similar convergence rate with the CDC algorithm. For the CES algorithm in the case of $T_e = 512$, the canceller diverges after an initial convergence because of the accumulating error on the tail weights. In Fig. 6.15, similar comparisons are performed at the CO receiver, where the step-sizes are chosen

to ensure similar slope during initial convergence. It can be seen that the results follow the same trends as above. In both RT and CO receivers, the constrained DTC algorithm performs similar to the time-domain LMS echo canceller. However, as explained in Section 5.5.2, the constrained DTC algorithm has increased computational complexity compared with those of the CDC, SDC and CES cancellers, due to the use of the constrained adaptive weight update.

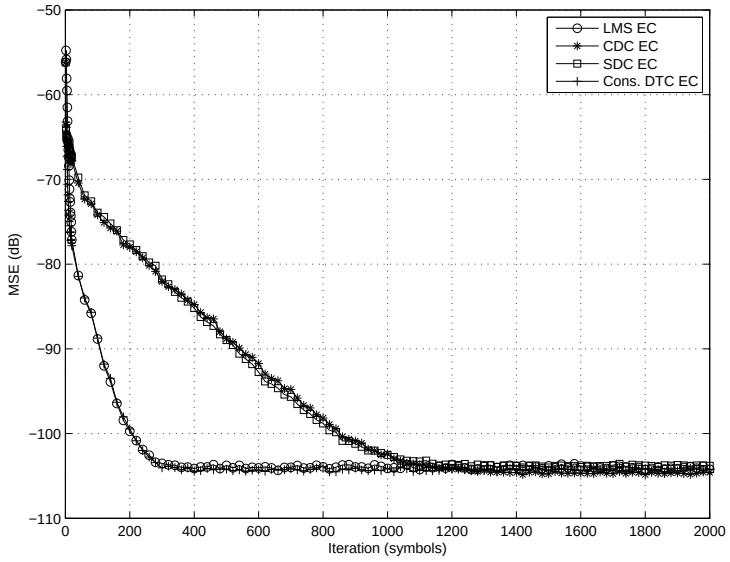

Fig. 6.13 Convergence behaviour of different echo cancellation methods for synchronous ADSL-RT, $T_e = 512$, similar error floor case

In the second set of simulations, the convergence rate of the unconstrained, constrained and combined DTC algorithms are examined. In the combined DTC algorithm, the adaptive update is mainly performed by unconstrained update as in (5.19), and infrequently by the constrained adaptive update in (5.34). For the combined algorithm, the intervals between the infrequent updates are denoted by parameter ϕ, where for $\phi = 1$, the constraint is applied in each iteration, which implements the

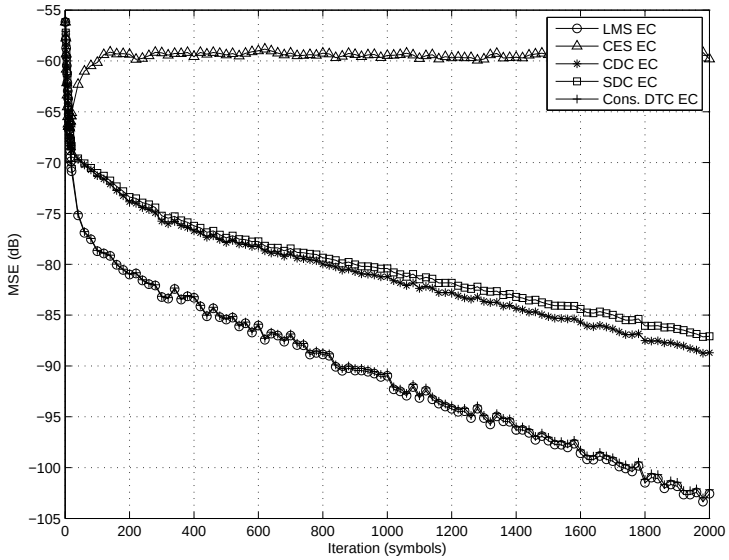

Fig. 6.14 Convergence behaviour of different echo cancellation methods for synchronous ADSL-RT, $T_e = 512$, similar initial slope case

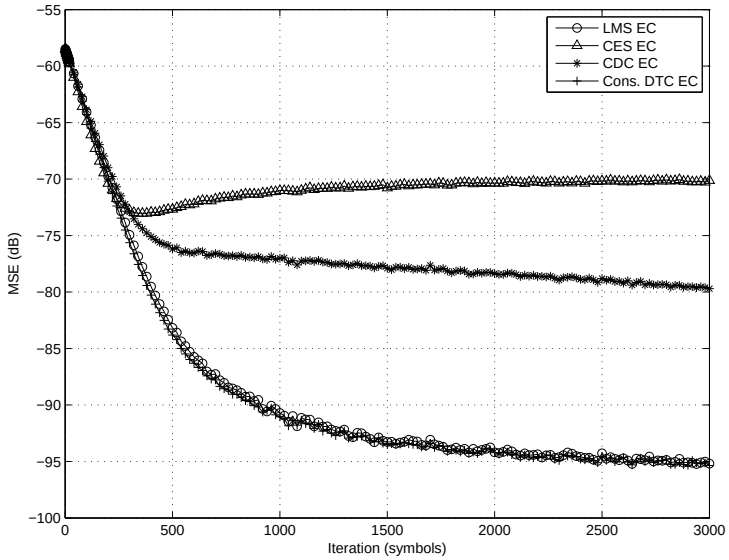

Fig. 6.15 Convergence behaviour of different echo cancellation methods for synchronous ADSL-CO, $T_e = 512$

constrained DTC algorithm; for $\phi = 10$ and 50, the constrained adaptive update in (5.34) is applied at every 10^{th} and 50^{th} iterations, respectively and for $\phi = \infty$, no constraint is applied and (5.19) is used to update the weights for all iterations, which implements the unconstrained DTC algorithm.

The simulations results for the above scenario for the RT receiver and the CO receiver are depicted in Fig. 6.16 and Fig. 6.17, respectively. In these simulations, for the interpolated canceller the value of $\mu = 0.5$ and for the decimated canceller the value of $\mu = 0.01$. As it can be seen, for both receivers, the unconstrained algorithm has the slowest convergence speed, as expected, and the constrained one has the fastest because of the reduced degrees of freedom. However, the combined DTC algorithms with $\phi = 10$ and 50 have a close performance to that of the constrained DTC algorithm, which shows that the loss of convergence speed by using the infrequent constrained update is small.

In the third set of simulations, the performance of the combined DTC algorithm is compared with those of the existing echo cancellers, for the case where the length of the echo canceller is shorter than the frame size, i.e., $T_e = 260$. The learning curves for the frame synchronous system at the RT receiver (interpolated echo canceller) are depicted in Fig. 6.18, and at the CO receiver (decimated echo canceller) are depicted in Fig. 6.19. In these simulations, for the interpolated canceller the value of $\mu = 0.4$ and for the decimated canceller the value of $\mu = 0.004$.

For the SDC method, in addition to the extension discussed above to make it compatible for multirate systems, we have modified the algorithm from its original form in [18] to be used for cases where the length of echo channel is smaller than the frame size, i.e., $T_e < \kappa N$. In the expanded version, the last $\kappa N - T_e$ weights in the time

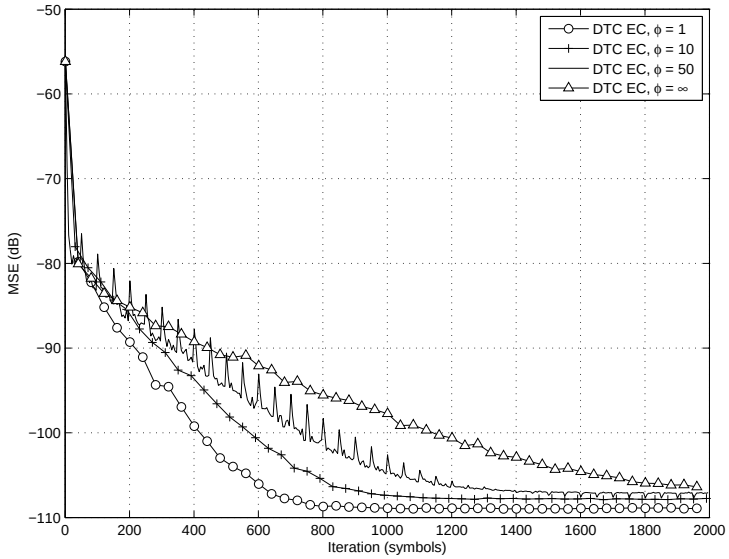

Fig. 6.16 Convergence behaviour of Combined DTC algorithm with different intervals of application of the constraint gradient for synchronous ADSL-CO, $T_e = 260$

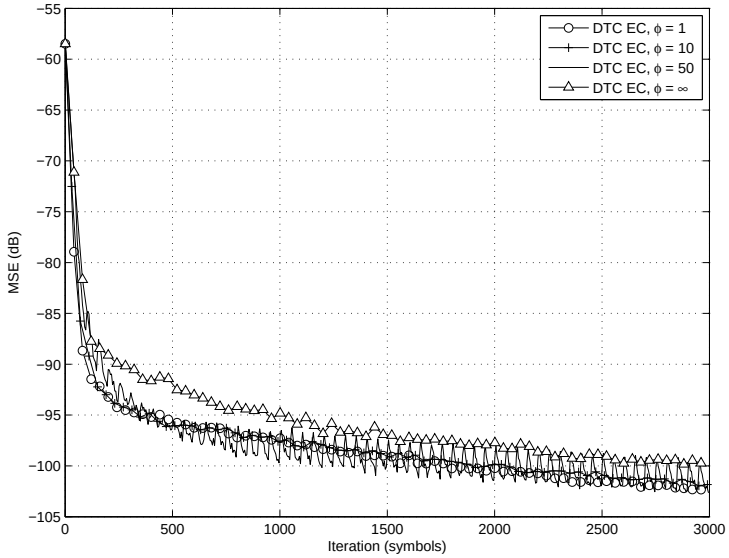

Fig. 6.17 Convergence behaviour of Combined DTC algorithm with different intervals of application of the constraint gradient for synchronous ADSL-CO, $T_e = 260$

domain are forced to zero, which generally improves the performance of the canceller. For the combined DTC algorithm, the use of different time intervals for applying the gradient constraint to the weight vectors are examined, i.e., $\phi = 1, 10, 50, \infty$.

As seen in Fig. 6.18 and Fig. 6.19, the DTC method with no gradient constraint performs better than the CDC and CES algorithms. It is interesting to note the improved performance of the extended SDC algorithm, which is similar to the performance of time-domain LMS canceller and the DTC method with $\phi = 10$. This improvement is due to the fact that the time-domain LMS, SDC and DTC algorithms calculate the estimated echo in the time domain. Consequently, the zeroing of the last $\kappa N - T_e$ weights of the weight vector reduces the error floor in these cancellers directly. On the other hand, in the CES and CDC algorithms, where a part of the echo emulation is done in the frequency domain, a higher error floor is observed, since the weights in the frequency domain do not correspond to the transformation of the time-domain weight vector with the last $\kappa N - T_e$ weights forced to zero.

The simulations results in this section show that the combined DTC canceller has convergence rate similar to that of the time-domain LMS canceller, which is faster than those of the CDC and CES algorithms. In terms of complexity, the combined DTC algorithm is comparable to the CDC and SDC methods, but while it has faster convergence rate. In addition, unlike the CES and (sometimes) the CDC algorithms, the combined DTC algorithm does not require the transmission of dummy data on the unused tones.

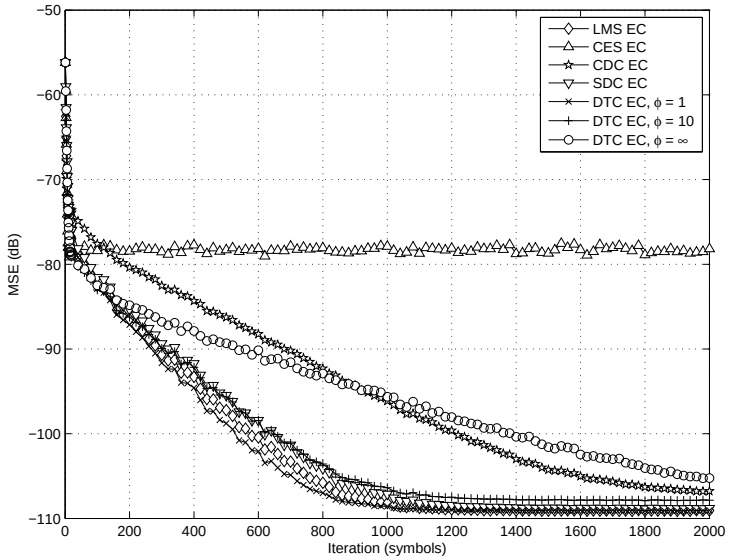

Fig. 6.18 Convergence behaviour of different echo cancellation methods for synchronous ADSL-RT, $T_e = 260$

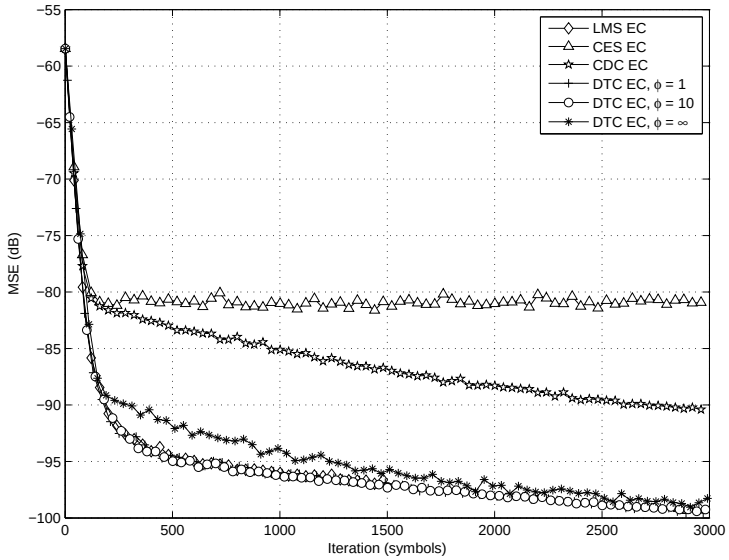

Fig. 6.19 Convergence behaviour of different echo cancellation methods for synchronous ADSL-CO, $T_e = 260$

Chapter 7

Conclusion

7.1 Summary of the Work

In this thesis, we introduced a general framework for studying and designing echo cancellers for DMT-based systems. This general form provides a unified representation of the existing echo cancellers. In addition, the proposed models offer a better understanding of different parts of the canceller and of the impacts of each part on the overall performance in terms of the convergence rate and the computational complexity. These models were also used to design new cancellers with improved performance.

In the first part of this thesis, where we studied linearly constrained echo cancellers, the focus was mainly on providing a structure with the capability to incorporate various constraints on the weight vectors in either the time or frequency domain. The linearly constrained cancellers were developed by considering the joint echo cancellation in the time and frequency domains as a constrained optimization, where linear constraints are imposed on the weight vectors. Using this viewpoint, two approaches for realizing the linearly constrained cancellers were presented, one based on the con-

strained LMS algorithm by Frost in [25] and the other one based on the generalized sidelobe canceller (GSC) structure by Griffiths and Jim in [26].

We showed that these realizations of the constrained cancellers can be implemented based on various echo emulation techniques, originated from the existing methods for the echo cancellation. In the proposed constrained cancellers, the constraints are mainly used to enforce a proper mapping of the weights between the time and frequency domains. It was also shown that the different choices of the constraint matrix can lead to an improved convergence rate of the adaptive canceller. In addition, we showed that the supplementary constraints can be added in the frequency domain or in the time domain to improve the performance of the system. For instance, appending proper constraints can improve the robustness of the canceller in the presence of radio frequency interference.

In the existing echo cancellation algorithms, the design procedure is initiated by deciding on the decomposition of the Toeplitz data matrix employed, and then the rest of the design follows from this decision. This order of design procedure has the disadvantage that the choice of the employed decomposition dictates some limitations on the canceller which directly affects its performance. Since the decomposition explicitly implies the domains in which the echo emulation and the adaptive weight update are performed and also defines the transformation matrices involved, its choice has a direct effect on the complexity and convergence of the algorithm.

In the second part of this thesis, we proposed to reverse the order of echo canceller design procedure. This was done by, firstly assuming a generic dual domain decomposition of the Toeplitz data matrix and designing a general dual domain echo canceller and secondly, choosing the decomposition to be used in this canceller. The proposed

design order has the advantage that the structure of the echo canceller can be optimized without having any limitations imposed by the choice of the decomposition.

Following the aforementioned two-step design procedure, a novel dual transform domain canceller (DTDC) was proposed. In this canceller, the time-domain signals and weight vectors are mapped into a dual domain defined by a pair of generic unitary matrices. This canceller performs an LMS adaptive weight update in the dual domain without any approximation with low computational complexity. Based upon this structure, the conditions for an appropriate decomposition, in the sense of reducing the computational complexity of the algorithm, have been determined. For the proposed DTDC structure, the symmetric decomposition performed by discrete trigonometric transformations satisfies the conditions of an appropriate decomposition. Consequently, the proposed dual domain canceller was implemented using the above decomposition, which is referred to as dual trigonometric canceller (DTC). As shown previously, the DTDC structure provides a unified representation of the existing echo cancellation algorithms and also provides an analytical tool to study this ensemble of algorithms.

We also developed linearly constrained dual domain cancellers, where linear constraints were added to ensure the proper mapping of the weights in the dual domain. These dual domain constrained cancellers are indeed the generalized form of the cancellers developed in Chapter 4, since in these cancellers it is assumed that the signals are mapped in any dual domain rather than being limited to only time and frequency domains.

The comprehensive study of the constrained and unconstrained dual domain cancellers showed that the constrained canceller has a faster convergence rate which is sim-

ilar to the convergence behaviour of the time-domain LMS canceller. This improved convergence rate is achieved at the expense of increased computational complexity compared with the unconstrained canceller. Therefore, we proposed a combined dual domain canceller which is based on the unconstrained dual domain canceller, while infrequently the constrained adaptive weight update is used. As it was shown later, the proposed combined dual domain canceller has a convergence rate very close to that of the time-domain LMS canceller with computational complexity similar to that of existing but slower cancellers.

7.2 Future Work

The following topics have been identified during the development of this thesis, which deserve particular attention:

In wired communication:

i) Issues regarding practical implementation of the proposed cancellers can be further examined, such as their fixed-point implementations and the effect of non-uniform bit loading.

ii) The framework developed in this work includes the echo cancellation for asynchronous systems. However, it may be of interest to examine the asynchronous dual domain echo cancellation systems further, where for instance the effect of the delay on the convergence and the complexity of the canceller is studied in detail.

iii) It is known that the convergence of the echo cancellers can be improved by combining them with double talk cancellers. It is of interest to examine

the implementation of double talk cancellers in the dual domain scenarios and their possible integration with the echo canceller.

iv) In recent year, an implementation of the multicarrier modulation systems based on the discrete trigonometric transformation instead of Fourier transform has been introduced [101]. The integration of the proposed dual domain cancellers based on trigonometric transformation for these systems can be studied further.

In wireless communication:

In this work, we have examined the problem of echo cancellation for DMT-based systems, with the main focus on the DSL networks. However, the main assumption made about the system is the use of the DMT modulation and therefore, the results of this work can be applicable to the OFDM-based wireless networks as well. Similar concepts to the echo cancellation have been already used in some wireless communication applications, such as intercarrier interference cancellation and full-duplex relaying [10, 11, 12, 13]. Further applications of the proposed methods in this work in the OFDM systems can therefore be of interest in this area.

Appendix A

Matrix Terminology

In this appendix, some of the matrix terminology used in the thesis is briefly reviewed.

A *square* $N \times N$ matrix, which has equal number of rows and columns, is defined as

$$\mathcal{A} = \begin{bmatrix} A(1,1) & A(1,2) & \cdots & A(1,N-1) \\ A(2,1) & A(2,2) & \cdots & A(2,N-1) \\ \vdots & & & \vdots \\ A(N-1,1) & A(N-1,2) & \cdots & A(N-1,N-1) \end{bmatrix}. \tag{A.1}$$

For such square matrix, the northwest-southeast diagonals above the main diagonal are referred to as super-diagonals, and the ones below are known as sub-diagonals [102]. In this work, the terms super-diagonal and sub-digonal are used to indicate the *first* super/sub-diagonals.

A matrix $\mathcal{A}$ is said to be *symmetric* if $\mathcal{A} = \mathcal{A}^T$, which means it is symmetric along the main northwest-southeast diagonal [102]. On the other hand, a matrix $\mathcal{A}$ is said to be *persymmetric* if it is symmetric along its northeast-southwest diagonal [89]. In addition, a matrix A is referred to as *skew-symmetric* or *anti-symmetric*, if $\mathcal{A}^T =$

$-\mathcal{A}$ [102, 103]. Finally, the sum of a square matrix with its transpose is symmetric, and the difference of a square matrix with its transpose is skew-symmetric. Therefore, any real square matrix can be written as a sum of a symmetric matrix with a skew-symmetric matrix, i.e.,

$$\mathcal{A} = \underbrace{(\mathcal{A} + \mathcal{A}^T)}_{\text{symmetric part}} + \underbrace{(\mathcal{A} - \mathcal{A}^T)}_{\text{anti-symmetric part}} . \tag{A.2}$$

It should be noted that for a complex square matrix, the equation above is true if the transpose replaced by conjugate transpose.

A matrix is called *Toeplitz* when the elements on each of its diagonals are identical [89]. For example,

$$\mathcal{A} = \begin{bmatrix} a & b & c & d \\ e & a & b & c \\ f & e & a & b \\ g & f & e & a \end{bmatrix}, \tag{A.3}$$

is a Toeplitz matrix. As it can be seen, a Toeplitz matrix can be defined by its first column and its first row. A closely related type of matrix to a Toeplitz matrix is *Hankel* matrix, where the elements on each of northeast-southwest diagonals are equal. Thus,

$$\mathcal{A} = \begin{bmatrix} a & b & c & d \\ b & c & d & e \\ c & d & e & f \\ d & e & f & g \end{bmatrix}, \tag{A.4}$$

is a Hankel matrix. One very useful type of matrices belonging to the larger class of

Toeplitz matrices are the *Circulant* matrices. A Circulant matrix is a Toeplitz matrix where each column is a *downshifted* version of the previous column [89]. Thus,

$$\mathcal{A} = \begin{bmatrix} a & b & c & d \\ d & a & b & c \\ c & d & a & b \\ b & c & d & a \end{bmatrix}, \tag{A.5}$$

is a Circulant matrix. It should be noted that a Circulant matrix can be completely defined by its first row or column.

Appendix B

Appendix to Chapter 5

B.1 Projection Matrix Calculations for the Constrained Dual Transform Domain Canceller

Assuming the constraint matrix in (5.30), in order to calculate the projection matrix $\mathcal{P}_c$, first the product $\mathcal{C}^H\mathcal{C}$ must be calculated, where

$$\mathcal{C}^H\mathcal{C} = \begin{bmatrix} \mathcal{I}_{N-T_e} & \tilde{\mathbf{M}}^T\mathbf{M} & \mathcal{O}_{N-T_e\times N-T_e} \\ \mathbf{M}^T\tilde{\mathbf{M}} & 2\mathcal{I}_{T_e} & \mathcal{O}_{T_e\times N-T_e} \\ \mathcal{O}_{N-T_e\times N-T_e} & -\tilde{\mathbf{M}}^T\mathbf{M} & \mathcal{I}_{N-T_e} \end{bmatrix}. \tag{B.1}$$

Since, $\tilde{\mathbf{M}}^T\mathbf{M} = \mathcal{O}_{N-T_e\times T_e}$ and $\mathbf{M}^T\tilde{\mathbf{M}} = \mathcal{O}_{T_e\times N-T_e}$, the resulting matrix is of the form below, which can easily be inverted:

$$\mathcal{C}^H\mathcal{C} = \begin{bmatrix} \mathcal{I}_{N-T_e} & \mathcal{O}_{N-T_e\times T_e} & \mathcal{O}_{N-T_e\times N-T_e} \\ \mathcal{O}_{T_e\times N-T_e} & 2\mathcal{I}_{T_e} & \mathcal{O}_{T_e\times N-T_e} \\ \mathcal{O}_{N-T_e\times N-T_e} & \mathcal{O}_{N-T_e\times T_e} & \mathcal{I}_{N-T_e} \end{bmatrix}. \tag{B.2}$$

Therefore, the projection matrix $\mathcal{P}_c$ can be obtained as

$$\mathcal{P}_c = \begin{bmatrix} \frac{1}{2}\mathcal{G}_1\tilde{\mathbf{M}}\tilde{\mathbf{M}}^T\mathcal{G}_1^H + \frac{1}{2}\mathcal{G}_1\mathbf{M}\mathbf{M}^T\mathcal{G}_1^H & -\frac{1}{2}\mathcal{G}_1\mathbf{M}\mathbf{M}^T\mathcal{G}_2^H \\ -\frac{1}{2}\mathcal{G}_2\mathbf{M}\mathbf{M}^T\mathcal{G}_1^H & \frac{1}{2}\mathcal{G}_1\mathbf{M}\mathbf{M}^T\mathcal{G}_1^H + \frac{1}{2}\mathcal{G}_2\tilde{\mathbf{M}}\tilde{\mathbf{M}}^T\mathcal{G}_2^H \end{bmatrix}. \tag{B.3}$$

The above matrix can be simplified by considering the relation between $\mathbf{M}$ and $\tilde{\mathbf{M}}$, where $\tilde{\mathbf{M}}\,\tilde{\mathbf{M}}^T + \mathbf{M}\,\mathbf{M}^T = \mathcal{I}_N$, which results in

$$\mathcal{P}_c = \begin{bmatrix} \mathcal{I}_N - \frac{1}{2}\mathcal{G}_1\mathbf{M}\mathbf{M}^T\mathcal{G}_1^H & -\frac{1}{2}\mathcal{G}_1\mathbf{M}\mathbf{M}^T\mathcal{G}_2^H \\ -\frac{1}{2}\mathcal{G}_2\mathbf{M}\mathbf{M}^T\mathcal{G}_1^H & \mathcal{I}_N - \frac{1}{2}\mathcal{G}_2\mathbf{M}\mathbf{M}^T\mathcal{G}_2^H \end{bmatrix}. \tag{B.4}$$

B.2 Eigenvalue Calculations for the Constrained DTDC algorithm

For the Constrained DTDC algorithm, as shown in [25], if the linearly constrained method based on the Frost method is used, the covariance matrix corresponding to the constrained algorithm can be derived based on the one of the unconstrained algorithm. In this case, the covariance matrix of the constrained algorithm denoted by $\mathcal{R}_{\text{C}}$ is given by

$$\mathcal{R}_{\text{C}} = \mathcal{P}_c^{\perp}\,\mathcal{R}_{\text{UC}}\,\mathcal{P}_c^{\perp}, \tag{B.5}$$

where $\mathcal{P}_c^{\perp}$ is the projection matrix and the $\mathcal{R}_{\text{UC}}$ is the covariance of the unconstrained algorithm. As explained in [25], the covariance matrix $\mathcal{R}_{\text{C}}$ has precisely l_c zero eigenvalues, where l_c is the number of constraints. In addition, this covariance matrix has $2N - l_c$ non-zero eigenvalues, which are bounded between the smallest and largest eigenvalues of $\mathcal{R}_{\text{UC}}$.

Using the above results, for the case where the length of echo channel is equal to the frame size ($T_e = N$) and the projection matrix $\mathcal{P}_c^{\perp} = \frac{1}{2}\mathcal{G}\,\mathcal{G}^H$, representing N linear constraints, the covariance matrix for the constrained case using (B.5) is as follows

$$\mathcal{R}_{\mathrm{C}} = \mathcal{G}\,\mathcal{G}^H\,\mathrm{E}[(\mathcal{S}^k)^H\,\mathcal{G}\,\mathcal{G}^H\,\mathcal{S}^k]\,\mathcal{G}\,\mathcal{G}^H, \tag{B.6}$$

where we drop the $1/2$ factor, since it does not affect the ratio of eigenvalues. Since the matrices $\mathcal{G}$ and $\mathcal{G}^H$ are deterministic, they can be moved inside the expectation operation, and (B.6) can be rewritten as

$$\begin{aligned} \mathcal{R}_{\mathrm{C}} &= \mathcal{G}\,\mathrm{E}[\mathcal{G}^H\,(\mathcal{S}^k)^H\,\mathcal{G}\,\mathcal{G}^H\,\mathcal{S}^k\,\mathcal{G}]\,\mathcal{G}^H \\ &= \mathcal{G}\,\mathrm{E}[(\mathcal{U}^k)^T\,\mathcal{U}^k]\,\mathcal{G}^H \end{aligned} \tag{B.7}$$

It can easily be verified that $\mathcal{R}_{\mathrm{LMS}} = \mathrm{E}[(\mathcal{U}^k)^T\,\mathcal{U}^k]$ is the covariance matrix determining the convergence rate of the time-domain LMS echo canceller. From results in [25], we know that $\mathcal{R}_{\mathrm{C}}$ has only N non-zero eigenvalues, in the following we show that these non-zero eigenvalues are equal to the eigenvalues of the covariance matrix $\mathcal{R}_{\mathrm{LMS}}$.

The eigenvalues of $\mathcal{R}_{\mathrm{C}}$ are given by the roots of the following characteristic polynomial given by

$$\begin{aligned} \det(\lambda\mathcal{I}_{2N} - \mathcal{R}_{\mathrm{C}}) &= \det(\lambda\mathcal{I}_{2N} - \mathcal{G}\,\mathcal{R}_{\mathrm{LMS}}\,\mathcal{G}^H) \\ &= \det(\lambda\mathcal{I}_N - \mathcal{G}_1\,\mathcal{R}_{\mathrm{LMS}}\,\mathcal{G}_1^H) \\ &\times \det(\lambda\mathcal{I}_N - \mathcal{G}_2\,\mathcal{R}_{\mathrm{LMS}}\,\mathcal{G}_2^H - \mathcal{G}_2\,\mathcal{R}_{\mathrm{LMS}}\,\mathcal{G}_1^H(\lambda\mathcal{I}_N - \mathcal{G}_1\,\mathcal{R}_{\mathrm{LMS}}\,\mathcal{G}_1^H)^{-1}\,\mathcal{G}_1\,\mathcal{R}_{\mathrm{LMS}}\,\mathcal{G}_2^H) \end{aligned} \tag{B.8}$$

As it can be seen the N non-zero eigenvalues are given by the roots of the first term

in the righthand side of (B.8), where since $\mathcal{G}_1$ is a unitary matrix, the eigenvalues are the same as the eigenvalues of the covariance matrix $\mathcal{R}_{\text{LMS}}$. This shows that the constrained DTDC algorithm has the same eigenvalue spread as time-domain LMS algorithm, which agrees with the simulation results in Chapter 6.

References

[1] M. Borgne and Y. Chen, "Next generation broadband access white paper." NextGenAccessWhitePaper.pdf, Aug. 2009. `http://www.broadband-forum.org/marketing/marketingdocuments.php`.

[2] T. Starr, J. M. Cioffi, and P. J. Silverman, *Understanding Digital Subscriber Line Technology*. Englewood Cliffs, NJ: Prentice- Hall, 1999.

[3] P. Golden, H. Dedieu, and K. S. Jacobsen, *Fundamentals of DSL Technology*. Boca Raton, FL: Auerbach Pub., 2004.

[4] G. Ysebaert, *Equalization and Echo Cancellation for DMT-Based Systems*. PhD thesis, Katholieke Universiteit Leuven, Belgium, 2001.

[5] F. Sjoberg, M. Isaksson, R. Nilsson, P. Odling, S. K. Wilson, and P. O. Borjesson, "Zipper: a duplex method for VDSL based on DMT," *IEEE Trans. Commun.*, vol. 47, pp. 1245–1252, Aug. 1999.

[6] D. Mestdagh, M. R. Isaksson, and P. Odling, "Zipper VDSL: a solution for robust duplex communication over telephone lines," *IEEE Commun. Mag.*, vol. 38, pp. 90–96, May 2000.

[7] S. Wilmoesterer, "Future proof telecommunications networks with VDSL2." VDSL2_WP_072005_v1.1_1.pdf, July 2005. `http://www.infineon.com/`.

[8] S. Haykin, *Adaptive Filter Theory*. Englewood Cliffs, NJ: Prentice- Hall, fourth ed., 2001.

[9] A. Goldsmith, *Wireless Communications*. New York, NY: Cambridge University Press, 2005.

[10] T. Riihonen, S. Werner, and R. Wichman, "Spatial loop interference suppression in full-duplex MIMO relays," in *43rd Asilomar Conf. on Signals, Systems and Computers*, (Pacific Grove, CA), pp. 1508–1512, Nov. 2009.

[11] T. Riihonen, S. Werner, R. Wichman, and Z. Eduardo, "On the feasibility of full-duplex relaying in the presence of loop interference," in *10th IEEE Workshop on Signal Process. Advances in Wireless Commun.*, (Perugia), pp. 275–279, June 2009.

[12] A. F. Molisch, M. Toeltsch, and S. Vermani, "Iterative methods for cancellation of intercarrier interference in OFDM systems," *IEEE Trans. Veh. Technol.*, vol. 56, pp. 2158–2167, July 2007.

[13] C.-Y. Hsu and W.-R. Wu, "Low-complexity ICI mitigation methods for high-mobility SISO/MIMO-OFDM systems," *IEEE Trans. Veh. Technol.*, vol. 58, pp. 2755–2768, July 2009.

[14] J. M. Cioffi and J. A. C. Bingham, "A data-driven multitone echo canceller," *IEEE Trans. Commun.*, vol. 42, pp. 2853–2868, Oct. 1994.

[15] M. Ho, J. M. Cioffi, and J. A. C. Bingham, "Discrete multitone echo cancelation," *IEEE Trans. Commun.*, vol. 44, pp. 817–825, July 1996.

[16] M. Ho, *Multicarrier Echo Cancellation and Multichannel Equalization.* PhD thesis, Dept. Elect. Eng., Stanford University, CA, 1995.

[17] G. Ysebaert, F. Pisoni, M. Bonaventura, R. Hug, and M. Moonen, "Echo cancellation in DMT-receivers: Circulant decomposition canceler," *IEEE Trans. Signal Process.*, vol. 52, pp. 2612–2624, Sept. 2004.

[18] F. Pisoni and M. Bonaventura, "A multi-carrier echo canceller based on symmetric decomposition," in *Proc. IEEE Workshop Signal Process. System Design and Implementation*, pp. 233 – 238, Nov. 2005.

[19] F. Pisoni, M. Bonaventura, and J. M. Cioffi, "Echo cancellation in DMT modems with frame-asynchronous operation," *IEEE Trans. Signal Process.*, vol. 55, pp. 246–255, Jan. 2007.

[20] D. C. Jones, "Frequency domain echo cancellation for discrete multitone asymmetric digital subscriber line transceivers," *IEEE Trans. Commun.*, vol. 43, pp. 1663–1672, Feb./Mar./Apr. 1995.

[21] G. Ysebaert, K. Vanbleu, G. Cuypers, M. Moonen, and K. Van Acker, "Double talk cancellation in echo cancelled DMT-systems," in *Proc. European Signal Process.Conf.*, vol. II, (Toulouse, France), pp. 381–384, Sept. 2002.

[22] G. Ysebaert, K. Vanbleu, G. Cuypers, M. Moonen, and J. Verlinden, "Echo cancellation for discrete multitone frame-asynchronous ADSL transceivers," in *Proc. IEEE Int. Conf. Communications*, vol. 4, (Seattle, WA), pp. 2421–2425, May 2003.

[23] H. Bogucka and K. Wesolowski, "Frequency-domain echo cancellation in digital multicarrier modulation systems," *IEEE Trans. Commun.*, vol. 48, pp. 333–342, Feb. 2000.

[24] K. Van Acker, M. Moonen, and T. Pollet, "Per-tone echo cancellation for DMT-based systems," *IEEE Trans. Commun.*, vol. 51, pp. 1582–1590, Sept. 2003.

[25] O. L. Frost, "An algorithm for linearly constrained adaptive array processing," *Proc. IEEE*, vol. 60, pp. 926–935, Aug. 1972.

[26] L. Griffiths and C. Jim, "An alternative approach to linearly constrained adaptive beamforming," *IEEE Trans. Antennas Propag.*, vol. 30, pp. 27–34, Jan. 1982.

[27] G. Kramer, *Ethernet Passive Optical Networks*. New York, NY: McGraw-Hill Professional, 2005.

[28] B. Skubic, C. Jiajia, J. Ahmed, L. Wosinska, and B. Mukherjee, "A comparison of dynamic bandwidth allocation for EPON, GPON, and next-generation TDM PON," *IEEE Commun. Mag.*, vol. 47, pp. S41–S48, Mar. 2009.

[29] K. Grobe and J. Elbers, "PON in adolescence: from TDMA to WDM-PON," *IEEE Commun. Mag.*, vol. 46, pp. 26–34, Jan. 2008.

[30] K.-C. Chung, K.-C. Chu, W.-T. Lee, and P.-C. Chung, "The comparison of performance issues on HFC networks," in *IEEE Region 10 Conf.*, vol. B, pp. 33–36, Nov. 2004.

[31] Cable Television Laboratories, Inc., SP-RFIv2.0-I06-040804, *Data-Over-Cable Service Interface Specifications, Radio Frequency Interface Specification*, Aug. 2004.

[32] A. Ghosh, D. R. Wolter, J. G. Andrews, and R. Chen, "Broadband wireless access with WiMax/802.16: current performance benchmarks and future potential," *IEEE Commun. Mag.*, vol. 43, pp. 129–136, Feb. 2005.

[33] J. G. Andrews, A. Ghosh, and R. Muhamed, *Fundamentals of WiMAX: Understanding Broadband Wireless Networking*. Englewood Cliffs, NJ: Prentice- Hall, 2007.

[34] D. McQueen, "The momentum behind LTE adoption," *IEEE Commun. Mag.*, vol. 47, pp. 44–45, Feb. 2009.

[35] K. Bogineni, R. Ludwig, P. Mogensen, V. Nandlall, V. Vucetic, B. K. Yi, and Z. Zvonar, "LTE Part I: Core network," *IEEE Commun. Mag.*, vol. 47, pp. 40–43, Feb. 2009.

[36] S. Baig and M. J. Mughal, "Multirate signal processing techniques for high-speed communication over power lines," *IEEE Commun. Mag.*, vol. 47, pp. 70–76, Jan. 2009.

[37] N. Pavlidou, A. J. H. Vinck, J. Yazdani, and B. Honary, "Power line communications: state of the art and future trends," *IEEE Commun. Mag.*, vol. 41, pp. 34–40, Apr. 2003.

[38] ANSI T1.601, *ISDN Basic Access Interface for Use on Metallic Loops for Application on the Network Side of the NT*, 1992.

[39] ANSI Committee T1, *High Bit-Rate Digital Subscriber Line (HDSL) Technical Report*, 1994.

[40] ANSI T1.418-2000, *High Bit-Rate Digital Subscriber Line Second Generation*, 2000.

[41] ETSI Tech. Specification TS 101 524, *Transmission and Multiplexing: Access Transmission System on Metallic Access Cables: Symmetric Single Pair High Bit-rate Digital Subscriber Line (SDSL)*, Nov. 2001.

[42] ITU-T Recommendation G.992.1, *Asymmetric Digital Subscriber Line (ADSL) Transceivers*, July 1999.

[43] ITU-T Recommendation G.992.2, *Splitterless Asymmetric Digital Subscriber Line (ADSL) Transceivers*, July 1999.

[44] ITU-T Recommendation G.992.3, *ITU02: Asymmetric Digital Subscriber Line Transceivers 2 (ADSL2)*, July 2002.

[45] W. Y. Chen, *DSL: Simulation Techniques and Standards Development for Digital Subscriber Line Systems*. Macmillan Technical Publishing, 1998.

[46] T. Starr, M. Sorbara, J. M. Cioffi, and P. J. Silverman, *DSL Advances*. Englewood Cliffs, NJ: Prentice- Hall, 2003.

[47] S. Lin and D. J. Costello, *Error Control Coding*. Englewood Cliffs, NJ: Prentice-Hall, second ed., 2004.

[48] J. G. Proakis and M. Salehi, *Digital Communications*. New York, NY: McGraw-Hill, fifth ed., 2008.

[49] ANSI T1.413-1998, *Network and customer installation interfaces asymmetric digital subscriber line (ADSL)*, 1998.

[50] P. S. Chow, J. M. Cioffi, and J. A. C. Bingham, "A practical discrete multitone transceiver loading algorithm for data transmission over spectrally shaped channels," *IEEE Trans. Commun.*, vol. 43, pp. 773 –775, Feb./Mar./Apr. 1995.

[51] P. Chow, J. M. Cioffi, and J. Bingham, "DMT-based ADSL: concept, architecture, and performance," in *IEE Colloq. High speed Access Technology and Services, Including Video-on-Demand*, vol. 3, pp. 1–6, Oct. 1994.

[52] P. Golden, H. Dedieu, and K. S. Jacobsen, *Implementation and Applications of DSL Technology*. Boca Raton, FL: Auerbach Pub., 2007.

[53] J. M. Cioffi, S. Jagannathan, M. Mohseni, and G. Ginis, "CuPON: the copper alternative to PON 100 Gb/s DSL networks," *IEEE Commun. Mag.*, vol. 45, pp. 132–139, June 2007.

[54] G. Ginis and J. M. Cioffi, "Vectored transmission for digital subscriber line systems," *IEEE J. Sel. Areas Commun.*, vol. 20, pp. 1085–1104, June 2002.

[55] W. Yu and J. M. Cioffi, "Competitive equilibrium in the Gaussian interference channel," in *Proc. IEEE Int. Symp. Information Theory*, p. 431, 2000.

[56] W. Yu, G. Ginis, and J. M. Cioffi, "Distributed multiuser power control for digital subscriber lines," *IEEE J. Sel. Areas Commun.*, vol. 20, pp. 1105–1115, June 2002.

[57] S. T. Chung and J. Cioffi, "Rate and power control in a two-user multicarrier channel with no coordination: the optimal scheme versus a suboptimal method," *IEEE Trans. Commun.*, vol. 51, pp. 1768–1772, Nov. 2003.

[58] S. T. Chung, S. J. Kim, J. Lee, and J. M. Cioffi, "A game-theoretic approach to power allocation in frequency-selective Gaussian interference channels," in *Proc. IEEE Int. Symp. Information Theory*, p. 316, July 2003.

[59] R. Cendrillon, J. Huang, M. Chiang, and M. Moonen, "Autonomous spectrum balancing for digital subscriber lines," *IEEE Trans. Signal Process.*, vol. 55, pp. 4241–4257, Aug. 2007.

[60] R. Cendrillon, W. Yu, M. Moonen, J. Verlinden, and T. Bostoen, "Optimal multiuser spectrum balancing for digital subscriber lines," *IEEE Trans. Commun.*, vol. 54, pp. 922–933, May 2006.

[61] S. Jagannathan and J. M. Cioffi, "Distributed adaptive bit-loading for spectrum optimization in multi-user multicarrier systems," in *Proc. IEEE Int. Conf. Communications*, (Beijing, China), pp. 625–630, May 2008.

[62] J. M. Cioffi, W. Rhee, M. Mohseni, and M. H. Brady, "Band preference in dynamic spectrum management," in *Proc. European Signal Processing Conf.*, (Vienna, Austria), Sept. 2004.

[63] R. Cendrillon, G. Ginis, E. Van den Bogaert, and M. Moonen, "A near-optimal linear crosstalk canceler for upstream VDSL," *IEEE Trans. Signal Process.*, vol. 54, pp. 3136–3146, Aug. 2006.

[64] R. Cendrillon, G. Ginis, E. Van den Bogaert, and M. Moonen, "A near-optimal linear crosstalk precoder for downstream VDSL," *IEEE Trans. Commun.*, vol. 55, pp. 860–863, May 2007.

[65] B. Lee, J. M. Cioffi, S. Jagannathan, K. Seong, Y. Kim, M. Mohseni, and M. Brady, "Binder MIMO channels," *IEEE Trans. Commun.*, vol. 55, pp. 1617–1628, Aug. 2007.

[66] B. Lee, J. M. Cioffi, S. Jagannathan, and M. Mohseni, "Gigabit DSL," *IEEE Trans. Commun.*, vol. 55, pp. 1689–1692, Sept. 2007.

[67] S. Jagannathan, V. Pourahmad, K. Seong, J. M. Cioffi, M. Ouzzif, and R. Tarafi, "Common-mode data transmission using the binder sheath in digital subscriber lines," *IEEE Trans. Commun.*, vol. 57, pp. 831–840, Mar. 2009.

[68] J.-J. Werner, "An echo-cancellation-based 4800 bit/s full-duplex DDD modem," *IEEE J. Sel. Areas Commun.*, vol. 2, pp. 722–730, Sept. 1984.

[69] L. Guidoux and B. Peuch, "Binary passband echo canceller in a 4800 bit/s two-wire duplex modem," *IEEE J. Sel. Areas Commun.*, vol. 2, pp. 711–721, Sept. 1984.

[70] S. Weinstein, "A passband data-driven echo canceller for full-duplex transmission on two-wire circuits," *IEEE Trans. Commun.*, vol. 25, pp. 654–666, July 1977.

[71] S. Nedic, "An approach to data-driven echo cancellation in OQAM-based multicarrier data transmission," *IEEE Trans. Commun.*, vol. 48, pp. 1077–1082, July 2000.

[72] D. Stopler and I. Reuven, "A fast convergence algorithm for echo cancellers in full duplex transmission using back projection from slicer," *IEEE Trans. Signal Process.*, vol. 53, pp. 1534–1549, Apr. 2005.

[73] R. C. Younce, P. J. W. Melsa, and S. Kapoor, "Echo cancellation for asymmetrical digital subscriber lines," in *Proc. IEEE Int. Conf. Communications*, vol. 1, (New Orleans, LA), pp. 301–306, May 1994.

[74] H.-Y. Wang and S.-W. Wei, "A window-gate for the echo canceller of DMT ADSL," in *Proc. Int. Symp. Circuits and Systems*, vol. 2, pp. 332–335, May 2003.

[75] F. Pisoni and M. Bonaventura, "Cyclic spectral analysis of multi-carrier DMT signals," in *IASTED, 24th Int. Conf. Modeling, Identification and Control*, 2005.

[76] M. Milosevic, T. Inoue, P. Molnar, and B. L. Evans, "Fast unbiased echo canceller update during ADSL transmission," *IEEE Trans. Commun.*, vol. 51, no. 4, pp. 561–565, 2003.

[77] H.-C. Yeh and L. Lin, "Frequency domain echo cancellation for discrete multitone systems," in *Proc. 4th IEEE Int. Symp. Signal Processing and Information Technology*, pp. 401–404, Dec. 2004.

[78] K. Van Acker, G. Leus, M. Moonen, O. van de Wiel, and T. Pollet, "Per tone equalization for DMT-based systems," *IEEE Trans. Commun.*, vol. 49, pp. 109–119, Jan. 2001.

[79] O.-S. Kwon, G.-O. Cho, and K.-W. Lee, "Asymmetric digital subscriber line echo cancellation," *Electron. Lett.*, vol. 36, pp. 274–276, Feb. 2000.

[80] S.-S. Lin and W.-R. Wu, "A low-complexity adaptive echo canceller for xDSL applications," *IEEE Trans. Signal Process.*, vol. 52, pp. 1461–1465, May 2004.

[81] A. Abousaada, T. Aboulnasr, and W. Steenaart, "An echo tail canceller based on adaptive interpolated FIR filtering," *IEEE Trans. Circuits Syst. II*, vol. 39, pp. 409–416, July 1992.

[82] R. M. Gray, "Toeplitz and Circulant matrices: A review," *Foundations and Trends in Commun. and Information Theory*, vol. 2, no. 3, pp. 155–239, 2006.

[83] J. J. Shynk, "Frequency-domain and multirate adaptive filtering," *IEEE Signal Process. Mag.*, vol. 9, pp. 14–37, Jan. 1992.

[84] D. Potts and G. Steidl, "Optimal trigonometric preconditioners for nonsymmetric Toeplitz systems," *Linear Algebra Appl.*, vol. 281, pp. 265–292, Sept. 1998.

[85] V. Britanak, P. C. Yip, and K. R. Rao, *Discrete Cosine and Sine Transforms: General Properties, Fast Algorithms and Integer Approximations*. Amsterdam: Academic Press Inc., 2006.

[86] ANSI T1E1.4/93-131, *Echo cancellation versus FDM for DMT-based ADSL: a comparative study of system performance and implementation complexity*, 1993.

[87] D. H. Brandwood, "A complex gradient operator and its application in adaptive array theory," *Proc. Inst. Elect. Eng.*, vol. 130, pp. 11–16, Feb. 1983.

[88] B. D. Van Veen, "Convergence of the SMI algorithm in partially adaptive linearly constrained beamformers," in *Proc. IEEE Int. Conf. on Acoustics, Speech, Signal Processing*, vol. 2, (Toronto, Canada), pp. 1373 –1376, Apr. 1991.

[89] G. H. Golub and C. F. Van Loan, *Matrix Computations*. Baltimore, MD: Johns Hopkins Univ. Press, third ed., 1996.

[90] C.-Y. Tseng and L. J. Griffiths, "A systematic procedure for implementing the blocking matrix in decomposed form," in *Proc. 22nd Asilomar Conf. Signals, System, Computation*, vol. 2, pp. 808–812, Nov. 1988.

[91] T. Zogakis, P. Chow, J. Aslanis, and J. M. Cioffi, "Impulse noise mitigation strategies for multicarrier modulation," in *Proc. IEEE Int. Conf. Communications*, vol. 2, (Geneva, Switzerland), pp. 784–788, May 1993.

[92] H. Cox, R. M. Zeskind, and M. M. Owen, "Robust adaptive beamforming," *IEEE Trans. Acoust., Speech, Signal Process.*, vol. 35, pp. 1365–1376, Oct. 1987.

[93] H. Guo, G. Sitton, and C. Burrus, "The quick Fourier transform: an FFT based on symmetries," *IEEE Trans. Signal Process.*, vol. 46, pp. 335–341, Feb. 1998.

[94] P. Z. Lee and F.-Y. Huang, "Restructured recursive DCT and DST algorithms," *IEEE Trans. Signal Process.*, vol. 42, pp. 1600–1609, July 1994.

[95] C. Alexander and M. Sadiku, *Fundamentals of Electric Circuits*. New York, NY: McGraw-Hill, fourth ed., 2008.

[96] W. Y. Chen, J. L. Dixon, and D. L. Waring, "High bit rate digital subscriber line echo cancellation," *IEEE J. Sel. Areas Commun.*, vol. 9, pp. 848 –860, Aug. 1991.

[97] L. D. Clercq, M. Peeters, S. Schelstraete, and T. Pollet, "Mitigation of radio interference in xDSL transmission," *IEEE Commun. Mag.*, vol. 38, pp. 168–173, Mar. 2000.

[98] J. A. C. Bingham, "RFI suppression in multicarrier transmission systems," in *Proc. IEEE Global Telecommunications Conf.*, vol. 2, pp. 1026–1030, Nov. 1996.

[99] G. Arslan and B. Lu, "Time domain equalizer design for discrete multitone modulation." dmtteq3_1.zip, May 2003. `http://users.ece.utexas.edu/bevans/projects/adsl/dmtteq/dmtteq.html`.

[100] R. Stolle, "Electromagnetic coupling of twisted pair cables," *IEEE J. Sel. Areas Commun.*, vol. 20, pp. 883–892, June 2002.

[101] P. Tan and N. C. Beaulieu, "An improved DCT-based OFDM data transmission scheme," in *Proc. IEEE 16th Int. Symp. Personal, Indoor and Mobile Radio Commun.*, vol. 2, pp. 745 –749, Sept. 2005.

[102] T. S. Shores, *Applied Linear Algebra and Matrix Analysis*. New York, NY: Springer, 2007.

[103] G. Williams, *Linear Algebra with Applications*. Boston, MA: Jones and Bartlett Publishers, fifth ed., 2005.